

PhD Thesis

# TOPOLOGICAL INDICES FOR THE CHARACTERIZATION OF ELECTRONIC LOCALIZATION IN MOLECULES AND SOLIDS

ALFONSO GALLO BUENO

PhD supervisor

ÁNGEL MARTÍN PENDÁS



DOCTORATE PROGRAMME IN THEORETICAL CHEMISTRY  
AND COMPUTATIONAL MODELLING

Quantum Chemistry Group  
Departament of Physical and Analytical Chemistry  
University of Oviedo  
March 2016



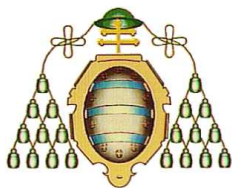
Tesis doctoral

# ÍNDICES TOPOLÓGICOS PARA LA CARACTERIZACIÓN DE LA LOCALIZACIÓN ELECTRÓNICA EN MOLÉCULAS Y SÓLIDOS

ALFONSO GALLO BUENO

Director de tesis

ÁNGEL MARTÍN PENDÁS



PROGRAMA DE DOCTORADO EN QUÍMICA TEÓRICA Y  
MODELIZACIÓN COMPUTACIONAL

Grupo de Química Cuántica  
Departamento de Química Física y Analítica  
Universidad de Oviedo  
Marzo de 2016





## RESUMEN DEL CONTENIDO DE TESIS DOCTORAL

1.- Título de la Tesis	
Español: Índices topológicos para la caracterización de la localización electrónica en moléculas y sólidos	Inglés: Topological indices for the characterization of electronic localization in molecules and solids
2.- Autor	
Nombre: Alfonso Gallo Bueno	DNI/Pasaporte/NIE:
Programa de Doctorado: Química teórica y modelización computacional	
Órgano responsable: Centro internacional de posgrado	

### RESUMEN (en español)

La química es una disciplina científica cuyos conceptos más arraigados han sido interpretados alegóricamente por Frenking y Krapp [J Comput Chem 28: 15–24, 2007] como unicornios, refiriéndose a algo que todo el mundo conoce pero que nadie ha visto. Como encargada de comprender las sustancias y sus transformaciones, la química ha ido introduciendo desde sus orígenes conceptos con un trasfondo en gran parte mítico, resilientes por haber servido para traerla hasta el estado en que se encuentra hoy en día, pero frágiles si atendemos al razonamiento científico sobre el que se basan. El enlace químico es uno de ellos que, como central a la ciencia química por ser el que rige las relaciones entre átomos y moléculas, y que por tanto define el comportamiento de las sustancias, ha sufrido numerosas transformaciones que han tratado de dotarlo de fondo físico.

Con el desarrollo de la mecánica cuántica como teoría del mundo microscópico a principios del siglo XX y su aplicación a sistemas químicos, el concepto de enlace ha ganado en sofisticación y contenido físico. Sin embargo, este avance se ha producido fundamentalmente en espacios abstractos diferentes al espacio real, por lo que entender las teorías que intentan explicarlo y sus consecuencias se hace muy complicado al exigir al lector una formación física avanzada.

De un tiempo a esta parte, se ha tratado de dar una vuelta de tuerca a la manera de entender el enlace, intentando buscar la forma de conciliar el rigor físico y matemático de su definición con las ideas tradicionales que tan útiles han demostrado ser, pero que se basan en la intuición. Esta nueva forma de entender la química cuántica se conoce como topología químico-cuántica (QCT). El paraguas QCT ampara diferentes herramientas, como los índices de localización (LI) y deslocalización (DI), definidos dentro de la teoría cuántica de átomos en moléculas (QAIM), así como las funciones de distribución electrónica (EDF) y los orbitales naturales adaptativos (NAdOs), todo en el espacio real, donde la mente del químico está acostumbrada a trabajar y donde el concepto de enlace químico toma sentido.

En la presente tesis doctoral ahondamos en la utilización de estas herramientas. Demostramos que los LIs y DIs son cantidades capaces de caracterizar sistemas metálicos y aislantes, tanto moleculares como en el estado sólido, desde un punto de vista teórico, es decir, con la gran ventaja de sólo necesitar de un cálculo computacional, sin involucrar ningún tipo de experimento. Se han aplicado en cadenas y anillos modelo, así como en cadenas y anillos de átomos de hidrógeno. Se analiza a su vez el efecto que tiene sobre ellos la correlación electrónica. También se extiende la aplicación de las EDFs, hasta ahora solo calculadas en moléculas, a sistemas en estado sólido: NaCl, diamante y grafito, y sodio metálico, como modelos de enlace iónico, covalente y metálico, respectivamente. Estas funciones de distribución electrónica permiten hacer un análisis pormenorizado de la “personalidad” de un sistema, cristal en nuestro caso, proporcionando así información del porqué de su comportamientos en cualquier tipo de ambiente. Tanto los LIs y DIs como las EDFs responden a la contemplación del enlace químico desde un punto de vista estadístico, lo que proporciona una mirada original a un concepto de larga trayectoria.



Por otro lado, los NAdOs son funciones representables gráficamente y que por su carácter monoeléctrico ofrecen una imagen del enlace químico similar a la de los orbitales moleculares, a los que la comunidad química está acostumbrada. Complementan por tanto la información de los DIs y las EDFs, haciendo que el enlace se comprenda mejor y además, pueda contemplarse mejor. En este trabajo se han aplicado los NAdOs, que hasta ahora solo se habían estudiado en moléculas, a los mismos sistemas cristalinos para los que se evaluaron las EDFs.

El resultado es un trabajo que recoge las más originales ideas sobre el enlace químico y que constituyen el *state of the art* de la ciencia química, y las extiende a nuevos territorios donde no se conocía su comportamiento, aumentando así su carácter general.

### RESUMEN (en Inglés)

Chemistry is a scientific discipline whose deepest concepts have been interpreted allegorically by Frenking and Krapp [J Comput Chem 28: 15-24, 2007] as unicorns, referring to something that everyone knows but no one has ever seen. As responsible for understanding substances and their transformations, chemistry has introduced since its inception, concepts with a largely mythical background, resilient for they have served to bring it to the state in which it is today, but fragile if we consider their scientific basis. The chemical bond is one those concepts, central to chemistry for it governs the relations between atoms and molecules, thus defining the behavior of the substances. Due to its relevance, it has undergone numerous transformations that have tried to give it a sound physical reasoning.

With the development of quantum mechanics as a theory of the microscopic world in the early twentieth century and its application to chemical systems, the bond concept has gained in sophistication and physical content. However, this progress has occurred mainly in abstract spaces other than the real space, which require from the reader an advanced physical background for proper understanding.

While ago, the scientific community has tried to give a twist to the way the chemical bond is looked at, pursuing to reconcile the physical and mathematical rigor of its definition with the traditional ideas, which have proved to be extremely useful, but are built on an intuitive basis though. This new look at quantum chemistry is known as quantum chemical topology (QCT). The QCT umbrella covers different tools, such as localization (LI) and delocalization indices (DI), defined within the quantum theory of atoms in molecules (QTAIM), the electron distribution functions (EDF) and the adaptive natural orbitals (NAdO), all defined in the real space, where the mind of the chemical is used to work in and where the concept of chemical bond makes sense.

In this thesis we delve into the use of these tools. We show that LIs and DIs are quantities capable of characterizing metal and insulating systems, both in molecules and in the solid state, from a theoretical point of view, that is, with the advantage that only a computer is needed in order to carry out the calculation and no experiment is involved. These indices have been applied in both model and real chains and rings of hydrogen atoms. The effect that the electron correlation exerts on them has been analyzed as well. The study is extended to the application of the EDFs, so far only calculated in molecules, to solid state systems: NaCl, diamond and graphite, and metallic sodium as model compounds of ionic, covalent and metallic bonding, respectively. EDFs allow a detailed analysis of the "personality" of a system, crystalline in our case, through the scrutiny of its electron distribution, offering that way an explanation of its behaviour in any environment. Both LIs and DIs, as well as EDFs respond to the observation of the chemical bond from a statistical point of view, providing an original look at the chemical



bond, a concept with a long career.

On the other hand, NAdOs are graphically representable one-electron functions that provide an image similar to that of the molecular orbitals, picture to which the chemical community is accustomed. They therefore complement the information provided by the DIs and EDFs, visually endorsing the understanding of the chemical bond. In this work have the NAdOs, so far only studied in molecules, have been applied in the same crystal systems as the EDFs.

The result is a PhD thesis that collects the most original ideas on chemical bonding that are the state of the art of quantum chemistry, and extends them to unexplored territories, thereby increasing their general character.

*Recuerde el alma dormida,  
avive el seso y despierte*  
J. M.





A esos amigos



To my mum  
To Tati y Tata



## ACKNOWLEDGMENTS

I wholeheartedly thank my supervisor Ángel Martín Pendás.

I am also sincerely thankful to the people from MPI, specially Miro,  
to the friends from the lab in Oviedo and from the master.



# CONTENTS

<b>I</b>	<b>Motivation</b>	<b>1</b>
<b>II</b>	<b>Theoretical basis</b>	<b>11</b>
<b>1</b>	<b>GENERAL QUANTUM CHEMISTRY</b>	<b>13</b>
1.1	The Schrödinger equation	13
1.1.1	The Born-Oppenheimer approximation	14
1.1.2	Antisymmetry and the Pauli exclusion principle	15
1.1.3	The orbital approximation	15
1.2	The Hartree-Fock approximation	17
1.3	Post-HF methods I: wave function-based	19
1.3.1	Configuration interaction	19
1.3.2	Configuration interaction single and doubles	20
1.3.3	Multi-configuration self-consistent field	21
1.4	Post-HF methods II: density-based	22
1.4.1	First Hohenberg-Kohn theorem	22
1.4.2	Second Hohenberg-Kohn theorem	24
1.4.3	The Kohn-Sham Approach	24
1.5	Electron Distribution and Density Matrices	29
1.5.1	Density Matrices	30
1.5.2	Cumulant densities	34
<b>2</b>	<b>SOLID STATE THEORY</b>	<b>37</b>
2.1	Basic crystallography	37
2.1.1	The Bravais lattice	37
2.1.2	The reciprocal lattice	40
2.2	Electronic structure methods in the solid state	41
2.2.1	Bloch's theorem	41
2.2.2	k-points sampling	43
2.3	The family of (L)APW methods	45
2.3.1	The APW method	46
2.3.2	The linearized augmented plane-wave method	47
2.3.3	LAPW with Local Orbitals: LAPW + LO	48
2.3.4	The APW-lo method	49
2.3.5	Mixed basis sets	50



<b>III</b>	<b>The decay of the delocalization index (DI) and metallicity</b>	<b>51</b>
3	CHEMICAL BOND DESCRIPTORS IN REAL SPACE: QTAIM	53
3.1	Localization and delocalization indices	54
3.2	The delocalization index in the solid state	58
4	DECAY OF DIS AND METALLICITY AT THE UNCORRELATED LEVEL	59
4.1	Introduction	59
4.2	Decay rate of 1-RDMs and delocalization indices	61
4.3	Models, computational details	63
4.4	Finite analytical models	64
4.4.1	The Hückel homoatomic chain	64
4.4.2	The Hückel AB heteroatomic chain	66
4.5	Periodic analytical models	68
4.6	Single determinant (HF, KS) results	71
5	DECAY OF DIS AND METALLICITY AT THE CORRELATED LEVEL	77
5.1	Introduction	77
5.2	Delocalization measures and the 1D Hubbard chain	79
5.2.1	The 1D Hubbard chain	81
5.3	Results	83
5.3.1	Saturation rate	83
5.3.2	Decay rate of $DI(1,j)$	85
<b>IV</b>	<b>The Electron Distribution Function (EDF) in the solid state</b>	<b>93</b>
6	ELECTRON DISTRIBUTION FUNCTIONS	95
6.1	The 2-center, 2-electron paradigm	97
6.1.1	Electron delocalization from the EDF	102
6.2	Electron distribution functions in the 1-determinantal case	103
7	EDF IN THE SOLID STATE	105
7.1	Natural adaptive orbitals	106
7.1.1	The domain average Fermi hole	106
7.1.2	Natural adaptive orbitals	108
7.2	EDF results	112
7.2.1	The ionic case: crystalline NaCl	112
7.2.2	The covalent cases: diamond and graphite	122
7.2.3	A metal: Na <i>bcc</i>	132

<b>V</b>	<b>The DI as a means to unveil the metal-to-insulator transition in MnO</b>	<b>137</b>
8	MOTT INSULATORS	139
	8.0.4 DFT and Hubbard alliance: LSDA+U approach	141
	8.0.5 Mott transitions	141
9	A FAILURE STORY: DIS AND THE MOTT INSULATOR TRANSITION IN MNO	143
	9.1 LSDA+U results in MnO	143
	9.2 A encouraging alternative: the reduced density matrix functional theory	146
<b>VI</b>	<b>Conclusions</b>	<b>151</b>
10	CONCLUDING REMARKS	153
	BIBLIOGRAPHY	155



# **Part I**

## **Motivation**



*Unlike Newton's mechanics, or Maxwell's electrodynamics, or Einstein's relativity, quantum theory was not created—or even definitively packaged—by one individual, and it retains to this day some of the scars of its exhilarating but traumatic youth. There is no general consensus as to what its fundamental principles are, how it should be taught, or what it really “means”. Every competent physicist can “do” quantum mechanics, but the stories we tell ourselves about what we are doing are as various as the tales of Scheherazade, and almost as implausible. Niels Bohr said, “If you are not confused by quantum physics then you haven't really understood it”; Richard Feynman remarked, “I think I can safely say that nobody understands quantum mechanics”.*

*Introduction to Quantum Mechanics*  
David J. Griffiths

At the end of the nineteenth century, and although the atomistic nature of matter was already known, it was felt that the laws of nature were well understood and that it was just a matter of time that a rationalization of all physical phenomena would be achieved. However, some scientists began to notice that Newtonian laws were not able to explain phenomena at the atomic level[160]. As the focus of their investigations changed from the dynamics of macroscopic bodies to entities of atomic dimensions, it was recognized that the older laws were not applicable to atoms or electrons without considerable modification[124]. The behaviour of atoms and molecules can be understood from the laws governing the motion of atoms and electrons. A new theory then appears, a theory of the very small: *the body of scientific principles that explains the behaviour of matter and its interactions with energy on the scale of atoms and subatomic particles*[163], which is not a smooth continuation of the classical mechanics, but a *conceptually rich and also technically difficult* theory[63]. Although clear analogies exist between classical mechanics and *quantum mechanics*, the name this new theory was given, the latter has a very distinct formulation that arises from a very different perspective regarding the way nature is observed.

The “old quantum theory”, as Pauling called it[124], was born at the beginning of the twentieth century with Planck's solution to the black body radiation conundrum[126]. Without explicitly stating the idea of light quantization, Planck had introduced during his investigations a finite constant  $h$  not existent in the classical theory[160]. It was in 1905 that Einstein introduced the idea of light quanta[41], for which he later received the Nobel price. This concept, as he showed in a posterior article[40], was implicitly used by Planck in his earlier work. With the idea of the electromagnetic energy being quantized in packages of energy  $h\nu$ , named photons, Einstein gave a satisfactory explanation of the photoelectric effect[39]. Armed with this ideas, Bohr introduced the atomic model by postulating a discrete number of allowed energy levels in the hydrogen atom[24].

In 1927, after the famous Solvay conference in Brussels, the field of *quantum physics* was widely accepted and applied to many different disciplines, including the one that interests us: chemistry. The application of the Schrödinger equation to the hydrogen atom in 1926[143], as well as the first quantum-mechanical approach to the hydrogen molecule in 1927[66] are considered as the true birth of quantum chemistry[90, 164]. The successful application of the quantum ideas and the subsequent description of simple systems from the perspective of a quantized nature of the matter, such as the harmonic oscillator, the oscillating and rotating diatomic molecule or the particle in a box, to cite a few examples, gave this theory the sufficient strength that led to the modern formulation of quantum mechanics[124, 165].

As a central discipline that is involved in every single natural process, the formation of substances and their transformations has been a main concern since the first attempts to understand nature. The chemical bond is the bridge between the original alchemical reasoning of the chemical transformations and the new perspectives of molecules changing into one another by breaking old bonds and making new ones. The bond concept extends its roots way back to the chemists that tried to overcome the spiritual view of chemistry as bunch of magical processes[145].

The new era in the study of the chemical bond is widely accepted to have started with the asseveration of Lewis that the electron pairs constitute the fundamental blocks of matter[91]. Previous to the development of the quantum chemistry as an appropriate tool to describe chemical processes, he introduced the cubical atom model and the electron pairing to explain the chemical bond. His observations consider the formation of electronic pairs as a phenomenon that cannot be understood just in terms of electrostatic interactions, and postulates a violation of the Coulomb law for the electronic coupling.

The quantum study of a chemical system consists in obtaining an approximation to its wave function, the quantum mechanical object that completely characterizes any physical system, by solving an approximation to the fundamental or Schrödinger equation. It was the great development of the quantum chemistry that came later which permitted the explanation of the underlying processes, and made it possible to recognize the Pauli principle as the reason for the violation that Lewis had stated.

The subsequent study of Heitler and London already mentioned [66], followed by the works of Pauling[122], Slater[155], Mulliken[119], Hund[70] or Hückel[69] among many others, made it clear that the new quantum theory was offering satisfactory explanations to the problems of chemistry. Several decades after, the chemical bond, despite its crucial importance, keeps intriguing the scientific community for various reasons. On the one hand, Lewis' classical ideas blend with difficulty with the quantum image. The former are based

on the concept of electron pairs and its sharing among the different chemical species are far from easy to be given a quantum-mechanical reasoning. There is not such a thing as a Lewis pair in the complex multidimensional mathematical object that a wave function is, whose analysis does not easily provide a intuitive representation of the various concepts used in chemistry, maybe with the exception of the simplest molecular systems.

On the other hand, there does not exist an observable operator for the chemical bond, so that it cannot be experimentally determined. For both reasons, chemists have been forced to develop theories, methods, concepts, ... to write the information contained in a wave function in a language that the chemists' mind understands.

In the subsequent years, the increasingly important study of the chemical systems in quantum-mechanical terms gave rise to many theories that tried to explain the experimental facts, and in particular the chemical bond. Two captured an special attention: the molecular orbital (MO) and the valence bond (VB) theories.

For different reasons that will not be discussed in this succinct introduction, the MO prevailed over the VB theory, and is still nowadays an extremely useful tool with great descriptive and predictive power. As it can be deduced from its name, the MO theory is based on the description of the spatial distribution of the electrons with monoelectronic functions known as orbitals. The orbitals have the great advantage that they can be graphically represented, and on the other side, mean a drastic reduction of the dimensionality of the wave function from a  $3N$  or  $(3+1)N$ -dimensional problem, to  $N$  3- or 4-dimensional problems.

Despite its crucial importance in the development of chemistry, the MO theory suffers from some limitations originated in its monoelectronic basis. The wave function is invariant under orbital transformations, opening the problem of which orbital representations should be taken as reference, since there are infinite for a given wave function. Additionally, the electron correlation must be considered in most chemical systems of interest in order to obtain a satisfying description of them and therefore one must search for alternative theories beyond the monoelectronic approach.

With this aim, the theoretical chemistry community has dedicated itself to the search for new physically rigorous theories, that rather than annihilating the widespread concepts originated from Lewis ideas, try conciliate them with the principles of quantum mechanics. The already mentioned idea of an electron pair shared between two atoms, together with the process of electron transfer from one atom to another and the notion of Pauling's resonance<sup>[123]</sup>, form a hard core that still stands to this day, and there is no advantage in putting them aside.



These overwhelmingly successful ideas conform the chemical intuition, deeply rooted in the chemist's mind, that is an invaluable tool in his every day's work. The new theories are required to i) recover these concepts by means of generic methods, not subject to a fixed procedure as it is the case of the MO and VB approaches. Besides, the search focuses on ii) theories in the real space—in contrast to the Fock space—, where all the aforementioned concepts reside, and where the chemist's mind is accustomed to work. They are iii) ideally of a not too high complexity, easily understandable by the not specialized scientific communities such as for instance the experimental chemists, and also iv) endowed with predictive power.

The best known approaches, collecting the enumerated preconditions are based on a partition of the real space by way of a gradient acting on some scalar field carrying chemical content, and are grouped under the umbrella of the quantum chemical topology (QCT) name[136, 137]. This standpoint, also known as the topological analysis of the wave function, started with the work of Richard F. W. Bader in the '60s, and is based in the widely used strategy of dividing the space of interest into smaller regions, endowed with physical meaning, to tackle chemical problems. Therefore, the topological analyses not only exhaustively partition the space, but also discretize it so that the examination of a scalar field can be enclosed to specific regions of particular importance, rather than extend the whole space.

Among the ream of scalar fields that can be used, as for instance the Laplacian of the electron density  $\nabla^2\rho$ , or the widely used ELF[21] or the ELI[81] functions, the electron density  $\rho$  is the most successful one. The quantum theory of atoms in molecules (QTAIM)[12] is a very well-known theory, central to this PhD thesis, that defines regions of zero-flux of  $\rho$ , which results in a division of the space into atomic regions.

The delocalization index (DI) is defined within Bader and Stephens' QTAIM theory[10] as a descriptor of how many pairs of electrons are shared—delocalized—between two atomic regions of the kind just described, in the real space. In order to calculate the DI, only the first- and second-order reduced density matrices, also referred to as 1-RDM and 2-RDM, respectively, are necessary. The 1- and 2-RDMs, as it will be described more in detail later on, are condensations of the total wave function that carry all the information that the wave function contains about one and two particle interactions, respectively. As the Schrödinger equation does not consider interactions between more than two particles, the 2-RDM is in principle the highest-order RDM necessary to characterize the chemical bond. The size of the problem is reduced to at most a two-particle quantity, which make the DIs an affordable tool in terms of the computational effort required to evaluate them. The DIs have been used to study many different chemical problems, as the bonding in aromatic compounds[95, 105, 106, 127]

and in solids[18, 56], the study of the bond transformation with reaction coordinates[57], among many others.

Kohn published a seminal paper in 1964[77], in which he showed that insulators and conductors do not differ, as it was believed until then[74], only in the nature of their excited states, which implies hence a description far from the real space, but also in the organization of their electrons in the ground state. Resta did in 1998[84] a reformulation of Kohn's ideas, which has as consequence that conductivity should leave scars in the RDMs, defined in the real space.

As deriving from the 2-RDM (the 1-RDM in the case of monodeterminantal wave functions), the DI is an attractive tool to study metallicity from the real space standpoint. A second connection is established by the naive association made by the chemist's mind between a material with conducting properties and highly delocalized electron networks. As a measure of the electron delocalization, the nature itself of the DI directly connects it to metallic or insulating character, but its ability to characterize the degree of metallicity of a system, being a priori appealingly clear, has yet never been put under study though.

It is a main goal of this work, after the corresponding introduction to the general ideas of the quantum chemistry and the solid state of Part II, to show that the DI is a suitable index to characterize from the ground state the behaviour of, not only in the solid state but also molecular systems, both in model and real cases, under electric fields. This is the content of Part III, divided into a first Chapter 4 where no correlation is considered and a second 5 at the correlated level.

Let us come back to a exhaustive partition of the real space occupied by a system. The particle number operator does not commute with the Hamiltonian of the system, so that if we ask how many electrons are there in a region of space, no definite number is obtained. On the contrary, we can only talk about average electron populations and for a given partition, an electron distribution will occur with a certain probability. The frontiers of the domains in which the space is divided must be considered as permeable, so the concept of fluctuation becomes central: the higher the fluctuation, the lower the localization.

Within this context, Daudel *et al.* occupied themselves in the search for a function that determines the probability to find a given number of electrons inside a region of space[37]. Savin gave later a turn to this approach by using these probabilities to study the electron distribution in the setting of a QTAIM partitioning[32, 141]. The thread was resumed around a decade ago by Martín Pendás and co-workers, introducing the electron distribution function (EDF)[54, 100, 101], an statistical interpretation of the chemical bond. For a given partition of the space, each electron distribution, or resonant structure in Pauling's terms, has a probability which is a weight of this probability in

the total set of resonant structures that the molecule can adopt. Part IV deals with the application of this original view of the chemical bond in solid state metallic, insulating and ionic systems.

The ubiquitous MO theory, for it is based in monoelectronic functions, fails when the electron correlation plays a fundamental role. Towards the search of an alternative standpoint to the MO theory, a generalization must be done that allows to explore the yet to a great extent unknown territory of the electron correlation, but at the same time tending to the MO ideas if the correlation is removed. We are entering a generalized electron population analysis.

RDMs are the suitable base for these new concepts, for they are condensations of the system wave function, and therefore less complex, but still carry the information we want. Although the traditional bond is basically a 2-centre, 2-electron bond, from higher-order RDMs also higher-order DIs can be obtained and that way multicentre bonds can be studied.

From a diagonalization procedure that involves cumulants, which are just special parts of the RDMs that are irreducible, in a certain spin orbital representation, a series of functions of particular interest can be obtained. These are representable monoelectronic functions obtained for multicentre bonds. Therefore one gets from them an orbital picture very similar to that yielded by the MO theory, but with information of 2 or higher-order bonding—for they derive from two- or higher-order cumulants, i.e., RDMs—. The brilliant idea of obtaining those functions is Ponec's idea, who gave them the name, in the case of just one-centre, of domain-average Fermi hole (DAFH) functions[129, 130]. A generalization of the DAFHs to  $\nu$ -centres was done at the quantum chemistry group in the University of Oviedo by Francisco *et al.*, who proposed the name of natural adaptive orbitals (NAdOs)[113]. In the case of three centres, the NAdOs can be seen as a partition of a traditional two-centre bond in monoelectronic contributions. The 2-NAdOs will be analyzed within this work, together with the EDFs, in the solid state systems of Part IV.

In the last Part V we tried to apply the DIs to map an insulator-to-metal transition in the MnO. Transition metal oxides (TMOs) are strongly correlated systems with partially filled d-bands that show insulating behaviour in the ground state. TMOs can suffer an inversion in their electric properties, becoming metals from an insulating state as a consequence of a change in the correlation strength triggered by some alteration in the physical properties. As the inversion, known as a Mott transition[26], is originated in the electronic structure of the TMO and after the success of the DI in differentiating metallic from insulating behaviour, it is tempting to check whether these indices capture the switch in the delocalization that takes place during a Mott transition.

The correct description of a Mott insulators, name given to the TMOs that undergo a Mott transition, as insulating systems although being oxides of transition metals has been yet not achieved. This is one of the biggest failures of the band theory, which predicts the Mott insulators to be metals in their ground state. The recent development of a new theory, known as the reduced density-matrix functional theory (RDMFT)[60] appeared as the solution to this problem for it was shown it could provide a correct theoretical description of a Mott insulator[147, 148]. However and although we established contact with the authors of these publications, their results were not reproducible, at least with our computational resources. The early stage of the development of the theory, as well as the rapidly scaling computational cost are the reasons behind this failure.

Part VI just wraps up summarizing some conclusions that we think important to stress from this thesis.



## **Part II**

# **Theoretical basis**



# 1 | GENERAL QUANTUM CHEMISTRY

Let us now briefly introduce the basic ideas, that will allow us to construct an eloquent exposition of the results of our research.

## 1.1 THE SCHRÖDINGER EQUATION AND THE MANY ELECTRON WAVE FUNCTION: THE ORBITAL APPROXIMATION

The main concern of quantum chemistry is the problem of many electrons moving in a field of fixed nuclei. We will introduce now the many-electron problem and what the approximations generally used to solve it are.

It is a basic tenet of quantum mechanics that all the information that can be obtained from a system is contained in its wave function  $\Psi$ , which is the solution of the so-called Schrödinger equation:

$$\hat{H}\Psi = i\partial_t\Psi. \quad (1)$$

In the above equation,  $\hat{H}$  is the Hamiltonian operator, whose spectrum yields the allowed energy values of the system. In the case of a time independent Hamiltonian, the energy of the system  $E$  results from the application of the Hamiltonian operator  $\hat{H}$  to the aforementioned wave function  $\Psi$ :  $\hat{H}\Psi = E\Psi$ . For a many body problem, the last equation can be rewritten as:

$$\hat{H}\Psi(\mathbf{r}_1, \dots, \mathbf{r}_N, \mathbf{R}_A, \dots, \mathbf{R}_M) = E\Psi(\mathbf{r}_1, \dots, \mathbf{r}_N, \mathbf{R}_A, \dots, \mathbf{R}_M), \quad (2)$$

where the positions of the  $N$  electrons and the  $M$  nuclei are denoted by  $\mathbf{r}_N$  and  $\mathbf{R}_M$ , respectively, and the Hamiltonian operator  $\hat{H}$  adopts the form:

$$\begin{aligned} \hat{H} = & -\sum_{i=1}^N \frac{1}{2} \nabla_i^2 - \sum_{A=1}^M \frac{1}{2M_A} \nabla_A^2 - \sum_{i=1}^N \sum_{A=1}^M \frac{Z_A}{r_{iA}} + \\ & + \sum_{i=1}^N \sum_{j>i}^N \frac{1}{r_{ij}} + \sum_{A=1}^M \sum_{B>A}^M \frac{Z_A Z_B}{R_{AB}}. \end{aligned} \quad (3)$$

Nuclei and electrons are designated by  $A, B$  and  $i, j$ , respectively. Nucleus  $A$  has nuclear charge  $Z_A$  and  $M_A$  is the ratio of its mass to



the mass of an electron, in any case using atomic units. The Laplace operator  $\nabla^2$  involves the second derivative with respect to the spatial coordinates of the  $i$ th electron and of the  $A$ th nucleus. The first two terms describe the kinetic energy of electrons and nuclei, respectively. The remaining three terms are potential ones and represent, in this order, the attractive electrostatic nucleus-electron interaction and the potential describing the electron-electron and the nucleus-nucleus repulsion.

#### 1.1.1.1 The Born-Oppenheimer approximation

The description of chemical systems with the tools of the quantum mechanics is a very difficult task, made feasible by means of different approximations. A paramount one within quantum chemistry is the Born-Oppenheimer approximation.

Due to their heavier nature, nuclei move very slowly when compared with the lightweight electrons,<sup>1</sup> This allows us to assume that, to a very good approximation, the electrons are the only mobile particles in a molecule. That way, the Born-Oppenheimer approximation assumes the electron motion uncoupled from the motion of the nuclei, which are now fixed, and considers both movements separately. Equation 3 is thus simplified by noticing that the nuclear kinetic energy vanishes, and the last term in this expression, which accounts for the nuclear repulsion is constant. Since addition of a constant to an operator does not change its eigenvectors, simply shifting its spectrum, this term can also be neglected and expression 3 reduces to

$$\hat{H}_{elec} = - \sum_{i=1}^N \frac{1}{2} \nabla_i^2 - \sum_{i=1}^N \sum_{A=1}^M \frac{Z_A}{r_{iA}} + \sum_{i=1}^N \sum_{j>i}^N \frac{1}{r_{ij}} = \hat{T} + \hat{V}_{Ne} + \hat{V}_{ee}, \quad (4)$$

which is the electronic Hamiltonian describing the motion of  $N$  electrons in the field of  $M$  fixed nuclei now represented by point charges.  $\hat{T}$  is the kinetic energy operator, and  $\hat{V}_{Ne}$  and  $\hat{V}_{ee}$  are the operators denoting the nucleus-electron and the electron-electron interactions, respectively.

The electronic Schrödinger equation is now formulated as

$$\hat{H}_{elec} \Psi_{elec} = E_{elec} \Psi_{elec}, \quad (5)$$

analogous to the general equation 3, but where the energy  $E_{elec}$  and the wave function  $\Psi_{elec}$  are now electronic objects. The total energy is recovered according to

$$E_{tot} = E_{elec} + E_{nuc}. \quad (6)$$

<sup>1</sup> The nucleus-electron mass ratio for the lightest nucleus (proton  $^1\text{H}$ ) is of 1,836152. For very common atoms as C, the ratio is increased to about 20,000.

A more detailed discussion on the nuclear Schrödinger equation and the treatment of a wave function where nuclei also move can be found in the cited literature, as for example in references [75, 157].

### 1.1.2 Antisymmetry and the Pauli exclusion principle

Although the Hamiltonian of equation 4 depends only on the spatial coordinates of the electrons, a complete description of a system demands to consider their spin coordinates as well. The wave function is then  $\Psi(\mathbf{x}_1, \mathbf{x}_2 \dots, \mathbf{x}_N)$ , where both the spatial  $\mathbf{r}_i$  and the spin  $\sigma_i$  coordinates of the  $i$ th electron are included in  $\mathbf{x}_i = (\mathbf{r}_i, \sigma_i)$ .

According to Max Born's interpretation, the square of the wave function yields the probability density of finding electron 1 in  $d\mathbf{x}_1$ , 2 in  $d\mathbf{x}_2$ , ... and  $N$  in  $d\mathbf{x}_N$ , simultaneously:

$$|\Psi(\mathbf{x}_1, \mathbf{x}_2 \dots \mathbf{x}_N)|^2 d\mathbf{x}_1 d\mathbf{x}_2 \dots d\mathbf{x}_N. \quad (7)$$

For indistinguishable particles this probability is not affected by the exchange of the coordinates of two of them. Nature offers two possible situations that can result from the permutation of the coordinates of two particles: either the  $N$ -wave function remains the same after the permutation, in which case the considered particles are called *bosons*, or its spin is also flipped (is antisymmetric), and then the particles we are dealing with are named *fermions*. Electrons are fermionic particles with spin = 1/2 and the wave function  $\Psi$  is therefore antisymmetric:

$$\Psi(\mathbf{x}_1, \mathbf{x}_2 \dots \mathbf{x}_N) = -\Psi(\mathbf{x}_2, \mathbf{x}_1 \dots \mathbf{x}_N). \quad (8)$$

The last equation is the quantum-mechanical expression of the Pauli exclusion principle.  $\Psi$  is of course normalized, so the probability to find the  $N$  electrons in the whole space equal to unity:

$$\int |\Psi(\mathbf{x}_1, \mathbf{x}_2 \dots \mathbf{x}_N)|^2 d\mathbf{x}_1 d\mathbf{x}_2 \dots d\mathbf{x}_N = 1. \quad (9)$$

### 1.1.3 The orbital approximation

After assuming the Born-Oppenheimer approximation, each of the electrons that form the system is moving under the influence of the frozen nuclei and the other electrons. Another vital approximation in quantum chemistry limits what kind of influence that is. If the electron is considered as a negatively charged particle moving under the influence of a mean field created, on the one hand by the potential of the positively charged, fixed nuclei, and on the other hand by an averaged interaction of the remaining electrons, this new approximation is known as the mean field electron model or the *orbital approximation*.

Within the so-called orbital approximation, notwithstanding their antisymmetry requirement, the electrons are treated as independent particles and consequently, the total electronic Hamiltonian of equation 4 can be written as a sum of one-particle effective Hamiltonians

$$\hat{H}_{elec} = \sum \hat{h}_{eff}, \quad (10)$$

and very importantly, the many-body wave function can then be expressed as an antisymmetrized product of one-particle functions  $\psi$

$$\Psi_{elec}(\mathbf{x}_1, \mathbf{x}_2) = \mathcal{A} \prod_i \psi_i. \quad (11)$$

As we will only consider the electronic structure of matter in this work, any reference to the total wave function of a system  $\Psi$  will be addressing namely the electronic wave function  $\Psi_{elec}$ .

### *Molecular orbitals*

The one-particle wave functions  $\psi_i$  introduced in equation 11 are spin orbitals of the form

$$\psi(\mathbf{x}_i) = \phi(\mathbf{r}_i)\sigma(s). \quad (12)$$

A spin orbital is a function that describes a mean-field electron formed by two parts: a spatial term  $\phi$  that accounts for the position of electron  $i$ , and a spinorial one,  $\sigma$ , describing its spin.  $s$  can adopt either the  $\alpha$  —spin-up— form with  $m_s = +\frac{1}{2}$  or alternatively the  $\beta$  —spin-down— one with  $m_s = -\frac{1}{2}$ .

In atomic or molecular systems, which unlike crystals span a finite volume, the spatial part  $\phi$  of the spin orbital is normally approximated as a linear combination of either Slater-type functions (STF) or more frequently Gaussian-type functions (GTF). The collection of atomic-centred functions  $\{\chi_i\}$  of either STF- or GTF-type, or a combination of both, is known as the *basis set*. The procedure of expanding a wave function  $\psi$  as a linear combination of functions of the basis set is given the name *linear combination of atomic orbitals* (LCAO) and has the form

$$\psi_j = \sum_{i=1}^N c_{ij}\chi_i, \quad (13)$$

where  $c_{ij}$  are the coefficients of the expansion.

In a molecular context, the total wave function  $\Psi$  is then expressed as an antisymmetrized product of one-particle wave functions  $\psi_i$ , the molecular orbitals, which are in turn approximated according to the LCAO procedure. The particular procedure of combining  $\psi$  functions

to recover  $\Psi$ , has been historically done through either of two different approaches. On the one hand, the *valence bond theory* sees the molecular orbitals as functions localized in the bonding region, while the second strategy provides a picture in which the molecular orbitals spread all over the molecular space. This latter approach is the *molecular orbital theory* (MO), which has had much more success and has been used in most of the quantum studies of chemical systems up to our days.

The electronic Schrödinger equation shown in the equation 5 consequently reduces to an effective one-electron Schrödinger equation,

$$\hat{h}_{\text{eff}}\psi_j = \varepsilon_j\psi_j. \quad (14)$$

## 1.2 THE HARTREE-FOCK APPROXIMATION

After all the approximations we have briefly introduced, a practical method is necessary in order for the previous ideas to be applicable to real systems: this role is played by the Hartree-Fock (HF) method. In the search for approximate solutions to the electronic Schrödinger equation 14, despite being founded on a strongly simplifying assumption that we will discuss immediately, the Hartree-Fock procedure still represents not only the cornerstone of all conventional, i.e., wave function based quantum chemical methods, but also a conceptually very relevant theory as a first step towards more accurate approximations.

The simplest antisymmetric wave function, i.e., a wave function that fulfills the Pauli exclusion principle, of the ground state  $\Psi_0$  of a closed-shell N-electron system, is a single Slater determinant

$$\begin{aligned} |\Psi_0\rangle &= |\psi_1\psi_2\cdots\psi_N\rangle = \\ &= \frac{1}{\sqrt{N!}} \begin{vmatrix} \psi_1(x_1) & \psi_2(x_1) & \cdots & \psi_N(x_1) \\ \psi_1(x_2) & \psi_2(x_2) & \cdots & \psi_N(x_2) \\ \vdots & \vdots & \ddots & \vdots \\ \psi_1(x_N) & \psi_2(x_N) & \cdots & \psi_N(x_N) \end{vmatrix}. \end{aligned} \quad (15)$$

The best wave function that satisfies the above equation is found variationally as that yielding the lowest energy:

$$E_0 = \langle\Psi_0|\hat{H}|\Psi_0\rangle, \quad (16)$$

where  $\hat{H}$  is the total Hamiltonian of the system. The main task of the variational principle resides in finding the best approximation to the unknown true ground state wave function  $\Psi_0$ , which would have associated a energy  $E_0$ . A priceless power of this principle is that the variationally determined energy  $E$  is an upper bound to the true

ground state energy  $E_0$ , which takes its lowest possible value. The variational principle carries out its task by finding the best choice of spin orbitals  $\psi_j$ , in turn expanded as stated in equation 13. That way, one is sure to be closer to the true wave function  $\Psi_0$  if a new choice of spin orbitals yields a lower (more negative) energy.

The minimization of the energy with respect to the spin-orbitals leads to the derivation of an eigenvalue equation for each particle  $i$ . These are collectively known as the Hartree-Fock equations

$$\hat{f}_i \psi(\mathbf{x}_i) = \varepsilon \psi(\mathbf{x}_i). \quad (17)$$

$\hat{f}_i$  is Fock's effective operator and  $\varepsilon$  the orbital energy (eigenvalue) of the spin orbital (eigenvector)  $\psi$ .

In short, the HF method could be said to simplify the construction of the complicated many-body wave function, reducing it to finding single-electron functions which describe averaged electron-electron repulsion. To that end, in the electronic Hamiltonian of equation 4 we replace the electron-electron repulsion term by  $v_i^{\text{HF}}$ :

$$\hat{f}_i = -\frac{1}{2} \nabla_i^2 - \sum_{A=1}^M \frac{Z_A}{r_{iA}} + v_i^{\text{HF}}, \quad (18)$$

where the sum over the  $N$  electrons has been removed since  $\hat{f}_i$  is a monoelectronic operator.  $v_i^{\text{HF}}$  is a one-electron effective potential explicitly defined as

$$v_i^{\text{HF}} = \sum_j \left( \hat{J}_j(\mathbf{x}_i) - \hat{K}_j(\mathbf{x}_i) \right), \quad (19)$$

the sum runs over all the spin orbitals  $\psi_j$  and  $\hat{J}_j$  and  $\hat{K}_j$  are the Coulomb and exchange operators, respectively.  $v_i^{\text{HF}}$  is the total average potential experienced by the electron  $i$  due to the influence of the remaining electrons.

Developing the parenthesis of this equation, the HF potential can be divided into two parts. The first one is the Coulomb potential

$$v_i^{\text{coul}} = \sum_j \hat{J}_j(\mathbf{x}_i) = \sum_j \int |\psi_j(\mathbf{x}_2)|^2 \frac{1}{r_{i2}} d\mathbf{x}_2, \quad (20)$$

which accounts for the repulsive interaction exerted by electron 2 on electron  $i$ . The interaction between both electrons is weighted by  $d\mathbf{x}_2 |\psi_j(\mathbf{x}_2)|^2$ , the probability of electron 2 to be found in the volume element  $d\mathbf{x}_2$ .

The second term in equation 19 is the exchange contribution to the HF potential. It arises from the antisymmetric character of the Slater

determinants and has no classical meaning. It can only be understood through its effect when operating on a spin orbital:

$$\hat{K}_j(\mathbf{x}_i)\psi'_j(\mathbf{x}_i) = \left[ \int \psi_j^*(\mathbf{x}_2)r_{12}^{-1}\psi'_j(\mathbf{x}_2)d(\mathbf{x}_2) \right] \psi_j(\mathbf{x}_i). \quad (21)$$

It can be seen comparing the previous equation with equation 20 that the action of  $\hat{K}_j$  produces an exchange of the variables of the two spin orbitals such that now  $\psi'_j$  is occupied by  $\mathbf{x}_2$ . The result of applying  $\hat{K}_j$  depends on the value of  $\psi'_j$  in all points of space, so the exchange operator is hence said to be *nonlocal*.

The total potential  $v_i^{\text{HF}}$  seen by electron  $i$  (equation 19) depends on the spin orbitals of the remaining electrons. In other words, the Fock operator (equation 18) depends on its own eigenfunctions, which requires that the solution of equation 17 is known in order to be able to solve this equation. This sort of dependency is solved by means of an iterative procedure named self-consistent field (SCF) method.

Every SCF loop starts with a initial guess of the spin orbitals that allows for the calculation of the mean potential  $v_i^{\text{HF}}$  seen by electron  $i$ . Equation 17 is then solved and a new set of spin orbitals obtained, from which again a potential  $v_i^{\text{HF}}$  is found closing one SCF loop and starting the iteration again until convergence of both the  $\psi$ 's and  $\epsilon$ 's is attained (a schematic description of the SCF iterative process can be seen in figure 1).

We have already mentioned that the second term in equation 4 is also a potential that describes the interaction electron-nucleus. The spatial arrangement of the nuclei is the unique part of the whole equation that changes with the system under consideration. Hence, whether our system is a solid, a molecule or an atom is determined by the spatial arrangement of the nuclei, which is specified in the electron-nucleus potential.

## 1.3 QUANTUM CHEMICAL METHODS BEYOND HARTREE-FOCK I: WAVE FUNCTION METHODS

### 1.3.1 Configuration interaction

Within the HF theory, the ground state wave function of a closed shell system is approximated by a single Slater determinant formed by  $N$  occupied spin orbitals. Approximations to the excited states of the system can also be proposed by constructing Slater determinants in which any of the occupied spinorbitals is substituted by excited solutions of the Hartree-Fock equations. It may be proven that the exact wave function,  $\Phi$ , may be expanded as a linear combination of

the ground state determinant and those formed by all possible excited ones. This is the basis of the Configuration Interaction (CI) method:

$$|\Phi_0\rangle = c_0|\Psi_0\rangle + \sum_{ra} c_a^r |\Psi_a^r\rangle + \sum_{\substack{a<b \\ r<s}} c_{ab}^{rs} |\Psi_{ab}^{rs}\rangle + \dots, \quad (22)$$

where  $|\Psi_0\rangle$  is the HF wave function,  $|\Psi_a^r\rangle$  are the single-excited determinants,  $|\Psi_{ab}^{rs}\rangle$  accounts for double excitations and so on, and  $c_0, c_a^r, \dots$  are the coefficients of the linear combination, which are also variationally optimized within the CI method.

By ignoring the contribution of the excited determinants, the HF approach neglects all of the instantaneous correlations that exists between electrons, beyond that related to antisymmetry. Neglecting the correlation implies then ignoring some of Coulomb repulsion, and electrons within HF are closer to each other than in the real situation. Consequently the “HF system” is less stable than it really is  $|E_{\text{HF}}| < |E_0|$ . As it is a variational method, the  $E_{\text{HF}}$  is an upper bound to the exact, non-relativistic energy  $E_0$ . The difference between both energies is a negative quantity called the correlation energy

$$E_{\text{corr}} = E_0 - E_{\text{HF}}. \quad (23)$$

A linear combination of Slater determinants of all the possible excitations of the  $N$  electrons to all the molecular orbitals of the system would yield the *full CI* wave function of the system, and would offer the exact energy within the one-electron basis set used. This energy will approach the true energy of the system as the basis set approaches completeness.

### 1.3.2 Configuration interaction single and doubles

The actual number of determinants that have to be considered in a full CI calculation can be reduced according to Brillouin’s theorem, which states that the ground-state determinant cannot directly mix with single-excited determinants (see for instance [157]). Although they can mix through double or higher order excitations, this cuts down the collection of determinants that must be considered. Despite this simplification and the conceptually simple mathematical full CI formulation, its computational cost grows with the size of the system at a rate that makes it a prohibitive approach for the majority of the real systems. Fortunately, the higher the order of the excitation, the lower the weight of the wave function terms. To a good approximation, one can thus accomplish a truncation of the full CI expansion of equation 24. Of course, the full CI expansion could be stopped at any excitation, but experience has demonstrated that the wave function of the system can be accurately approximated by considering only those Slater determinants differing from the ground state in only one or two

spin-orbitals. In other words, by neglecting the Slater determinants involving excitations of more than two electrons. The procedure that corresponds to a truncated full CI at the double excitations is known as single and doubles CI (CISD). Equation 24 becomes

$$|\Phi_{\text{CISD}}\rangle = c_0|\Psi_0\rangle + c_S|\Psi_S\rangle + c_D|\Psi_D\rangle, \quad (24)$$

where  $|\Psi_S\rangle$  and  $|\Psi_D\rangle$  are the terms that account for the single and double excitations, respectively.

### 1.3.3 Multi-configuration self-consistent field

Within HF, the molecular orbitals  $\psi_j$  are optimized, but combined in just a single Slater determinant to approximate the wave function. Differently, in CI not the molecular orbitals but the coefficients  $c$  of the expansion are varied, optimizing that way the linear combination in terms of which the wave function is pictured. The multi-configuration self-consistent field (MCSCF) is a combination of both

$$|\Phi_{\text{MCSCF}}\rangle = \sum_I c_I |\Psi_I\rangle, \quad (25)$$

in which the coefficients of the expansion  $c_I$ , as well as the Slater determinants  $\Psi_I$  are optimized. Let us recall that Slater determinants are made of molecular orbitals as shown in equation 15, that in turn are a linear combination of basis functions (equation 13).

As equation 25 is a truncation of a CI expansion, it still remains to be decided how many Slater determinants are to be included in the linear combination. A particularly important strategy to do so is the complete active space or CASSCF, which in brief consists of a full CI done in a restricted space of determinants of adjustable size. The user specifies an active space, which consists of a number of active electrons and a set of active and virtual orbitals that those electrons occupy and can be excited to. All possible excitations of the selected electrons among the chosen orbitals are taken into account. An active space including all electrons in all the molecular orbitals available according to the chosen basis set would be a full CI exactly as that described above. CASSCF can also be considered as a truncated CI.

On the water molecule with a basis of let us say 12 orbitals, a CASSCF[4,10] calculation would mean that the  $1s^2 2s^2$  electrons of the oxygen and the 2 electrons of the hydrogen atoms are fixed and fully occupy the 3 lowest orbitals. The remaining 4 p-electrons of the oxygen are allowed to occupy any of the 10 next orbitals, so that it can be said that a full CI is performed for this 4 weight electrons in the active space formed by 10 orbitals.



## 1.4 QUANTUM CHEMICAL METHODS BEYOND HARTREE-FOCK II: DENSITY FUNCTIONAL METHODS

One among the most successful post-HF methods, which was worth a Nobel price to one of its major developers Walter Kohn in 1998, is known as the density functional theory (DFT). It is endowed with a good treatment of the electron correlation, concept that will be explained more in detail in the next section 1.5, at a very low computational cost when compared to wave function post-HF methods, which opened up the possibility to theoretically treat complex real systems, such as solid state compounds, to which DFT is systematically applied.

The wave function of a system depends on  $4N$  variables (3 spatial coordinates per electron plus the spin) which makes it a complicated object that can be fully analyzed only in very small systems. Most of the chemical structures of interest in biology, materials science, etc. are therefore entirely intractable. In addition to the large computational expense, the complexity of the wave function makes it very difficult to obtain a clear description of the system and an intuitive interpretation of it. Those reasons make it desirable to find an alternative, in which more simple quantities are used, without losing all the information necessary to describe a chemical system. Additionally, the total Hamiltonian is a function of only one- and two-particle operators (see Section 1.5 and equation 43 in particular), which suggests that the wave function needs not to be considered as a whole. The low-order (first- and second-order specifically) density matrices are in principle sufficient to provide us with the information necessary to solve the majority of the problems of quantum chemistry, for they mainly consist on 1- and 2-body interactions.

The DFT is characterized by taking one of these density matrices as its central quantity: the first-order density matrix or simply its diagonal part the electron density  $\rho(\mathbf{r})$  —a real space quantity that depends only on the 3 spatial coordinates of the electron— rather than the whole wave function  $\Psi$ . It assumes that, in principle, the Schrödinger equation can be solved by using functionals of the electron density, a promising solution to the aforementioned problems.

### 1.4.1 First Hohenberg-Kohn theorem

Many attempts were done in order to find a practical way of solving the Schrödinger equation using  $\rho$ . The most successful one is established by the first Hohenberg-Kohn theorem.

The electron density  $\rho$  is firstly proved to be a suitable quantity to solve the Schrödinger equation (equation 1) in the paper published by Hohenberg and Kohn in 1964 [67]. In there —quoting literally [67]— is stated that “the external potential  $V_{\text{ext}}(\mathbf{r})$  is (to within a constant) a

unique functional of  $\rho(\mathbf{r})$ ; since in turn  $V_{\text{ext}}(\mathbf{r})$  fixes  $\hat{H}$  we see that the full many body particle ground state is a unique functional of  $\rho(\mathbf{r})$ ". A proof for this statement is easily found by *reductio ad absurdum*, in which the consideration of two different external potentials  $V_{\text{ext}}$  and  $V'_{\text{ext}}$  can not lead to the same density  $\rho(\mathbf{r})$ . The role of the external potential is therefore crucial in the aforementioned assertion, the foundation upon which the whole DFT is built. Once proven that the ground state density  $\rho_0(\mathbf{r})$  uniquely determines the external potential  $V_{\text{ext}}$ , one can conclude it also decides all the other properties of the system in its ground state, as this sketch summarizes

$$\rho_0 \longrightarrow \{N, Z_A, R_A\} \longrightarrow \hat{H} \longrightarrow \Psi_0 \longrightarrow E_0 \quad (26)$$

In our case, the external potential is the attractive potential exerted on the electrons by the nuclei  $V_{\text{ext}} = V_{\text{Ne}}$ . The total energy of the ground state  $E_0$  can be divided in three components: the electron-electron repulsion  $E_{ee}$ , the kinetic energy  $T$  and the external potential now in the form of an attractive nucleus-electron interaction  $E_{\text{Ne}}[\rho_0] = \int \rho_0(\mathbf{r}) V_{\text{Ne}} d\mathbf{r}$ . As the complete ground state energy is fully determined by the ground electron density  $\rho_0$ , so are its components,

$$E_0[\rho_0] = E_{\text{Ne}}[\rho_0] + E_{ee}[\rho_0] + T[\rho_0] \quad (27)$$

which are in turn functionals  $\rho_0$ . The kinetic  $T$  as well as the electron-electron repulsion energy  $E_{ee}$  in the expression above are system-independent quantities. However, the term accounting for the nucleus-electron electrostatic interaction  $E_{\text{Ne}}$  is the term that defines the kind of system that is considered:

$$E_0[\rho_0] = \underbrace{\int \rho_0(\mathbf{r}) V_{\text{Ne}} d\mathbf{r}}_{\text{System-dependent}} + \underbrace{T[\rho_0] + E_{ee}[\rho_0]}_{\text{Universal}}, \quad (28)$$

The last two terms on the right hand side of equation 28 can be gathered under a new quantity called the *Hohenberg-Kohn functional*, defined as

$$F_{\text{HK}}[\rho_0] = T[\rho_0] + E_{ee}[\rho_0], \quad (29)$$

which remains unchanged no matter the system and is acknowledged to be the holy grail of DFT.

Equation 28 can now be rewritten as

$$E_0[\rho_0] = \int \rho_0(\mathbf{r}) V_{\text{Ne}} d\mathbf{r} + F_{\text{HK}}[\rho_0]. \quad (30)$$

Apart from the electron kinetic energy  $T$  it contains information about the electron-electron interaction:

$$E_{ee}[\rho] = \frac{1}{2} \int d\mathbf{r}_1 \int \frac{\rho(\mathbf{r}_1)\rho(\mathbf{r}_2)}{r_{12}} d\mathbf{r}_2 + E_{ncl}[\rho]. \quad (31)$$

The first term is the classical part known as the Coulomb repulsion  $J[\rho]$ , whereas the second  $E_{ncl}[\rho]$  is *non-classical* and accounts for the self-interaction correction and the inter particle correlation.

#### 1.4.2 Second Hohenberg-Kohn theorem

We know now from the first H-K theorem that the ground state electron density suffices to determine any of the properties of the system. The next step, also solved by Hohenberg and Kohn in their work [67], is to ensure that the electron density  $\rho$  we are using is indeed the density of the ground state that we are looking for. In that sense the second H-K theorem establishes that the energy  $E_0$  given by the H-K functional will be the lowest energy only if the density  $\rho$  is the density of the ground state  $\rho_0$ . This theorem is hence also variational and can be expressed as

$$E_0 = \min_{\Psi \rightarrow \rho} \langle \Psi | \hat{T} + \hat{V}_{Ne} + \hat{V}_{ee} | \Psi \rangle. \quad (32)$$

In other words, for any trial density the  $E$  obtained is an upper limit to the true ground state energy  $E_0$ :

$$E_0 \leq E[\rho] = T[\rho] + E_{Ne}[\rho] + E_{ee}[\rho]. \quad (33)$$

#### 1.4.3 The Kohn-Sham Approach

Many attempts have been performed to attain a practical solution to the H-K equation 30. The most successful one is formulated in the second most important article within the development of the density functional theory by W. Kohn and L. Sham in 1965 [79].

The success of this new approach starts by considering that most of the problems that make DFT inaccurate were related to the way the kinetic energy is treated. In their article, Kohn and Sham proposed a Hartree-Fock-like method to more accurately calculate the kinetic energy. A part of it is then determined exactly by introducing the concept of a non-interacting reference system built from a set of orbitals (one-electron functionals), i.e., the electrons are treated as non-interacting fermions. The remaining contribution to the kinetic energy, a small part of the total, is treated by a non-classical approximate functional.

### The Kohn-Sham orbitals

The HK functional, expressed in equation 30 has the form

$$F[\rho(\mathbf{r})] = T[\rho(\mathbf{r})] + J[\rho(\mathbf{r})] + E_{\text{ncl}}[\rho(\mathbf{r})]. \quad (34)$$

$J[\rho]$  is a classical term and can be exactly determined but the other two terms remain unknown. Regarding the kinetic energy  $T[\rho]$  it became clear that it was not properly described by the simple expression used by other approaches such as the Thomas-Fermi-Dirac model (see [75] for further information on alternative methods to the Kohn-Sham one).

The kinetic energy is now obtained from a system of non-interacting electrons. A new *effective potential*  $V_S$  is added to account for the electron-electron interaction and the Hamiltonian of the non-interacting system  $\hat{H}_S$  has now the form:

$$\hat{H}_S = -\frac{1}{2} \sum_i^N \nabla_i^2 + \sum_i^N V_S(\mathbf{r}_i), \quad (35)$$

where consequently no electron-electron term appears. A pseudo-wave function  $\Psi_S$  is now constructed in a Hartree-Fock manner (see equation 15):

$$\Psi_S = \frac{1}{\sqrt{N!}} \begin{vmatrix} \varphi_1(\mathbf{x}_1) & \cdots & \varphi_N(\mathbf{x}_1) \\ \vdots & \ddots & \vdots \\ \varphi_1(\mathbf{x}_N) & \cdots & \varphi_N(\mathbf{x}_N) \end{vmatrix}, \quad (36)$$

where the Kohn-Sham orbitals  $\varphi_j$  fully recover the density

$$\rho_S(\mathbf{r}) = \sum_j \sum_s |\varphi_j(\mathbf{r}, s)|^2 = \rho_0(\mathbf{r}). \quad (37)$$

As mentioned above the main idea of the Kohn-Sham Ansatz consists of finding a new way to more accurately determine the kinetic energy, calculating as much as possible of it exactly. The kinetic energy of the non-interacting system is described exactly using KS orbitals  $\varphi$  instead of the HF molecular orbitals  $\psi$  of equation 13:

$$T_S = -\frac{1}{2} \sum_j \langle \varphi_j | \nabla^2 | \varphi_j \rangle. \quad (38)$$

The non-interacting kinetic energy  $T_S$  does not carry all the kinetic energy  $T \neq T_S$ . The difference with the interacting system is included

into a new functional named  $E_{XC}$  that contains all the non-classical interactions

$$E_{XC}[\rho] = (T[\rho] - T_S[\rho]) + (E_{ee}[\rho] - J[\rho]) = T_C[\rho] + E_{ncl}[\rho]. \quad (39)$$

The *exchange-correlation functional*  $E_{XC}$  still remains unknown and the search for the exact one is the main challenge of DFT. It includes:

- effects of the self-interaction correction
- exchange (antisymmetry)
- correlation
- a portion belonging to the kinetic energy

After this, the expression for the energy of the true, interacting system is written as follows:

$$E[\rho(\mathbf{r})] = T_S[\rho] + J[\rho] + E_{XC}[\rho] + E_{Ne}[\rho], \quad (40)$$

where  $J$  is the Coulomb term,  $T_S$  the part of the kinetic energy, exactly determined by the non-interacting system,  $E_{XC}$  the unknown non-classical exchange-correlation functional and the external potential that accounts for the nuclei-electron interaction  $E_{Ne}$ .

The next step will be to find the proper orbitals for the non-interacting system. To that end we will expand equation 40 to:

$$\begin{aligned} E[\rho(\mathbf{r})] = & -\frac{1}{2} \sum_j \langle \varphi_j | \nabla^2 | \varphi_j \rangle + \\ & + \frac{1}{2} \sum_j \sum_{j'} \iint |\varphi_j(\mathbf{r}_1)|^2 \frac{1}{r_{12}} |\varphi_{j'}(\mathbf{r}_2)|^2 d\mathbf{r}_1 d\mathbf{r}_2 + \\ & + E_{XC}[\rho(\mathbf{r})] - \sum_j \int \sum_A^M \frac{Z_A}{r_{1A}} |\varphi_j(\mathbf{r}_1)|^2 d\mathbf{r}_1. \end{aligned}$$

Note that the unknown exchange-correlation term cannot be given any explicit form.

### LCAO Ansatz for the resolution of the Kohn-Sham Equations

By variationally minimizing the expression 40 of the true energy with respect to the KS single-particle orbitals, we get the following 1-electron equation

$$\varepsilon_j \varphi_j(\mathbf{r}_1) = \left( -\frac{1}{2} \nabla_1^2 + \left[ \sum_j \int \frac{|\varphi_j(\mathbf{r}_2)|^2}{r_{12}} d\mathbf{r}_2 + V_{XC}(\mathbf{r}_1) - \sum_A^M \frac{Z_A}{r_{1A}} \right] \right) \varphi_j(\mathbf{r}_1), \quad (41)$$

or

$$\varepsilon_j \varphi_j = \hat{f}^{KS} \varphi_j. \quad (42)$$

The set of KS orbitals are expanded in an analogous way as within the Hartree-Fock context (see equation 14), in terms of a finite basis set that does not provide the exact orbitals but only approximations to them. The larger the basis set the better the approximation but also the more expensive the calculation. For an infinite basis set every KS orbital will be exactly described.

Equation 42 has to be solved, the orbitals expanded as a linear combination of the basis set. The Coulomb operator  $J$  and the exchange-correlation operator  $E_{XC}$  of equation 40 are dependent on the electron density  $\rho$ , which is a function of the orbitals  $\varphi$ . However these orbitals are being searched in order to determine the electron density, entering in a *Self-Consistency problem* as that of solving the HF equation (figure 1).

A guessed initial density  $\rho_0$  needed to calculate the orbitals is introduced. The KS Hamiltonian  $H_{KS}$  is found from the Coulomb (also called Hartree-Fock potential) and the exchange-correlation potentials. There are many different approaches to approximate this exchange-correlation potential as LDA, LSDA, GGA, meta-GGA... which will not be discussed here for this lies out of the scope of this work. For a more detailed description of the approximations to the  $E_{XC}$  functional, the reader is referred to the specialized works [29, 42, 75]. When the KS Hamiltonian, named  $\hat{f}^{KS}$  within the Kohn-Sham approach has been found, the secular equation (see equation 42) is solved and a set of orbitals  $\varphi_n$  is obtained. From these orbitals a new density  $\rho_n$ , different from the previous one  $\rho_{n-1}$ , is calculated. Once we have arrived to a point where the difference between both densities is under a threshold, the self-consistent loop has converged and the calculation comes to an end.

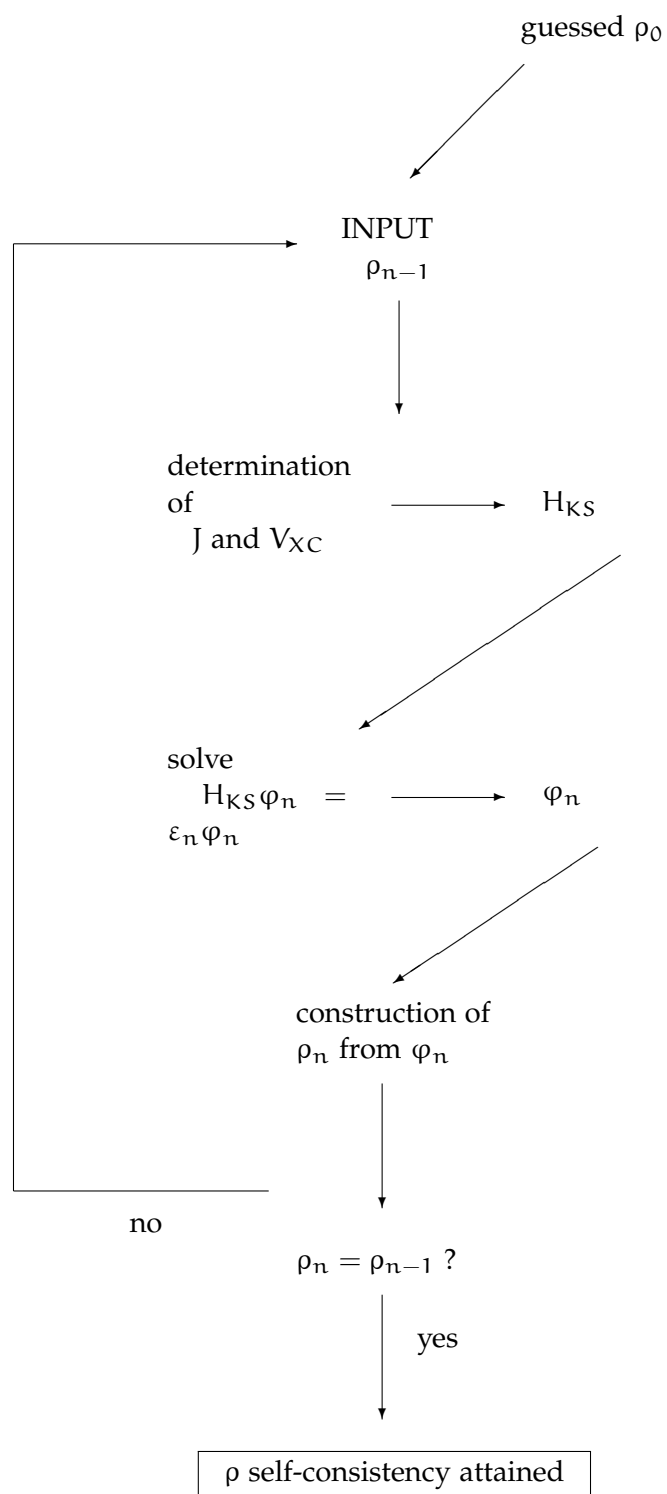


Figure 1: Scheme of the iterative self-consistent procedure to solve the Kohn-Sham equations [34].

## 1.5 ELECTRON DISTRIBUTION AND DENSITY MATRICES

We find it necessary to include a —brief— selection of the ideas explained in [112] about what a density matrix is, for it is a central concept of the present work, to which we will be referring often.

Thanks to the increasing sophistication of the theoretical methods used in quantum chemistry, the computational treatment of complex chemical systems is now in reach. However, the associated wave function can be so complicated that its study as a whole provides no clear information of the actual electron distribution. Many of the chemical and physical properties of a system are inferred from this electron distribution and therefore it is crucial to have as much information as possible about it. The fact that the full Hamiltonian of the system  $\hat{H}$  depends on only 2-particle operators,

$$\hat{H}_{\text{elec}} = \underbrace{\hat{T} + \hat{V}_{Ne}}_{1\text{-particle}} + \underbrace{\hat{V}_{ee}}_{2\text{-particle}}, \quad (43)$$

where  $\hat{T}$ , and  $\hat{V}_{Ne}$  and  $\hat{V}_{ee}$  keep the same meaning as in equation 4, suggests that the high complexity of the wave function contains redundant information that does not need to be unavoidably considered. The electronic Hamiltonian operator can be actually re-written in terms of the one- and two-particle density matrices, on which we will take soon in this section[75].

It is usually admitted that all the physical information of a system can be obtained from the square of the wave function (equation 7)

$$\rho_N(\mathbf{x}) = |\Psi(\mathbf{x})|^2, \quad (44)$$

where  $\rho_N(\mathbf{x})$  is the *N-electron density function*.

By integrating all electrons in 7 over spin and all electrons but one over the spatial coordinates we get, due to the indistinguishable character of the electrons, N-times the probability of finding one electron of any spin in  $d\mathbf{r}_1$  whereas the rest of the electrons may be anywhere in space. This quantity is known as simply the *electron density*<sup>2</sup>

$$\rho_1(\mathbf{r}_1) = N \int \Psi(\mathbf{x}_1, \mathbf{x}_2 \dots \mathbf{x}_N) \Psi^*(\mathbf{x}_1, \mathbf{x}_2 \dots \mathbf{x}_N) d\mathbf{s}_1 d\mathbf{x}_2 \dots d\mathbf{x}_N. \quad (45)$$

The electron density is a non-negative quantity and an observable of the wave function —it can be obtained by acting on the wave func-

<sup>2</sup> Strictly speaking it is a probability density but it is usually given the name electron density, since the electrons can be understood as “smeared out” within the volume element, with a certain density P.



tion with an hermitian operator—that integrates to the total number of electrons  $N$  (equation 9) and vanishes at infinity for a finite system:

$$\rho_1(\mathbf{r} \rightarrow \infty) = 0.$$

The pair function is the corresponding probability density of two particles, also known as the *electron pair density*:

$$\rho_2(\mathbf{r}_1, \mathbf{r}_2) = N(N-1) \int |\Psi(\mathbf{x}_1, \mathbf{x}_2 \dots \mathbf{x}_N)|^2 d\mathbf{s}_1 d\mathbf{s}_2 d\mathbf{x}_3 \dots d\mathbf{x}_N. \quad (46)$$

Similarly, the electron pair density is defined as the probability of finding one electron within the volume element  $d\mathbf{r}_1$  and simultaneously another one in  $d\mathbf{r}_2$ , whereas the remaining  $N-2$  electrons are anywhere in space, regardless of their spin.

How the motions of two electrons are correlated is described by the pair function. It is normalized to the total number of ordered-electron pairs that can be formed  $N(N-1)$ , according to McWeeny's normalization[112]. For non-interacting particles, the probability of finding one of them at one point of the space and simultaneously another one at any other point, would be just the product of the individual probabilities:

$$\rho_2(\mathbf{r}_1, \mathbf{r}_2) = \frac{N-1}{N} \rho_1(\mathbf{r}_1) \rho_1(\mathbf{r}_2). \quad (47)$$

The term  $(N-1)/N$  arises due to the indistinguishability of the electrons.

### 1.5.1 Density Matrices

It is extremely useful to slightly generalize the density functions of equations 45 and 46. For a 1-electron system, the expectation value of any operator  $\hat{F}$  when the electron is located in the spin orbital  $\psi$  is given by

$$\langle \hat{F} \rangle = \int \psi^*(\mathbf{x}) \hat{F} \psi(\mathbf{x}) d\mathbf{x}. \quad (48)$$

When  $\hat{F}$  is a real operator that acts only on the right term  $\psi(\mathbf{x})$ ,  $\psi^*(\mathbf{x})$  being unaffected by it. Hence the factors order matters and it cannot be expressed as

$$\langle \hat{F} \rangle = \int \hat{F} \psi^*(\mathbf{x}) \psi(\mathbf{x}) d\mathbf{x}.$$

This can be solved by changing the name of the variables in  $\psi^*$  from  $\mathbf{x}$  to  $\mathbf{x}'$  making them immune to the action of  $\hat{F}$ . The electron

density from equation 45 is now generalized to the *non-diagonal reduced 1-density matrix*, which takes the form

$$\rho_1(\mathbf{r}_1; \mathbf{r}'_1) = N \int \Psi(\mathbf{x}_1, \mathbf{x}_2 \dots \mathbf{x}_N) \Psi^*(\mathbf{x}'_1, \mathbf{x}_2 \dots \mathbf{x}_N) d\mathbf{s}_1 d\mathbf{x}_2 \dots d\mathbf{x}_N. \quad (49)$$

The prime plays its role during the action of the operator  $\hat{F}$  and does nothing just before the integration. That way  $\hat{F}$  acts only on the unprimed wave function while the subsequent integration affects all terms.

Of course the same applies to the two-electron case, where the *non-diagonal reduced 2-density matrix*, has the following expression.

$$\begin{aligned} \rho_2(\mathbf{r}_1, \mathbf{r}_2; \mathbf{r}'_1, \mathbf{r}'_2) = \\ N(N-1) \int \Psi(\mathbf{x}_1, \mathbf{x}_2 \dots \mathbf{x}_N) \Psi(\mathbf{x}'_1, \mathbf{x}'_2 \dots \mathbf{x}_N) d\mathbf{s}_1 d\mathbf{s}_2 d\mathbf{x}_3 \dots d\mathbf{x}_N. \end{aligned} \quad (50)$$

Both the electron density and the electron pair density are recovered as the diagonal part of the corresponding density matrices

$$\rho(\mathbf{r}) = \rho_1(\mathbf{r}_1; \mathbf{r}_1), \quad \rho_2(\mathbf{r}_1, \mathbf{r}_2) = \rho_2(\mathbf{r}_1, \mathbf{r}_2; \mathbf{r}_1, \mathbf{r}_2).$$

The information about the correlation of the electronic motion is contained in the electron pair density function. This electron correlation can be of two distinct types:

- **Fermi or exchange correlation:** In equation 50 the 2-RDM is defined, where the primed coordinates are not integrated. The antisymmetry of the wave function established by the Pauli principle states that interchanging the positions of two electrons ( $\mathbf{r}_1$  and  $\mathbf{r}_2$ ) for example, will cause  $\rho_2(\mathbf{r}_1, \mathbf{r}_2; \mathbf{r}'_1, \mathbf{r}'_2)$  to have its sign changed

$$\rho_2(\mathbf{r}_1, \mathbf{r}_2; \mathbf{r}'_1, \mathbf{r}'_2) = -\rho_2(\mathbf{r}_2, \mathbf{r}_1; \mathbf{r}'_1, \mathbf{r}'_2)$$

In the specific case where we take the diagonal part of this matrix ( $\mathbf{r}_1 = \mathbf{r}'_1$  and  $\mathbf{r}_2 = \mathbf{r}'_2$ , cf. Section 1.5.1) we recover the pair density  $\rho_2(\mathbf{r}_1, \mathbf{r}_2)$  as defined on equation 46. For the special case in which two same-spin electrons are sharing the same position  $\mathbf{r}_1 = \mathbf{r}_2$ ,

$$\rho_2(\mathbf{r}_1, \mathbf{r}_1) = -\rho_2(\mathbf{r}_1, \mathbf{r}_1), \quad (51)$$

which is the probability that both electrons are identical and occupy exactly the same location, relation that is satisfied solely by

the condition  $\rho_2(\mathbf{r}_1, \mathbf{r}_1) = 0$ . This type of interaction is the exchange correlation, inherently considered by the HF approach as it is one of the properties of Slater determinants. It has however nothing to do with the correlation included in the correlation energy  $E_C^{\text{HF}}$  in the previous chapter (see equation 23).

- **Coulomb correlation:** Unlike in the case of alike spins, electrons of opposite spin do not suffer Fermi correlation but are subject to an electrostatic interaction coming from the term  $1/r_{ij}$  in equation 4. This is a repulsion force that applies to all electrons—regardless of the spin—due to their charge that prevents them to approximate to each other. The interaction between the motion of the electrons due to their charge is the Coulomb correlation or simply the electron correlation and is not treated at all by the HF approach.

Whereas for the parallel spin situation the Pauli principle is fulfilled, as already mentioned  $\rho_2^{\text{HF}, \sigma_1=\sigma_2}(\mathbf{r}_1, \mathbf{r}_2) = 0$ , if the electrons have opposite spin, the pair probability equals the product of the individual probabilities and does not take into account the electron correlation  $\rho_2^{\text{HF}, \sigma_1 \neq \sigma_2}(\mathbf{r}_1, \mathbf{r}_2) = \rho_1(\mathbf{r}_1)\rho_1(\mathbf{r}_2)$ .

The Fermi and Coulomb correlation can now be included into a correlation factor  $f(\mathbf{r}_1; \mathbf{r}_2)$ , a term that allows the correlation of electronic motion to be separated from the non-interacting situation, yielding an alternative definition of the pair density expression also known as the *second-order reduced density matrix* or 2-RDM in short, which is as follows:

$$\rho_2(\mathbf{r}_1, \mathbf{r}_2) = \rho(\mathbf{r}_1)\rho(\mathbf{r}_2)[1 + f(\mathbf{r}_1; \mathbf{r}_2)]. \quad (52)$$

This correlation factor will vanish in case the electrons do not feel each other.

After developing the product, the right term on the last equation is the *exchange-correlation density*, which describes to what extent the electrons differ from the independent particle situation.

$$\rho_{xc}(\mathbf{r}_1, \mathbf{r}_2) = \rho(\mathbf{r}_1)\rho(\mathbf{r}_2) - \rho_2(\mathbf{r}_1, \mathbf{r}_2). \quad (53)$$

We will be often referring to this equation later on, as it is in  $\rho_{xc}$  where many of the tools of this study have their origin.

A new function can now be defined: the *conditional probability*  $\Omega(\mathbf{r}_1; \mathbf{r}_2)$ . As its name indicates, it describes the probability of finding one electron at position  $\mathbf{r}_2$  subject to the condition that another one is already at  $\mathbf{r}_1$

$$\Omega(\mathbf{r}_1; \mathbf{r}_2) = \frac{\rho_2(\mathbf{r}_1, \mathbf{r}_2)}{\rho_1(\mathbf{r}_1)}. \quad (54)$$

This conditional density integrates to  $N - 1$ , the total number of electrons except the reference electron at  $\mathbf{r}_1$ . If we make the difference between the conditional density and the uncorrelated probability of finding an electron at  $\mathbf{r}_2$ , we get the *exchange-correlation hole*

$$h_{\text{XC}}(\mathbf{r}_1; \mathbf{r}_2) = \frac{\rho_2(\mathbf{r}_1, \mathbf{r}_2)}{\rho_1(\mathbf{r}_1)} - \rho(\mathbf{r}_2). \quad (55)$$

This hole describes the change in the conditional probability provoked by the self-interaction correction, and the Fermi and Coulomb correlation in comparison to the totally uncorrelated situation. It is called a hole for it normally causes depletion of electron density at  $\mathbf{r}_2$  compared to the independent particle situation. Since the pair density integrates to  $N - 1$  and the density at  $\mathbf{r}_2$  to  $N$ , the exchange-correlation hole integrates to  $-1$ . In other words, it contains exactly the charge of one electron

$$\int h_{\text{XC}}(\mathbf{r}_1; \mathbf{r}_2) d\mathbf{r}_2 = -1.$$

There are no many-body interactions among electrons in the Coulomb approximation, and consequently there is no need to consider distribution functions of higher order than the pair function  $\rho_2$  to get the energy of a system.

#### *The orbital expansion of the RDMs*

Within the orbital approximation the wave function is approximated as a linear combination of 1-electron spin orbitals  $\{\psi\}$  (see equation 12 and Section 1.1.3), and so are the density matrices. It is hence common to find the 1- and 2-RDM expanded as:

$$\rho(\mathbf{r}; \mathbf{r}') = \sum_{ij}^M {}^1D_j^i \psi_i^*(\mathbf{r}') \psi_j(\mathbf{r}), \quad (56)$$

$$\rho_2(\mathbf{r}_1, \mathbf{r}_2; \mathbf{r}'_1, \mathbf{r}'_2) = \sum_{ijkl}^M {}^2D_{kl}^{ij} \psi_i^*(\mathbf{r}'_1) \psi_j^*(\mathbf{r}'_2) \psi_k(\mathbf{r}_1) \psi_l(\mathbf{r}_2), \quad (57)$$

where  ${}^1D_j^i$  and  ${}^2D_{kl}^{ij}$  are the matrices with the coefficients of the linear combination, and the spin coordinates are dropped off.

The actual computation of  $\nu$ -RDMs is extremely demanding with today's computers for orders  $\nu > 4$  because of high memory demands. Fortunately, the 1- and 2-RDM are easy to obtain, and even 3- and 4-RDMs[55] are affordable in simple systems.

The form of the 2-RDM is particularly simple in the case of a 1-determinantal wave function, for it is written in terms of the 1-RDM:

$$\rho_2^{SD}(\mathbf{r}_1, \mathbf{r}_2; \mathbf{r}'_1, \mathbf{r}'_2) = \rho_1(\mathbf{r}_1; \mathbf{r}'_1)\rho_1(\mathbf{r}_2; \mathbf{r}'_2) - \rho_1(\mathbf{r}_1; \mathbf{r}'_2)\rho_1(\mathbf{r}_2; \mathbf{r}'_1). \quad (58)$$

If the primes drop, equation 58 becomes

$$\rho_2^{SD}(\mathbf{r}_1, \mathbf{r}_2) = \rho(\mathbf{r}_1)\rho(\mathbf{r}_2) - \rho_1(\mathbf{r}_1; \mathbf{r}_2)\rho_1(\mathbf{r}_2; \mathbf{r}_1). \quad (59)$$

The analogy with equation 53 is perceptible: the first term is the direct product of the 1-particle densities and the second is the exchange-correlation contribution, whose form in the monodeterminantal case is worth writing

$$\rho_{xc}(\mathbf{r}_1, \mathbf{r}_2) = \rho_1(\mathbf{r}_1; \mathbf{r}_2)\rho_1(\mathbf{r}_2; \mathbf{r}_1) = \sum_{i,j} \psi_i(\mathbf{r}_1)\psi_j(\mathbf{r}_1)\psi_i(\mathbf{r}_2)\psi_j(\mathbf{r}_2), \quad (60)$$

where the sum runs over all occupied states.

It is important to note that, even in the unprimed case, the 2-RDM of 59 still contains non-zero terms out of the principal diagonal that correspond to 1-RDMs with non-diagonal terms of the kind  $\rho(\mathbf{r}_i; \mathbf{r}_j)$   $i \neq j$ .

The factorization of the 2-RDM in terms of the 1-RDM is possible only in case of 1-determinantal wave functions (thus within both HF and DFT), and implies that any magnitude of the system is determined by  $\rho(\mathbf{r}_1; \mathbf{r}'_1)$ , which is also known as the Fock-Dirac density matrix.

### 1.5.2 Cumulant densities

The  $\nu$ th-order (reduced) density matrices ( $\nu$ -RDMs) play a fundamental role in the analysis of the chemical bond in the real space. The attentive analysis of their structure reveals that there are parts that cannot be expressed in terms of RDMs of lower-order than  $\nu$ . Those terms are given the name  *$\nu$ -th order cumulant densities* ( $\nu$ -CDs) or simply  $\nu$ th-order cumulants and are denoted by  $\rho_c^\nu$ . In general, a  $\nu$ th-order cumulant determines the irreducible part of the central moments of the same order in a statistical distribution function, which is saying that part of this distribution cannot be expressed in terms of lower-order moments[87].

The cumulants are key objects in the determination of chemical bond indices in the real space, for they determine the level of fluctuation of  $\nu$  particles in a statistical distribution, that is to say, their correlation. Francisco and co-workers published in 2013 a procedure

to obtain the  $\nu$ -CDs from the diagonal terms of the RDMs[55]. The expressions for the 1- and 2-CDs are

$$\begin{aligned}\rho_c^1(\mathbf{r}_1) &= \rho(\mathbf{r}_1), \\ \rho_c^2(\mathbf{r}_1, \mathbf{r}_2) &= \rho(\mathbf{r}_1)\rho(\mathbf{r}_2) - \rho_2(\mathbf{r}_1, \mathbf{r}_2).\end{aligned}\tag{61}$$

The 1-CM  $\rho_c^1 = \rho_c$  is the electron density  $\rho$  and the 2-CM the exchange-correlation density  $\rho_{xc}$ .

It is worth noting that one important property of the CDs is their recurrence: the  $(\nu - 1)$ -CD can be obtained from the  $\nu$ -CD by integrating the  $\nu$ th electron:

$$\rho_c^{\nu-1}(\mathbf{r}_1, \dots, \mathbf{r}_{\nu-1}) = \int \rho_c^\nu(\mathbf{r}_1, \dots, \mathbf{r}_\nu) d\mathbf{r}_\nu.\tag{62}$$

The successive application of equation 62 from  $\nu, \nu - 1, \dots, 1$  recovers the total number of electrons  $N$

$$\rho_c(\mathbf{r}_1, \dots, \mathbf{r}_\nu) d\mathbf{r}_1 \dots d\mathbf{r}_\nu = N,\tag{63}$$

which is the second relevant property of the CMs: their extensivity.



# 2

## INTRODUCTION TO SOLID STATE THEORY[7, 74]

### 2.1 BASIC CRYSTALLOGRAPHY

In principle, the treatment of a solid, understood as a huge molecule with an Avogadro number of ions or atoms, cannot be theoretically tackled and is as well computationally unworkable. In the particular case of a solid with crystalline structure, the atoms are arranged with translational symmetry, meaning that an atomic pattern can be found that is invariant under translation operations. Although a crystal is a finite macroscopic object, due to its huge number of atoms it can be said that this invariance is applied *ad infinitum*. The ratio between the number of atoms on the surface and the number of atoms in the crystal  $N$  is small and proportional to  $N^{-1/3}$ . If  $N$  is large and we are dealing with a neutral surface, the effects of the superficial limits affect only a few layers of the crystal, not reaching its internal part. Therefore the macroscopic solid shows the properties of the nucleus of the crystal and the surface effects can be disregarded, unless we are intentionally interested in the surface itself. Under such conditions, the crystallographic model is adequate for the description of an infinite crystal showing translational invariance, and there exist many computational procedures to treat it. It is therefore important to clearly state that all the references to a solid or condensed system in the following will be referring to a system with crystalline structure.

#### 2.1.1 The Bravais lattice

A 3D Bravais lattice is a collection of points indefinitely repeated in intervals of length  $a_1$ ,  $a_2$  and  $a_3$  along three different directions. In figure 2 a 2-dimensional Bravais lattice of vectors  $\mathbf{a}_1$  and  $\mathbf{a}_2$  is shown as an example. The three magnitudes  $a_1$ ,  $a_2$  and  $a_3$  are named the *lattice parameters* and the vectors  $\mathbf{a}_1$ ,  $\mathbf{a}_2$  and  $\mathbf{a}_3$ , oriented in the same three non-coplanar directions with the three lattice parameters as norm are the *primitive vectors* (see figure 2 for a 2-dimensional example).

Any vector  $\mathbf{R}$  connecting two points of the lattice is a *lattice vector* and can be expressed as a linear combination of the primitive vectors with the corresponding coefficients  $n_1$ ,  $n_2$  and  $n_3$

$$\mathbf{R} = n_1 \mathbf{a}_1 + n_2 \mathbf{a}_2 + n_3 \mathbf{a}_3, \quad (64)$$



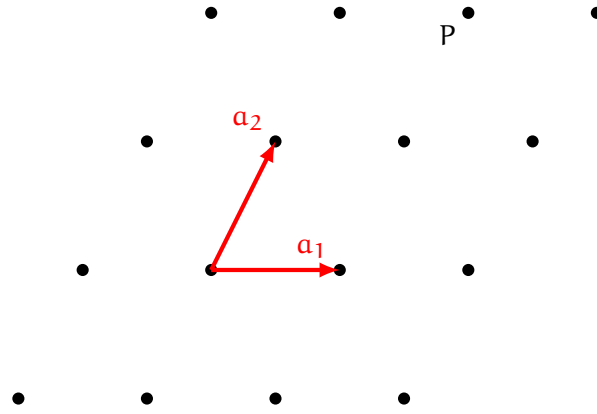


**Figure 2:** General 2-dimensional Bravais lattice. Primitive vectors  $\mathbf{a}_1$  and  $\mathbf{a}_2$  are shown. Any point of the net can be expressed as a linear combination of the primitive vectors; for instance  $P = \mathbf{a}_1 + 2\mathbf{a}_2$ .

as in the example for 2-dimensions of figure 2.

The primitive vectors define a parallelepiped that receives the name of *unit cell*. The definition of the unit cell of a system is arbitrary and there are an infinite number of them, since all the cells containing the same number of lattice points are equivalent. By translating a unit cell in the 3 dimensions, one can completely fill the space. Each of these unit cells is tagged by a vector  $\mathbf{R}$  that characterizes it and that allows us to differentiate it with respect to the original unit cell.

The unit cell of a crystal can be of two types: it is a *primitive cell* if it contains only one lattice point, i.e., one atom in the particular case of a crystal. The geometry of the primitive cell characterizes the lattice, but it does not show intuitively the symmetry of the crystal. Alternatively, a unit cell containing in general a larger number of lattice points can be defined which presents the symmetry of the crystal. This other unit cell is a centered or *conventional cell*.

As an example, a *body centered cubic* (bcc) crystal structure has a conventional cell that is represented in figure 3. The three vectors drawn within this cell delimit a parallelepiped, which is its primitive cell. The primitive lattices in the 3-dimensional space are divided in 7 different crystalline systems, each of them characterized by a particular relative length of the lattice vectors and the angles between them. Additionally, another 7 non-primitive cells complete the full set of possible lattices in the ordinary space, which are all the possible Bravais lattices, summarized in figure 3.

Now if at any of the points of a Bravais lattice we place a motif, which can be an atom, an ion or a molecule and we translate the lattice repeatedly in all the 3 directions of the space, the crystal is created. The symmetry of the motif, applying the crystallographic restriction theorem[16], is one among the 32 so called *point groups*. A point group consists in a set of five different symmetry operations, all of which leave a central point fixed: reflection, rotation, improper

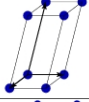
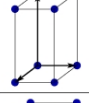
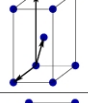
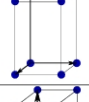
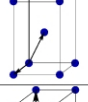
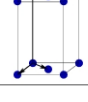
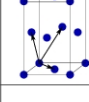
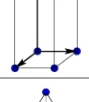
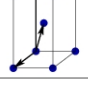
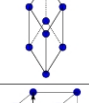
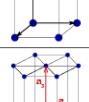
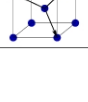
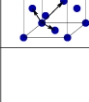
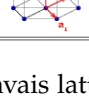
Bravais lattice	Parameters	Simple (P)	Volume centered (I)	Base centered (C)	Face centered (F)
Triclinic	$a_1 \neq a_2 \neq a_3$ $\alpha_{12} \neq \alpha_{23} \neq \alpha_{31}$				
Monoclinic	$a_1 \neq a_2 \neq a_3$ $\alpha_{23} = \alpha_{31} = 90^\circ$ $\alpha_{12} \neq 90^\circ$				
Orthorhombic	$a_1 \neq a_2 \neq a_3$ $\alpha_{12} = \alpha_{23} = \alpha_{31} = 90^\circ$				
Tetragonal	$a_1 = a_2 \neq a_3$ $\alpha_{12} = \alpha_{23} = \alpha_{31} = 90^\circ$				
Trigonal	$a_1 = a_2 = a_3$ $\alpha_{12} = \alpha_{23} = \alpha_{31} < 120^\circ$				
Cubic	$a_1 = a_2 = a_3$ $\alpha_{12} = \alpha_{23} = \alpha_{31} = 90^\circ$				
Hexagonal	$a_1 = a_2 \neq a_3$ $\alpha_{12} = 120^\circ$ $\alpha_{23} = \alpha_{31} = 90^\circ$				

Figure 3: The 14 Bravais lattices in 3 dimension.

rotation, the screw axis and the glide plane. The combination of one of the 32 point groups and the 14 Bravais lattices gives the *space group*, which gathers the full symmetry of the crystal. In the ordinary space, there exist 230 of these possible combinations. See the bibliography for a deeper exposition of group theory and symmetry [35, 65, 111].

The 230 space groups are fully characterized in the “International tables for crystallography”, a collection of eight volumes published nowadays by the International Union of Crystallography [138].

Some points of the crystal are invariant under one or more symmetry operations. In this case, the number of symmetry equivalent points, known as *multiplicity*, is smaller than the total number of symmetry operations of the space group. Those points are the *special positions*, whereas the remaining are called the *general positions*. The minimum set of atoms, both in general and special positions, that fully generates the unit cell after applying all the symmetry operations that define the space group is named the *asymmetric unit*.

The full characterization of a crystal requires information about

- the space group,
- the cell parameters,
- the type and position of the atoms in the asymmetric unit.

The position of an atom  $\mathbf{r}$  in the unit cell can be expressed either in Cartesian or in crystallographic coordinates, also known as *fractional*

*coordinates*. The edges of the unit cell are used as the basic vectors, and the position of the atoms are given by fractions of them as

$$\mathbf{r} = x_1 \mathbf{a}_1 + x_2 \mathbf{a}_2 + x_3 \mathbf{a}_3, \quad (65)$$

where  $x_1$ ,  $x_2$  and  $x_3$  are real numbers.

### 2.1.2 The reciprocal lattice

Any direct lattice allows a geometric construction such that

$$\begin{aligned} \mathbf{b}_1 &= 2\pi \frac{\mathbf{a}_2 \times \mathbf{a}_3}{\mathbf{a}_1 \cdot (\mathbf{a}_2 \times \mathbf{a}_3)}, \\ \mathbf{b}_2 &= 2\pi \frac{\mathbf{a}_3 \times \mathbf{a}_1}{\mathbf{a}_1 \cdot (\mathbf{a}_2 \times \mathbf{a}_3)}, \\ \mathbf{b}_3 &= 2\pi \frac{\mathbf{a}_1 \times \mathbf{a}_2}{\mathbf{a}_1 \cdot (\mathbf{a}_2 \times \mathbf{a}_3)}, \end{aligned} \quad (66)$$

and the primitive vectors of the reciprocal lattice  $\mathbf{b}_1$ ,  $\mathbf{b}_2$  and  $\mathbf{b}_3$  are obtained from the primitive vectors of the direct lattice. Additionally,  $\mathbf{b}_i$  satisfies that

$$\mathbf{b}_i \cdot \mathbf{a}_j = 2\pi \delta_{ij}, \quad (67)$$

where  $\delta_{ij}$  is the Kronecker delta

$$\begin{aligned} \delta_{ij} &= 0 \text{ if } i \neq j, \\ \delta_{ij} &= 1 \text{ if } i = j. \end{aligned}$$

Equivalently as in direct space, any vector in the reciprocal lattice can be expressed as a linear combination of its primitive vectors with integer coefficients so that

$$\mathbf{k} = k_1 \mathbf{b}_1 + k_2 \mathbf{b}_2 + k_3 \mathbf{b}_3. \quad (68)$$

Every point in the reciprocal space represents a family of planes of the direct lattice evenly spaced. The reciprocal lattice is a Bravais lattice. Let us now define a primitive cell of a lattice point, known as the *Wigner-Seitz cell*, as the primitive cell that includes all points of the space that are closer to that lattice point than to any other. The Wigner-Seitz cell in the reciprocal space is known as the *first Brillouin zone* (BZ). Although there are higher-level Brillouin zones, we are only interested here in the first one for it plays a fundamental role within Bloch's interpretation of solids, according to which the description of a crystal is restricted to the treatment of states lying within the first Brillouin zone only.

## 2.2 ELECTRONIC STRUCTURE METHODS IN THE SOLID STATE

The Schrödinger equation 1 in its most general form, involves a wave function dependent on the coordinates of the particles and on time  $\Psi(\mathbf{r}, t)$ . For stationary states, this wave function can be separated into a term independent of time, and time-dependent phase terms  $\Psi(\mathbf{r}, t) = \Psi(\mathbf{r})f(t)$ . If we consider the time-independent wave function, it is now the time-independent Schrödinger equation which must be solved

$$\hat{H}\Psi_k = E_k\Psi_k, \quad (69)$$

where  $\hat{H}$  is now the time-independent Hamiltonian of equation 3. Relativistic effects are also neglected in equation 69. Therefore, the state  $k$  described by  $\Psi_k$  has an energy  $E_k$  that does not change with time. In general, we will be interested in the determination of the ground state of the system, denoted by equation 2, in which the state indices  $k$  are dropped off. We will also assume the BO approximation already described in Section 1.1.1.

### 2.2.1 Bloch's theorem

Because the entities forming a perfect crystal are arranged in a regular periodic array, the electrons are considered under a potential  $U(\mathbf{r})$  with the periodicity of the underlying Bravais lattice vectors  $\mathbf{G}$

$$U(\mathbf{r} + \mathbf{G}) = U(\mathbf{r}). \quad (70)$$

In the mean field approximation, electrons move independently in the average field created by the others. One of these independent electrons, ruled by a one-electron Schrödinger equation, is known as a *Bloch electron*, in contrast to a *free electron*, which is just a special case of a Bloch electron when the periodic potential is zero. A Bloch electron is then subject to

$$\hat{h}\psi = \left( -\frac{\hbar^2}{2m}\nabla^2 + U(\mathbf{r}) \right)\psi = \varepsilon\psi, \quad (71)$$

a special case of which, if  $U(\mathbf{r}) = 0$ , is the free-electron Schrödinger equation. For this one-electron Hamiltonian, the Bloch theorem states that the eigenstate  $\psi$  can be chosen to be a plane wave times a function with the periodicity of the Bravais lattice:

$$\psi_{n,k}(\mathbf{r}) = e^{i\mathbf{k}\cdot\mathbf{r}}u_{n,k}(\mathbf{r}), \quad (72)$$

where  $\mathbf{k}$  is the *wave vector*, fixed in the last expression, which labels the different solutions to equation 71, and  $u_{n,\mathbf{k}}(\mathbf{r})$  has the periodicity of the Bravais lattice, all  $\mathbf{k}$ -vectors being in the reciprocal space. The number  $n$  is the *band index* and tags the different independent eigenstates for a given wave vector  $\mathbf{k}$ .

Once the wave function  $\psi$  has acquired the form stated by the Bloch theorem, the Fockian equation shown in equation 71 becomes

$$\hat{h}_{\mathbf{k}} u_{n,\mathbf{k}}(\mathbf{r}) = \left[ \frac{\hbar^2}{2m} \left( \frac{1}{i} \nabla + \mathbf{k} \right)^2 + U(\mathbf{r}) \right] u_{n,\mathbf{k}}(\mathbf{r}) = \epsilon_n(\mathbf{k}) u_{n,\mathbf{k}}(\mathbf{r}). \quad (73)$$

The periodic function  $u_{n,\mathbf{k}}$  must satisfy that

$$u_{n,\mathbf{k}}(\mathbf{r} + \mathbf{G}) = u_{n,\mathbf{k}}(\mathbf{r}), \quad (74)$$

for all vectors  $\mathbf{G}$  in the Bravais lattice, which is equivalent to confine the solutions of equation 71 to the primitive cell of the crystal. Equations 72 and 74 imply that

$$\psi_{n,\mathbf{k}}(\mathbf{r} + \mathbf{G}) = e^{i\mathbf{k} \cdot \mathbf{r}} \psi_{n,\mathbf{k}}(\mathbf{r}), \quad (75)$$

for all  $\mathbf{G}$  in the Bravais lattice, which is another common form of stating Bloch's theorem.

As they are  $\psi$ -modulated plane waves, Bloch functions span the whole space and do not decay to zero at infinite. Therefore no normalization is in principle possible. To overcome this problem, we can consider a finite crystal formed by  $N = N_1 \times N_2 \times N_3$  cells, where  $N$  tends to infinity. To maintain the periodicity, we impose the Born-von Karman boundary condition, so that if there are  $N_j$  cells along the  $j$  direction ( $j = 1, 2, 3$ ) in the macroscopic crystal, it must be satisfied that for any integer  $m$  and any  $j$

$$\psi_{n,\mathbf{k}}(\mathbf{r} + mN_j \mathbf{a}_j) = e^{imN_j \mathbf{k} \cdot \mathbf{a}_j} \psi_{n,\mathbf{k}}(\mathbf{r}), \quad (76)$$

since the crystal is a infinite 3-dimensional lattice of identical finite juxtaposed crystals, with the shape of a parallelepiped, each of them formed by  $N$  primitive cells.

Comparing equations 75 and 76, it becomes clear that

$$e^{imN_j \mathbf{k} \cdot \mathbf{a}_j} = e^{i\mathbf{k} \cdot \mathbf{r}} = 1. \quad (77)$$

If we define the component  $\mathbf{k}_j$  of the wave vector as

$$\mathbf{k}_j = \frac{n_j}{N_j} \mathbf{b}_j, \quad (78)$$

$n_j$  being an integer,  $\mathbf{k}$  can be interpreted from equation 67 as a point in the reciprocal space, and therefore there are  $N\mathbf{k}$  points per cell.

Each of those points can be described as a combination of the primitive vectors of the reciprocal lattice as

$$\mathbf{k} = \left( \frac{n_1}{N_1} \mathbf{b}_1 + \frac{n_2}{N_2} \mathbf{b}_2 + \frac{n_3}{N_3} \mathbf{b}_3 \right). \quad (79)$$

When  $N_1$ ,  $N_2$  and  $N_3$  tend to infinity, the number of  $\mathbf{k}$ -points in all the cells of the reciprocal lattice also tends to infinity until it completely fills the space, and  $\mathbf{k}$  can be considered a continuous variable.

The periodicity has reduced the problem of solving the Schrödinger equation 71 for an infinite system to that of solving it for the finite first BZ through the Born-von-Karman boundary condition. This confinement implies an infinite number of solutions  $u_{n,\mathbf{k}}(\mathbf{r})$  with eigenvalues  $\varepsilon_n(\mathbf{k})$ , distributed in a discrete manner. The term  $\varepsilon_n(\mathbf{k})$  contains the wave vector as a parameter and is therefore a continuous function of it. In spite of the boundary condition imposed,  $\mathbf{k}$  appears as a continuous variable since in a although macroscopic, finite lattice, the density of  $\mathbf{k}$ -points is so high that it becomes a continuous variable that can take any possible value within the BZ.

The Bloch theorem reduces the problem of calculating an infinite number of functions by that of calculating a finite number of them in an infinite number of  $\mathbf{k}$ -points. As a consequence of the continuous nature of  $\mathbf{k}$ , the electrons occupy a dense set of states that form a band structure, analogous to the discrete set of orbitals in a molecule. Each band  $n$  has associated an energy  $\varepsilon_n(\mathbf{k})$ . As in the case of atoms and molecules, the Pauli principle rules the filling of the bands with the electrons. The energy of the highest occupied state is known as the Fermi energy, and the surface of the  $\mathbf{k}$  space with energy constant and equal to the Fermi energy is the Fermi level  $E_F$ . This surface separates the occupied from the empty electronic states. The bands are separated from each other by gaps of forbidden energies, known as *band gaps*. According to this scheme, an insulator is characterized by the existence of a large band gap between the occupied and the empty states. Contrarily, in a metal, the existence of partially occupied states causes that there is no gap between the occupied and the empty states, allowing the electrons to wonder between both regions.

### 2.2.2 $\mathbf{k}$ -points sampling

The integration of the functions of  $\mathbf{k}$  in the first BZ is a crucial aspect in the actual *ab initio* calculations of periodic structures. A numerical integration using a standard numerical technique, though feasible in principle, turns to be computationally prohibitive, for it involves the integration of a huge number of wave vectors. For sufficiently smooth functions, one can take advantage of the fact that the functions suffer almost no change within small distances in the  $\mathbf{k}$ -space and approximate the integral by a sum over a discrete set  $\mathbf{K}$

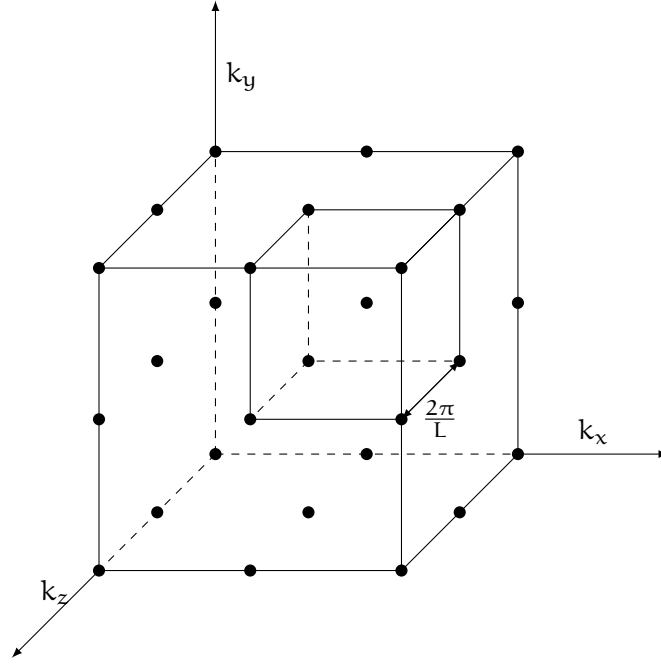


**Figure 4:** Simplified cubic net of side  $L$ , with the  $k$ -points are located at  $k_r = 2\pi n_r/L$  forming a 3-dimensional  $k$ -space. To each point corresponds a volume of  $(2\pi L)^3$ .

of sampling points  $k_i (i = 1, \dots, I)$  (see figure 4), carefully selected to ensure convergence.

The number  $I$  of  $k$ -points is usually indicated by a vector  $\mathbf{k} = (k_i, k_j, k_k)$  with the number of points along each direction. As very often the same number of points is used in the three directions, one might also see the notation  $k_i^3$ , if  $k_i = k_j = k_k$ . The final number  $I$  of  $k$ -points used in the calculation determines the actual number of bands available to be occupied by the electrons, and therefore the number of electrons considered in the calculation, as the periodicity of the crystal makes that the last  $k$ -point of the original cell  $k_I$  is the first of the second, in a sort of cyclic loop. This is then specially relevant for the calculation of the electron distribution functions that we will be dealing with further on in this work, for the number of them that can be obtained is directly related to the number of electrons (bands) that the wave function consists of.

Starting from the lowest  $k = 0$  level, electrons will be placed according to the Pauli principle on each electron level, filling up a region which in the non-interacting particle situation will be a sphere of radius  $k_F$ . The sphere containing all the occupied one-electron levels is known as the *Fermi sphere* and the surface that represents the frontier between occupied and unoccupied states is named *Fermi surface*.

## 2.3 THE FAMILY OF (L)APW METHODS

Elk [1] is an all-electron full-potential linearized augmented-plane wave (FP-LAPW) code, one of the most accurate computational schemes for solving solid-state DFT equations [3], originally written at Karl-Franzens-Universität Graz as a milestone of the EXCITING EU Research and Training Network. As it is the code we use for all solid state calculations throughout this study we believe it necessary to give a brief explanation of the basic theoretical concepts it is built upon.

The Kohn-Sham equations (see expressions 41 and 42) are solved using a basis set that approximates the wave function of the solid state Hamiltonian. Ideally this basis set satisfies two requirements: it should be *unbiased*: approximate wave functions carry too much information from the basis functions and errors are introduced to the system wave function; and *efficient*, only a few basis functions are necessary if they are similar to the wave function that is to be expanded. In summary, we are seeking a basis set efficient and simple; both requirements are satisfied by plane waves in real space.

Bloch's theorem, discussed in Section 2.2.1, states that any one-electron eigenfunction  $\psi_{n,\mathbf{k}}$  of a periodic Hamiltonian can be expanded using a basis set of the form:

$$\psi_{n,\mathbf{k}}(\mathbf{r}) = \sum_{\mathbf{G}} c_{\mathbf{k}-\mathbf{G}}^n e^{i(\mathbf{k}+\mathbf{G})\cdot\mathbf{r}}, \quad (80)$$

where  $\mathbf{G}$  is any reciprocal lattice vector.

The part to be determined are the coefficients  $c_{\mathbf{k}-\mathbf{G}}^n$ . It can be seen from the previous expression that the wave function is both dependent on the Brillouin zone designated by  $n$  (also called the *band index*) and  $\mathbf{k}$ . For a certain  $\mathbf{k}$  value within a determined Brillouin zone  $n$ , the wave function is hence expanded as a sum over the discrete though infinite basis set determined by  $\mathbf{G}$ . However, in practice the infinite sum is truncated limiting the set of all  $\mathbf{G}$  to  $G \leq G_{\max}$ . This limits the choice of  $\mathbf{G}$  to only the vectors contained within a sphere with radius  $G_{\max}$ . This "cut-off" value, also known as *energy cut-off* or *plane-wave cut-off* is of great importance in solid state calculations since it controls the number of plane-waves that are to be used by the code.

The usage of plane-waves to approximate the wave function of spatially periodic Hamiltonians, namely Hamiltonians for crystal systems, was first introduced by Slater in 1937[156]. It is certainly advantageous to use such an expansion because of the aforementioned simplicity and moderate computational cost of the plane-wave treatment. Nevertheless a serious problem arises when trying to properly describe the region close to the nucleus.



The oscillating behaviour of the wave function affects its tails, that stretch into regions close to the nucleus. However, the nuclear region in a solid is quite shielded from the outer chemically relevant levels. The electrons occupying these low-lying regions of a solid behave not different from electrons forming part of free atoms. The potential they suffer can therefore be replaced by a smoother *pseudopotential* that yields very smooth tails in the region close to the nucleus and require only a few plane-waves to describe it.

### 2.3.1 The APW method

The pseudopotential method is very useful in many situations but:

- the choice of a pseudopotential is to a certain extent arbitrary,
- information contained in regions close to the nucleus is lost.

The first improvement of the quality of the basis set was achieved by the *augmented plane-wave* (APW) basis set  $\{\phi_{\mathbf{G}}^{\text{APW}}\}$ . The APW method is motivated by the different behaviour of electrons depending on whether they are close or far from the nucleus. The space is partitioned into the *muffin tin* (MT) and the *interstitial* (I) regions. The muffin tin region is delimited by a sphere of radius  $R_{\alpha}$  around each atom, where electrons behave in a manner similar to that of the electrons in a free atom: the MT sphere comprises the region where a pseudopotential used to be applied. The interstitial region is the space between muffin tin regions where electrons, far from the nucleus, are free-like. Plane-waves are appropriate to treat free-like electrons as those in the I region (see below), while atomic-like functions are suitable to describe the low-lying electrons within the MT region. Such a prescription is mathematically formulated as

$$\phi_{\mathbf{G}}^{\text{APW}}(\mathbf{r}, E) = \begin{cases} \frac{1}{\sqrt{V}} e^{i(\mathbf{k}+\mathbf{G})\cdot\mathbf{r}} & \mathbf{r} \in \text{I} \\ \sum_{l,m} a_{l,m}^{\alpha,(\mathbf{k}+\mathbf{G})} u_l^{\alpha}(r', E) Y_{l,m}(\hat{\mathbf{r}}') & r' < R_{\text{MT}}^{\alpha}, \end{cases} \quad (81)$$

where  $\alpha$  is an index to differentiate among MTs.

The APW basis functions  $\phi_{\mathbf{G}}^{\text{APW}}$  consist of plane-waves in the interstitial region that are augmented inside the MT spheres with radial solutions of atomic Schrödinger equations.

The symbols  $\mathbf{k}$ ,  $\mathbf{G}$  and  $\mathbf{r}$  maintain their usual meaning and  $V$  is the volume of the unit cell in the real space. The coefficient  $a_{l,m}^{\alpha,(\mathbf{k}+\mathbf{G})}$  and  $E$  are still undetermined and  $u_l^{\alpha}$  are radial functions, through which the Schrödinger equation is numerically solved. Every radial function corresponds to a solution for the electron  $\alpha$  with energy  $E$ .

The determination of the parameters  $a_{l,m}^{\alpha,(\mathbf{k}+\mathbf{G})}$  is done by imposing the condition to the plane-wave that it must match the function inside the MT over the whole sphere surface. Each plane-wave is then expanded at  $r = r_{MT}$  into spherical harmonics, which yields an infinite number of coefficients that have to be truncated at some value  $l_{max}$ <sup>1</sup>.

The APW method is not of much practical use today due to its energy dependence. In order to describe an eigenstate  $\psi_{n,\mathbf{k}}(\mathbf{r})$  properly, the energy  $E$  of that state has to be set equal to its eigenvalue (or band energy)  $\epsilon_{n,\mathbf{k}}$ . But this eigenvalue is exactly what we are looking for. The search must hence start from an initial guess of  $\epsilon_{n,\mathbf{k}}$ , for which the APW functions are evaluated, and whose result feeds the  $E$  of the next iteration and so on. The method becomes thus too slow to be applied to real systems and further improvements must be achieved.

### 2.3.2 The linearized augmented plane-wave method

Among the numerous works where the linearized augmented plane-wave (LAPW) method is discussed (as for instance those by Andersen[4] or by Koelling[76]), we precisely cite the book by Singh[152], for it contains a very detailed description on the method. Within the LAPW, the radial function  $u_l^\alpha(r', \epsilon_{n,\mathbf{k}})$  is expressed as a two-term Taylor expansion, which introduces a correction to the APW analogous term. The LAPW radial function consists then of the same radial function evaluated at some fixed linearization energy  $E_0$  and a new term: its energy derivative computed also at energy  $E_0$ :

$$u_l^\alpha(r', \epsilon_{n,\mathbf{k}}) = u_l^\alpha(r', E_0) + (E_0 - \epsilon_{n,\mathbf{k}}) \underbrace{\left. \frac{\partial u_l^\alpha(r', E)}{\partial E} \right|_{E=E_0}}_{\dot{u}_l^\alpha(r', E_0)} . \quad (82)$$

The energy difference of the second term is yet unknown and as a consequence a new coefficient  $b_{l,m}^{\alpha,\mathbf{k}+\mathbf{G}}$  appears in the expression of the complete LAPW basis function  $\phi_{\mathbf{G}}^{LAPW}$ :

$$\phi_{\mathbf{G}}^{LAPW}(\mathbf{r}) = \begin{cases} \frac{1}{\sqrt{V}} e^{i(\mathbf{k}+\mathbf{G}) \cdot \mathbf{r}} & \mathbf{r} \in I \\ \sum_{l,m} \left( a_{l,m}^{\alpha,(\mathbf{k}+\mathbf{G})} u_l^\alpha(r', E_{1,l}^\alpha) + \right. & \\ \left. + b_{l,m}^{\alpha,(\mathbf{k}+\mathbf{G})} \dot{u}_l^\alpha(r', E_{1,l}^\alpha) \right) Y_{l,m}(\hat{\mathbf{r}}') & r' < R_{MT}^\alpha \end{cases} \quad (83)$$

<sup>1</sup> The boundary condition that both functions have to match at the sphere boundary requires the number of nodes per unit length of the plane-waves ( $G_{max}$ ) to be similar to that of the angular functions ( $l_{max}$ ):  $R_\alpha G_{max} = l_{max}$  [34].

The relative weight of  $u$  and  $\dot{u}$  does the matching between the radial function and the plane-wave both in value and slope at the MT radius, i.e. the coefficients  $b_{lm}^{\alpha, k+G}$  and  $a_{lm}^{\alpha, k+G}$ . The LAPWs provide the basis flexibility necessary to properly describe eigenfunctions with eigenenergies close to the linearization energy, which is kept fixed.

The linearization energy  $E_0$  is not universally chosen. On the contrary, a different energy is used for each angular momentum  $l$ , conferring s-, p-, d- or f- character to the basis set and hence adequately describing the state. Consequently,  $E_0$  is replaced by a set of well-chosen  $E_{l,l}^\alpha$  up to  $l = 3$ . If  $l > 3$ , a fixed energy value can be used for all those  $l$ 's. The same procedure can now be used as in the APW case, but the secular equation that must be solved here becomes linear in energy and all eigenvalues can be obtained with a single diagonalization of the secular matrix, unlike in the APW method.

### 2.3.3 LAPW with Local Orbitals: LAPW + LO

The LAPW method, though being among the most accurate applicable techniques for density-functional-based electronic-structure and total-energy calculations, has some shortcomings, the most important one arising from the linearization itself. The electrons lying close to the nucleus are called “core states” and behave quite like electrons in a free atom. They do not have an important role in chemical bonding and must lay completely inside the MT sphere. However, states situated far from the nucleus leak out of the MT, sticking into the interstitial region. Such states are named “valence states” and actively participate on the chemical bond.

As a third group, electrons with the same  $l$  but different principal quantum number than valence electrons, the so-called *low-lying valence states*, located inbetween core and valence states, may have also an important role in the chemical bond. For atoms with such states, called “semicore states”, the basis functions are only approximately orthogonal to the semicore states. The energies may then have a dependency on the linearization energy  $E_l$  that has been chosen. LAPW basis is a good basis set only for eigenvalues close to this energy. Valence electrons sharing  $l$  with semicore states are poorly described, since the  $E_l$  chosen is close to the eigenvalue of the semicore bands. As  $E_l$  is arisen towards the valence bands semicore state will become poorer described and its eigenvalue will increase. At some point  $E_l$  will overlap with valence eigenenergies and a ghost state will appear, making that the correct total energy cannot be calculated.

Singh *et al.*[151] proposed a method to solve these difficulties, based on a change in the linearization that brings sufficient variational freedom to properly treat both semicore and valence states. All  $l$ 's except those for which there are semicore states are treated exactly as within

the LAPW method, with both  $u_l(r)$  and  $\dot{u}_l(r)$  functions. Those  $l$ 's that have semicore states accompanied are described by the usual  $u_l(r)$  and  $\dot{u}_l(r)$  at the linearization energy  $E_{1,l}$  in the valence region, but supplemented with a second  $u_l(r)$  for the  $l$  of the semicore states, at a second linearization energy  $E_{2,l}$ . A new type of basis function  $u_l^\alpha(r', E_{2,l}^\alpha)$  named *local orbital* (LO) is added to the standard LAPW basis set,

$$\phi_{l,m}^{\alpha,LO}(\mathbf{r}) = \begin{cases} 0 & \mathbf{r} \in I \\ \left[ a_{l,m}^{\alpha,LO} u_l^\alpha(r', E_{1,l}^\alpha) + b_{l,m}^{\alpha,LO} \dot{u}_l^\alpha(r', E_{1,l}^\alpha) + \right. & (84) \\ \left. + c_{l,m}^{\alpha,LO} u_l^\alpha(r', E_{2,l}^\alpha) \right] Y_{l,m}(\hat{\mathbf{r}}') & r' < R_{MT}^\alpha \end{cases}$$

This new type of basis function is called *local* since it does not match the plane-waves in the interstitial region. A new boundary condition is hence added: the basis function must be continuous in value and slope at the MT radius and additionally, goes to zero at the sphere boundary  $r \geq R_{MT}$ . These boundary conditions allow to find the coefficients  $a_{l,m}^{\alpha,LO}$ ,  $b_{l,m}^{\alpha,LO}$  and  $c_{l,m}^{\alpha,LO}$ .

#### 2.3.4 The APW-lo method

The linearization of the pure APW basis functions made in the LAPW method is energy-dependent. This was removed at the cost of a somewhat larger basis set in the LAPW+LO method. Sjöstedt *et al.* [153] proposed a new method that expands the wave function by means of an energy-independent basis set that still has the same size as the APW basis set.

The APW+lo method provides higher variational freedom using a complementary basis set consisting of local orbitals for physically important  $l$ -quantum numbers, generally  $l \leq 3$ . The orbitals used in the APW+lo are local in the same sense as used by Singh [151], i.e., to treat semicore states: they are totally confined inside the MT spheres. It therefore consists of two different kinds of basis functions: APWs and los. The first kind are exactly the same as described in 2.3.1 (equation 81). The second have the form:

$$\phi_{l,m}^{\alpha,lo}(\mathbf{r}) = \begin{cases} 0 & \mathbf{r} \in I \\ \sum_{l,m} \left( a_{l,m}^{\alpha,lo} u_l^\alpha(r', E_{1,l}) + \right. & (85) \\ \left. + b_{l,m}^{\alpha,lo} \dot{u}_l^\alpha(r', E_{1,l}) \right) Y_{l,m}(\hat{\mathbf{r}}') & r' < R_{MT}^\alpha \end{cases}$$

The energies  $E_{1,l}^\alpha$  used are again the same as for the corresponding APWs. The coefficients  $a_{lm}^{\alpha,lo}$  and  $b_{lm}^{\alpha,lo}$  are found by requiring the functions to be normalized and that they must vanish at the MT sphere boundary, respectively. Energies are found as in the LAPW+LO method by a single matrix diagonalization but requiring a lower plane-wave cut-off and hence similar number of functions than in APW but smaller than in the LAPW+LO case.

The APW+lo basis set appears not only to be faster than LAPW but also to provide a better description of eigenfunctions close to  $E_{1,l}^\alpha$ . Both  $u_l(r, E_{1,l}^\alpha)$ , as used within the APW method for efficient description of the eigenfunctions close to  $E_{1,l}^\alpha$ , and a more relaxed linear combination of  $u_l(r, E_{1,l}^\alpha)$  and  $\dot{u}_l(r, E_{1,l}^\alpha)$ , to make an accurate description of states away from  $E_{1,l}^\alpha$ , are included in the APW+lo method.

### 2.3.5 Mixed basis sets

A combination of some of these methods may be suitable to treat certain special systems:

**LAPW WITH APW+LO** basis sets can solve situations hardly handled by LAPW as atoms with d- and f- valence states or systems whose atoms have very different muffin tin spheres. APW+lo basis set is used only where it is needed while the rest of the electrons are treated with LAPW.

**APW+LO WITH LO.** The same problem with semicore states that the APW method had, solved with LAPW+LO in section 2.3.3 is encountered in the APW+lo. LOs used for APW+lo look however differently:

$$\phi_{l,m}^{\alpha,LO}(\mathbf{r}) = \begin{cases} 0 & r \in I \\ \left[ a_{lm}^{\alpha,LO} u_l^\alpha(r', E_{1,l}^\alpha) + \right. \\ \left. + c_{lm}^{\alpha,LO} u_l^\alpha(r', E_{2,l}^\alpha) \right] Y_{l,m}(\hat{r}') & r' < R_{MT}^\alpha \end{cases} \quad (86)$$

## **Part III**

# **The decay of the delocalization index (DI) and metallicity**



## 3

CHEMICAL BOND  
DESCRIPTORS IN REAL SPACE:  
THE QUANTUM THEORY OF  
ATOMS IN MOLECULES

Many quantum chemical concepts introduced on an empirical basis several decades ago can be assigned a physical reasoning through the quantum theory of atoms in molecules (QTAIM). Taking the electron density  $\rho$  as the central observable, the QTAIM is able to confer physical meaning, via the topology of the electron density, to basic chemical concepts as bonds or atoms. A full, authoritative account of the theory is found in [8, 9].

In order to obtain a well-behaved quantum-mechanical description of an open region of a quantum system, this region must be bounded by a surface whose flux of the gradient of the electron density vanishes [97]. Defined within the QTAIM, equation 87, is the mathematical formulation of such a region

$$\nabla\rho(\mathbf{r}_s) \cdot \mathbf{n} = 0, \quad (87)$$

where  $\mathbf{n}$  is a vector normal to the boundary surface and  $\mathbf{r}_s$  indicates that the electron density is evaluated at each point of the surface.

The result is a division of the space into non-overlapping basins  $\Omega_i$ , enclosed by a surface of zero-flux of the electron density  $\rho$ . These basins are assigned to a nucleus, conferring this way physical meaning to the resulting regions. The atomic basins satisfying equation 87 are also space-filling since the procedure is exhaustive  $\cup_a \Omega_a = \mathbb{R}^3$ .

Alternatively, the partition of the space can be done according to scalar fields other than the electron density, such as the electron localization function (ELF) of Becke and Edgecombe[21] or the electron localisability indicator (ELI) of Kohout[81], which result in a finer division of the space into core, valence, bonding or lone-pair regions.



### 3.1 LOCALIZATION AND DELOCALIZATION INDICES

Within the QTAIM theory developed by professor R.F.W. Bader [9], a description of the localization (LI) and delocalization (DI) indices is given that allows us to determine the extent to which electrons are tied to a portion of the total space. For a more detailed description of LI and DI the reader is referred to the references [10, 11, 13, 47, 48]. Surely, information about localization and delocalization of electronic charge is contained in the quantum mechanical distribution function  $\Psi^*\Psi d\mathbf{r}_1 d\mathbf{r}_2 \dots d\mathbf{r}_N$  (see equation 7). For a system of  $N$  electrons divided into an  $m$  number of  $\Omega$  regions,  $P_n(\Omega)$

$$P_n(\Omega) = \frac{N!}{n!(N-n)!} \int_{\Omega} d\mathbf{r}_1 \dots \int_{\Omega} d\mathbf{r}_n \cdot \int_{\Omega'} d\mathbf{r}_{n+1} \dots \int_{\Omega'} d\mathbf{r}_N \rho_N(\mathbf{r}_1, \mathbf{r}_2, \dots, \mathbf{r}_N), \quad (88)$$

is the event probability that  $n$  electrons occupy  $\Omega$  while the other are in  $\Omega'$ ,  $\rho_N$  is the diagonal part of the spinless  $N$ -particle density matrix as given by equation 7 —after integrating over spin—.  $\mathbf{r}_i$  keeps its usual meaning. Since the wave function is normalized, summation over all possible events leads to certainty,

$$\sum_n P_n(\Omega) = 1. \quad (89)$$

Just like the integration of the electron density over the whole space yields the total number of electrons  $\int_{\mathbb{R}^3} \rho(\mathbf{r}) d\mathbf{r} = N$ , integration of the same function over an atomic basin  $\Omega$  yields the average number of particles within that region

$$\langle N_{\Omega} \rangle = \sum_n n P_n(\Omega) = \int_{\Omega} \rho(\mathbf{r}) d\mathbf{r}. \quad (90)$$

In order for the electrons of a system to be almost fully localized, one of the events described in equation 88 must have a probability close to one, whereas the remaining should have very low contributions. In other words, it would be very convenient to have an expression that carries the information of to what extent the condition 89 is determined by just one probability, whilst the rest are negligible and can be left out  $\sum_n P_n(\Omega) = 1 \approx P(\Omega)$ . The fluctuation function closely describes this situation and does not require the evaluation of the full  $N$ th-order density matrix  $\rho_N$ , but is on the contrary expressed in terms of the diagonal elements of the 2-RDM  $\rho_2$  defined in equation 46.

The fluctuation in the average number of electrons in a region  $\Omega$  is evaluated as

$$\sigma^2(\Omega) = \langle N_\Omega^2 \rangle - \langle N_\Omega \rangle^2 = \sum_n n^2 P_n(\Omega) - \left( \sum_n n P_n(\Omega) \right)^2, \quad (91)$$

which can be also expressed in terms of  $\rho_2$ . That possibility entails a “great conceptual advantage since the extent to which a set of indistinguishable particles is spatially localized is determined by the system’s pair density”, literally quoting R.F.W. Bader [9], and the distribution that also determines the fluctuation  $\sigma^2$ . The relevant properties of the pair density function are a consequence of the Fermi correlation, which results from the antisymmetrization of the wave function required by the Pauli principle. The correlation causes the pair density function to deviate from a simple product of independent densities. This correlation is carried by the function  $f(\mathbf{r}_1, \mathbf{r}_2)$ , defined in equation 52 and the pair density is expressed as in equations 52 and 53. This correlation term measures not only the Fermi correlation—which exists among electrons with identical spins—but also the Coulomb correlation—affecting opposite-spin electrons—as it is explained more in deep in section 1.5. According to the Pauli exclusion principle, the exchange of the coordinates of two electrons of identical spin—recall that Fermi correlation occurs between same-spin electrons—causes the sign of the pair density to change (see equation 51).

The aim of the present section is to show the expression which describes “the spatial extent of the effects of the self-pairing correlation on the motion of electrons, as well as whether or not the net effect of this correlation for any one particle, the correlation hole, may be localized to one particular region of space” [9]. In that sense the Fermi correlation is of capital relevance since it solely determines the extent to which sets of electrons may be localized in some region of real space.

The average number of pairs of  $\sigma$ -spin electrons in a region can be expressed in terms of event probabilities

$$D_2(\Omega, \Omega) = \frac{1}{2} \sum_n P_n(\Omega) (n-1)n = \frac{1}{2} \langle N_\Omega^2 \rangle - \langle N_\Omega \rangle. \quad (92)$$

This average number of electron pairs can also be expressed by integrating both coordinates of the pair density over  $\Omega$  region yielding

$$D_2(\Omega, \Omega) = \int_\Omega d\mathbf{r}_1 \int_\Omega \rho(\mathbf{r}_1, \mathbf{r}_2) d\mathbf{r}_2 = \frac{1}{2} [\langle N_\Omega^2 \rangle + F(\Omega, \Omega)], \quad (93)$$

$F(\Omega, \Omega)$  accounts for the correlation of the  $\sigma$ -spin electrons

$$F(\Omega, \Omega) = \int_{\Omega} d\mathbf{r}_1 \int_{\Omega} \rho(\mathbf{r}_1) \rho(\mathbf{r}_2) f(\mathbf{r}_1, \mathbf{r}_2) d\mathbf{r}_2. \quad (94)$$

A limiting situation will occur when the probability of one particular event  $P_n(\Omega)$  equals unity whereas the other probabilities of the remaining events vanish. In such situation the summatory in equation 92 reduces to just one term. The pair population within the region will be  $n(n-1)/2$  and it is referred to as a “pure pair” population. Electrons are uncorrelated and hence perfectly localized within region  $\Omega$ . They behave as distinguishable particles that do not see each other and the wave function for the total system could be written as a simple product of separately antisymmetrized wave functions, with  $n$  electrons in  $\Omega$  and the remaining  $N-n$  in  $\Omega'$ . The magnitude  $F(\Omega)$  is a measure of the total Fermi hole of the  $N_{\Omega}$  particles that lies within region  $\Omega$ . In such limiting situation the Fermi hole for any of the  $n$  electrons in  $\Omega$  is entirely contained in this region.

The term  $F(\Omega, \Omega)$  is in general far from this ideal situation and normally the Fermi hole of the electrons in  $\Omega$  extends out of this region. The magnitude  $F(\Omega, \Omega)$  is given the name atomic *localization index* LI, or  $\lambda^{\Omega}$  [45].

It can be also measured how much of the Fermi hole generated by the electrons occupying a region  $A$  is localized not in the same but within a different region  $B$ . This information is contained in  $F(A, B)$ , which is defined in the expression for the average number of electron pairs formed from the electrons located at  $A$  and those at  $B$ . It is obtained by integrating the coordinates of one electron over region  $A$  and the coordinates of the other over region  $B$

$$D_2(A, B) = \int_A d\mathbf{r}_1 \int_B \rho(\mathbf{r}_1, \mathbf{r}_2) d\mathbf{r}_2 = \frac{1}{2} [\langle N_A \rangle \langle N_B \rangle + F(A, B)], \quad (95)$$

where  $F(A, B) = F(B, A)$ . The sum of both magnitudes  $F(A, B) + F(B, A)$  defines the delocalization index  $\delta^{A,B}$ , or DI and quantitatively measures the sharing of electrons between regions  $A$  and  $B$  [45]. A reorganization of equation 95, equivalent to equation 53 where the exchange-correlation density  $\rho_{xc}$  is defined, leads to the most usual definition of the DI

$$\delta^{A,B} = 2 \int_A d\mathbf{r}_1 \int_B d\mathbf{r}_2 \rho_{xc}(1, 2). \quad (96)$$

Equivalently, the LI has the shape

$$\lambda^A = \int_A d\mathbf{r}_1 \int_A d\mathbf{r}_2 \rho_{xc}(1, 2). \quad (97)$$

Within the HF approach, the exchange-correlation density can be expanded in terms of the spin orbitals as in equation 60, which would yield a very common definition of the DI

$$\delta^{A,B} = 2 \sum_{i,j} \int_A \psi_i(\mathbf{r}_1) \psi_j(\mathbf{r}_1) d\mathbf{r}_1 \int_B \psi_i(\mathbf{r}_2) \psi_j(\mathbf{r}_2) d\mathbf{r}_2 \quad (98)$$

$$= 2 \sum_{i,j} S_{ij}^A S_{ij}^B, \quad (99)$$

where each of the integrands is the domain-restricted atomic overlap matrix (AOM)  $S_{ij}^A$  between spin orbitals  $\psi_i$  and  $\psi_j$ , whose spin coordinates have been left out

$$S_{ij}^A = \int_A \psi_i(\mathbf{r}_1) \psi_j(\mathbf{r}_1) d\mathbf{r}_1. \quad (100)$$

The number of electrons  $\langle N_A \rangle$  —charge— in the region  $A$  can be expressed as

$$\langle N_A \rangle = \lambda^A + \frac{1}{2} \sum_{X \neq A} \delta^{A,X}, \quad (101)$$

and the fluctuation  $\sigma^2(A)$  of equation 91 may be now rewritten as

$$\sigma^2(A) = D_2(A) + \langle N_A \rangle - \langle N_A^2 \rangle \quad (102)$$

$$= \langle N_A \rangle - \lambda^A = \frac{1}{2} \sum_{X \neq A}^{\text{nearest}} \delta^{A,X}, \quad (103)$$

from where it can be seen that the variance is given by the electron and electron pair populations. For situations where the electrons are perfectly localized, that is  $\lambda^A = \langle N_A \rangle$ , the fluctuation  $\sigma^2(A)$  will attain a value of zero.

The fluctuation defined in 91 measures the variance between the number of electrons occupying a region of the space and the localization of electrons within this region. It is also useful to consider whether electrons are shared between *close* or *distant* regions. We name close regions those having common zero-flux surfaces, that is, having direct contact with the region occupied by the electrons, whereas distant refers to regions located beyond the first neighbourhood. As defined in [18], the number of close shared pairs  $\sigma_c(A)$  for basin  $A$  is the sum of the DI of the nearest basins

$$\sigma_c(A) = \sum_{B \neq A} \delta^{A,B}. \quad (104)$$

The difference between twice the fluctuation (total shared pairs) and the sharing among the closest basins  $\sigma_c(A)$  yields the distant shared pairs  $\sigma_d(A)$  for basin  $A$

$$\sigma_d(A) = 2\sigma^2(A) - \sigma_c(A). \quad (105)$$

Finally, it will be meaningful to express the fraction of the total shared electron pairs that are shared with distant basins  $\chi(A)$

$$\chi(A) = \frac{\sigma_d(A)}{2\sigma^2(A)}. \quad (106)$$

### 3.2 THE DELOCALIZATION INDEX IN THE SOLID STATE

The exchange-correlation part of the pair density is not explicitly available from DFT and a workaround has to be used in order to build it from the Kohn-Sham orbitals using a HF-like formula (see [18] and references therein). This approach is known to yield good results in molecules and it may be also used in solid-state DFT, although partially occupied KS orbitals may appear (mostly in metals, where there are partially occupied bands).

In solid state calculations, the integration to find the DI is done over the Brillouin Zone (BZ) with volume  $V_{BZ}$  which is transformed into a summation over a user-chosen number of  $k$ -points within it ( $K_{BZ}$ )

$$\delta^{A,B} = \frac{2}{K_{BZ}^2} \sum_{n,n'} \sum_{k,k'} S_{nk,n'k'}(A) S_{n'k',nk}(B) \theta(n,k) \theta(n',k'), \quad (107)$$

which is the Ángyán formulation of the DI [5]. Also, an alternative form of the LI and the DI is given by Ponec in [131]. The index  $n$  runs over the bands and the occupation number  $\theta(n,k)$  selects only occupied states.  $S$  are the overlap integrals between the KS orbitals of the crystal calculated over the region  $\Omega$

$$S_{nk,n'k'}(\Omega) = \int_{\Omega} \psi_{n,k}^*(\mathbf{r}) \psi_{n',k'}(\mathbf{r}) d\mathbf{r}. \quad (108)$$

In a equivalent manner the LI over the region  $A$  are calculated as

$$\lambda^A = \sum_{n,n'} \sum_{k,k'} S_{nk,n'k'}^2(A). \quad (109)$$

Kohout and Baranov have explained in detail how to obtain the DI and LI for extended systems (see reference [18]).

## 4

DECAY OF DIS AND  
METALLICITY AT THE  
UNCORRELATED LEVEL

## 4.1 INTRODUCTION

Real space theories of the chemical bond[14, 109] have provided a physically sound alternative to the molecular orbital (MO) paradigm over the last two decades (see Section 1.1.3),[61] incorporating orbital invariant descriptors endowed with chemical meaning to the chemical bonding toolbox. Among several proposals, commonly gathered together under the Quantum Chemical Topology (QCT) umbrella, the QTAIM described in Section 3 is of special interest because of a key distinguishing feature that separates it from other techniques: its energetic face. All the standard components of the Coulomb Hamiltonian may be examined over QTAIM real space domains, providing a unique route to bind the physicist and the chemist points of view. In order to do so, the non-diagonal first order RDM (1-RDM) as well as the diagonal 2-RDM are needed. The first is a standard ingredient of the orthodox QTAIM, and the second was shown to provide a measure of electron delocalization in a seminal paper by Bader and Stephens[10], as we have discussed. The 2-RDM was finally added to the energy-related descriptors of the QTAIM in the interacting quantum atoms (IQA) scheme.[50]

As the set of systems for which the QTAIM was applied increased (including molecules, clusters, and solids), it soon became clear that  $\rho$  and/or  $\nabla^2\rho$  contain a wealth of information about chemical bonding, and that a simple classification of systems into shared-shell or closed-shell types, in quite good agreement with the standard covalent/non-covalent (including ionic) bonding models was possible. This knowledge is now mainstream, reaching general chemistry textbooks, and its success encouraged researchers to look for features in  $\rho$  peculiar to metallic systems, an enterprise with little initial success. The density of conducting materials seemed not different from that of standard covalent ones. A proposal that non-nuclear maxima (or non-nuclear attractors, NNAs), known in the  $\text{Li}_2$  molecule since 1956,[22] and found in other lithium clusters[31, 58] might signal metallic behaviour was received with hope. Its chemical image matched well with the qualitative idea that conducting electrons were transferred to interstitial positions in crystalline lattices. However, when reliable calculations of the topology of the electron density in solid alkali met-

als were available, this initial hope vanished.[93] Only Li displayed NNAs at equilibrium geometries. Since then, experimental densities have demonstrated that NNAs may appear in Beryllium,[72] but are absent in the metals of largest conductivity, like Cu, Al, or Ag. Whatever the origin of NNAs,[103] they do not signal conductivity. Other attempts have shown that the density of metallic systems is characterized by its interstitial flatness,[114] again in agreement with conventional chemical wisdom, but no salient feature of the density determining conductivity has ever been found.

From the purely theoretical side, the naïve difference between electrical conductors and insulators lies in their excitation spectra,[74] i.e. in the nature of their excited states, far from the real space realm. However, a seminal paper by Kohn in 1964[77] showed that insulators and conductors also differ essentially in the organization of electrons in their ground state. In the former, the wave function is composed of many-body building blocks localized in disconnected regions of the many-particle configuration space. Long forgotten, Kohn's theory was reformulated by Resta in 1998,[139] in what today is known as the modern theory of polarization, offering a new view deeply linked to Berry phases.[84] Resta has shown that the finiteness or divergence of Kohn's localization tensor (LT) is the key to conductivity, and that for one-determinant descriptions, the LT is closely related to Boys theory of localization,[25] very familiar to the quantum chemical audience. Application of the LT (or total position spread tensor, TPS) to chemical problems has been pioneered by Evangelisti and co-workers.[27] An important point for what follows here is that Resta's formulation lies in real space. Thus, conductivity may not leave scars in the plain density, but should lead to a recognizable imprint if we examine other RDMs in real space.

Notwithstanding the role that the TPS should play in this important problem, in this contribution let us focus on how the standard real space measures of (de)localization may be related to metallic behaviour in molecular systems. To that end, we will start recalling some known results based on Kohn's near-sightedness principle.[78] They show that the decay behaviour of the 1-RDM,  $\rho(\mathbf{r};\mathbf{r}')$ , determines the locality of all relevant observables. We will then relate the 1-RDM to the real space DI defined within the QTAIM by Bader and Stephens,[10]  $\delta^{A,B}$  (see equation 107). Armed with this, we will examine the analytical decay rate of  $\delta$  for Hückel and tight binding (TB) models of metals and insulators, comparing with simple calculations in toy systems. The results will show that, as expected, the decay rate of delocalization measures differs in insulating- or metallic-like systems, being exponential in the former and algebraic in the latter. Other interesting links, like that between the well known oscillations of  $\delta$  in conjugated molecules, clearly related to resonance and chemical behaviour, and Friedel oscillations in metals will be put forward.

## 4.2 DECAY RATE OF 1-RDMS AND DELOCALIZATION INDICES

As commented, the decay rate of the density matrix, a fundamental issue after Kohn's insights on near-sightedness[78] has been widely studied in the physical literature, usually under a one-electron picture within the DFT (see Section 1.4), or within a tight binding (TB) Hamiltonian approximation. For instance, Goedecker[62] showed that assuming the electronic structure of an isotropic 3D metal to be dominated by its free-electron band structure, the 1-RDM  $\rho(\mathbf{r}; \mathbf{r}') = \rho(|\mathbf{r} - \mathbf{r}'|) = \rho(s)$  decays algebraically at zero temperature,

$$\rho(s) = \frac{-k_F}{\pi^2 s^2} (\cos(sk_F) - \sin(sk_F)) / (sk_F), \quad (110)$$

where  $k_F$  is the Fermi vector modulus, related to the valence electron density  $k_F^3/(3\pi^2) = N_{el}/V$ . As it can be seen,  $\rho(s)$  oscillates on decaying like  $s^{-2}$ , with zeros at  $sk_F \approx 4.49, 7.73, 10.90$ , etc. For reasonable valence density values, it can readily be found that these zeros are close to lattice vectors. As we will see, this oscillatory behaviour, which is closely related to the well known Friedel oscillations of metals,[74] has close relatives in finite molecules.

Taraskin and co-workers[159] have refined these results for 1D to 3D TB metals in simple linear, square, or cubic cells, showing that  $\rho$  decays as  $s^{-(d+1)/2}$ ,  $d$  being the dimensionality of the system. These authors[158] have also shown that, for two bands TB models of insulating lattices the 1-RDM falls exponentially with  $s$ ,

$$\rho(s) \approx s^{d/2} e^{-\lambda s}, \quad (111)$$

where the inverse decay length  $\lambda$  depends on the gap,  $\Delta$ , scaling linearly with it as  $\Delta \rightarrow 0$ .  $\rho(s)$  turns out to be anisotropic, showing its slowest decay along the (1,1) or (1,1,1) diagonals in 2D or 3D, respectively. Effective  $\lambda$  values have been shown to lie between 1-5.

Once these results have been presented, let us turn to delocalization measures in real space. Several indicators have been proposed over the years, among which the electron localization function (ELF) of Becke and Edgecombe,[21] very popular in theoretical chemistry after the work of Savin and Silvi,[150] is probably best known. Other possibilities like the electron localizability indicator (ELI) introduced by Kohout,[80] valid for correlated descriptions, also exist. All of these are local descriptors, bearing no decay information, and do not serve our purposes.

Fortunately, the DI describes how many pairs of electrons are shared (thus delocalized) between two finite regions A and B in real space (see equation 107). In this expression, the integrand is the standard exchange-correlation density,  $\rho_{xc}(\mathbf{r}_1, \mathbf{r}_2)$ , obtained after integration



of equation 53 over the spin coordinates of both electrons.  $\delta^{A,B}$  is a scalar parameter between any two regions —notice that if  $A = B$  we usually talk about a localization index (see equation 109)— that due to the extensivity of  $\rho_{xc}$ , adds to the total electron population ( $N$ ),  $1/2 \sum_{A,B} \delta^{A,B} = N$ .

The DI may be understood as a simple generalization of the Wiberg-Mayer (WM) bond order,[110, 162] to which it reduces upon identification of real space averaging with atom-centred, Mulliken-like basis set condensation. Actually, for single determinant expansions with one-electron spinorbitals  $\psi_i$ , the DI can be defined in terms of the AOMs, defined in equation 100, as  $\delta^{A,B} = 2 \sum_{i,j} S_{ij}^A S_{ij}^B$ . To compare this expression to the WM bond order, which is usually written as

$$W_{AB} = 2 \sum_{\mu}^A \sum_{\nu}^B (PS)_{\mu\nu} (PS)_{\nu\mu}, \quad (112)$$

with sums running over primitive functions  $\chi_{\mu}$  centred on the A or B nuclei, and P denoting the density matrix written in terms of primitives,  $P_{\mu\nu} = \sum_i c_{i\mu} c_{i\nu}^*$  such that  $\phi_i = \sum_{\mu} c_{i\mu} \chi_{\mu}$ , it is useful to turn to a set of orthogonalized primitives  $\chi'_{\mu}$ . Using them,

$$W_{AB} = 2 \sum_{\mu}^A \sum_{\nu}^B P'_{\mu\nu} P'_{\nu\mu}, \quad (113)$$

that can immediately be recast as  $\delta^{A,B}$  if the Mulliken condensation

$$S_{ij}^A = \sum_{\mu} c'_{i\mu} c'_{j\mu} \quad (114)$$

is made. Although any orthogonalization procedure will destroy the original ascription of primitives to centres, it is very often the case that orthogonalization tails are not dominant, and that one can still formally assign the new orthogonal primitives to nuclei. Although this lies at the core of many of the problems of Mulliken or Löwdin population analysis, it plays no role in the following.

The chemist bond order is a measure of delocalization that the DI simply puts into a proper physical context. The above condensation procedure will be used soon in what follows. DIs have been widely used, providing a number of interesting insights. Particularly important in this context is the general finding that electron correlation tends to decrease the covalent bond order well below the standard integer numbers used by chemists.

It is also important to recognize that, being a domain condensation of the exchange-correlation density, the DI reflects the two-domain statistics of electron populations. For instance

$$\delta^{A,B} = -2\text{cov}(n_A, n_B) = -2[\langle n_A n_B \rangle - \langle n_A \rangle \langle n_B \rangle]. \quad (115)$$

Here,  $n_A, n_B$  are the domain electron counts, so that  $\langle n_A \rangle$  is the average electron population in region A. Delocalization, as sensed by the DI, is a measure of the fluctuation of electron populations. In chemical terms, two regions display a non-vanishing mutual bond order (if we like, they are bonded) when fluctuations in the electron population of one of them are sensed in the other, and vice versa.

At this point it was also noticed that most of the known results about the decay rates that we have commented above are based on TB Hamiltonians or effective one-electron formulations within DFT. In such cases, which can be assimilated to one-determinant expansions in a theoretical chemistry context, the exchange-correlation density reduces to its Fock-Dirac expression of equation 60.

This means that the decay rate of DIs with A – B distance should be a reason that allow to distinguish between metallic-like and insulating-like behaviour in not only extended but also finite systems.

It is the purpose of the work presented here to show with the help of Hückel and TB model Hamiltonians that the above insights hold indeed for molecules and solids. DIs should fall algebraically in metallic-like systems, possibly showing Friedel-like oscillations, and exponentially in insulating-like molecules, with decay lengths depending on the gap.

### 4.3 MODELS, COMPUTATIONAL DETAILS

The study will be restricted to the simplest possible cases that can be solved both analytically and modeled via single determinant, Hartree-Fock (HF) or Kohn-Sham (KS) DFT, expansions. To simplify as much as possible, we will consider homoatomic  $A_n$  linear chains of growing size with one electron per node to model metallic-like cases, and heteroatomic  $(AB)_n$  ones with also one valence electron sites to understand insulating-like behaviour. We will obtain DIs from analytical Hückel solutions with Mulliken condensation, and compare them to HF results in H and LiH chains obtained with the GAMESS[142] code using 6-311G(p) and 6-311+G(p) basis sets, respectively. In these cases, DIs for QTAIM topological partitions have been computed through our PROMOLDEN[2] program.

We have also obtained TB solutions for linear, square, and simple cubic one-electron per site extended lattices, and compared the decay rate of their DIs to that obtained from hydrogen lattices computed through the all-electron, full-potential linearized augmented plane

wave (FP-LAPW) code ELK.[1] QTAIM DIs from Elk solutions were obtained through the DGrid code.[82]

We will start considering our finite analytical models. Then we will generalize to 1D-3D extended systems, and finally we will compare results with HF and KS real data.

## 4.4 FINITE ANALYTICAL MODELS

### 4.4.1 The Hückel homoatomic chain

The Hückel homoatomic chain is an excellent semi-empirical model not only of hydrogen chains, but also of the  $\pi$  skeleton of alternate conjugated hydrocarbons, where a  $p$ , instead of an  $s$  function is placed at each node. We will freely switch between the  $s$ -H chain and the  $p$ -alternate hydrocarbon interpretations in what follows.

Let us label the  $n$  nodes of the chain with Latin indices, and build each one-electron function  $\psi_\mu = \sum_i c_\mu^i \chi_i$ , where  $\chi_i$  denotes each node's primitive and the orbital index  $\mu$  runs from 1 to  $n$ . We can both consider open-ended or closed chain conformations. Both admit well-known analytical solutions, so to simplify, we will stay with the open-ended, linear chain case. This is characterized by a Hamiltonian matrix  $\mathbf{H} = \alpha\mathbf{I} + \beta\mathbf{T}$ , where  $\alpha, \beta$  are the standard Hückel Coulomb and resonance parameters, respectively, and  $\mathbf{T}_{ij}$  is a Toeplitz tridiagonal adjacency matrix, with elements equal to 1 whenever  $|i - j| = 1$  and equal to zero otherwise. Toeplitz systems are easily diagonalized by discrete Fourier transforms.[20] To simplify further, let us assume that  $n$  is even. Then, the eigenvalues of  $\mathbf{H}$  and its associated spinor-bital coefficients are

$$\begin{aligned} \epsilon_\mu &= \alpha + 2\beta \cos \frac{\mu\pi}{n+1}. \\ c_\mu^i &= \sqrt{\frac{2}{n+1}} \sin \frac{\mu i \pi}{n+1}. \end{aligned} \quad (116)$$

Similar solutions may be obtained for a closed chain, now by solving a circulant matrix problem.

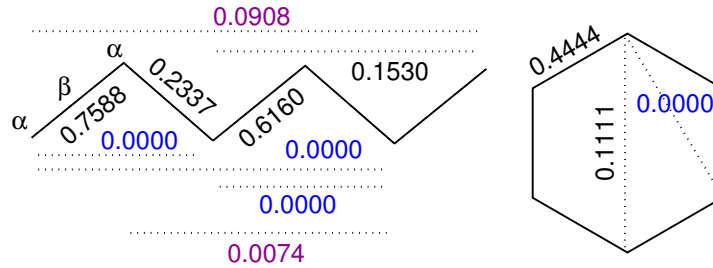


Figure 5: Hückel DIs for  $n = 6$  cyclic and open-ended homoatomic chains.

Using Mulliken's condensation,  $\delta^{i,j} = 2(\sum_{\mu} c_{\mu}^i c_{\mu}^j)^2$  (change the prefactor from 2 to 4 if the sum runs over occupied orbitals). Notice that the DI is built up from trigonometric functions, so a clearly oscillating behaviour is expected. Figure 12 shows all the DIs for both open and closed  $n = 6$  chains, which may be seen as models of hexatriene and benzene, respectively. DIs obtained with this simple prescription have already been reported in several model systems.[104]

There are several points to be commented. First, notice that the DI between nodes separated by an even number of edges is exactly zero, which is valid for any value of  $n$  and for cyclic or open chains. A chemically appealing connection between electron delocalization via DIs and mesomerism thus appears.

The resonance link is very clear when the covariance interpretation of the DI is taken into account. For instance, it is straightforward to check that on building the standard Pauling resonance structures of the hexatriene analogue, if the charge of node (atom) 1 (at one edge) is altered, then only those charges of atoms 2, 4, or 6 will also be found altered in the possible resonance schemes. This means that only the 1-even populations will display non-zero covariance, thus non-vanishing DIs. This interpretation may be generalized to other dimensions.

The *ortho* (or 1,2) DI in Hückel's benzene is 4/9, so adding the classical  $\sigma$  bond order would add to a total C-C bond order of 1.44, different from the naïve value 1.5. HF or DFT C-C DIs in benzene have been calculated many times, giving values clustered around 1.4. The 1,4 (*para*) DI, or PDI is quite large in benzene (although smaller than in the open chain), and has been successfully related to aromaticity in real calculations.[128]

Secondly, DIs in the open-ended chain show the expected bond order alternation of alternant hydrocarbons, with an oscillatory pattern of partial double (if the  $\sigma$  component is added) bonds, in good agreement with chemical wisdom. If the open chain is taken as a model for  $H_n$ , DIs predict the Peierls distortion (dimerization) of the hydrogen chain.[74] If, on the contrary, it is understood as an alternant hydrocarbon model, then DIs predict bond length alternation. Finally, this very simple example shows that DIs decay slowly in chains: the 1,6 value is as large as 0.0908.

Let us examine now the infinite chain ( $n \rightarrow \infty$ ) limit. It is easy to show that

$$\delta^{i,j} = \begin{cases} \frac{16}{\pi^2} \frac{j^2}{(i^2-j^2)^2} & (i+j) \text{ odd} \\ 0 & (i+j) \text{ even} \end{cases} \quad (117)$$

This analytical expression has several interesting readings. For instance, the open chain does not lead to bond equalization at its ends. The 1,2 and 2,3 DIs tend to 0.721 and 0.259, respectively. Equalization

is however achieved far from the edges, i.e. when  $n \approx n/2$ , where the DI tends to  $4/\pi^2 \approx 0.405$ .

As our main objective is regarded, if we take  $s = |j - i|$ ,  $\delta(s) \rightarrow 16/(\pi^2 s^2)$  (when non-zero), decaying algebraically as  $s^{-2}$ , in agreement with Taraskin and co-workers.[159] Figure 13 nicely shows the oscillating behaviour and the decay of the non-vanishing envelope for different sizes. Notice that, although the inverse square decay is only strictly valid at the  $n \rightarrow \infty$  limit, this is reached very quickly. This means that even for relatively small sized systems the polynomial decay should be clearly visible, should these model results extrapolate successfully to real systems.

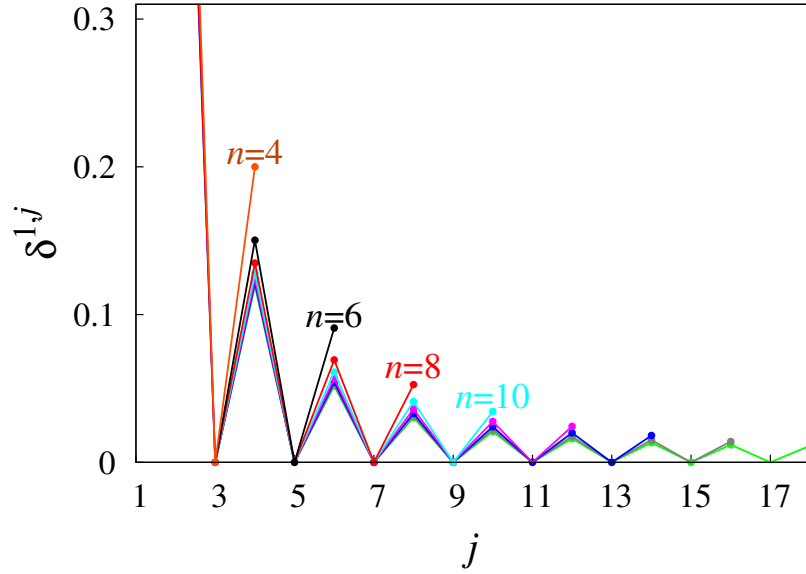


**Figure 6:** Hückel  $DI(1,i)$  for the homoatomic linear chain as its size ( $n$  sites) grows. Different lines correspond to different length chains. At the end of the chain  $j = n$ .

Let us finally recall that according to the eigenvalue expression shown above, the set of orbital energies is always enclosed in the  $\alpha \pm \beta$  range, evolving in such a way that the HOMO-LUMO gap  $\Delta$  closes as  $n$  increases. Expanding with respect to  $\gamma = 1/n$ , we get that  $\Delta(\gamma) = 2\pi(\gamma - \gamma^2) + \mathcal{O}(\gamma^3)$ . Similar expansions can be performed with the mid-chain first neighbour DI, so the DI may be used as an indicator of the gap for large chains, as figure 14 shows.

#### 4.4.2 The Hückel AB heteroatomic chain

A model for a chain insulator may be easily constructed by interpenetrating two different  $\alpha$  homoatomic lattices. Since all the physics is contained in  $\Delta\alpha = \alpha - \alpha'$ , we can arbitrarily set one of them (e.g.  $\alpha'$ ) to zero. This is a model for the valence electrons in LiH, for instance. Let us construct a chain with  $n$  ( $n$  even) sites, and order them

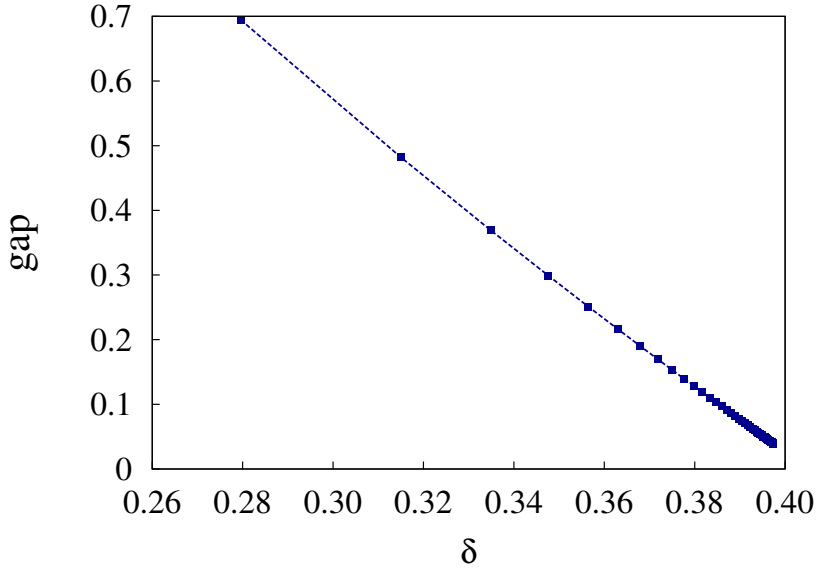


**Figure 7:** Evolution of the HOMO-LUMO gap against the midchain DI for the Hückel homoatomic chain. The length of the chain increases as the gap approaches zero (and the DI reaches its  $4/\pi^2$  limit). All data in a.u.

such that the first  $n/2$  are A ( $\alpha$ ) and the second  $n/2$  B (with  $\alpha' = 0$ ). Then the Hückel matrix is square-blocked,

$$\mathbf{H} = \begin{pmatrix} \alpha \mathbf{I} & \beta \mathbf{T} \\ \beta \mathbf{T}^t & \mathbf{0} \end{pmatrix}, \quad (118)$$

where  $\mathbf{T}_{ij}$  is again a Toeplitz tridiagonal matrix. Splitting eigenvectors into A and B components, the eigensystem is easily solved with a simple generalization of the Coulson-Rushbrook[36] theorem. The set of eigenvalues is

$$\epsilon_\mu = \frac{1}{2} \left( \alpha \pm \sqrt{\alpha^2 + 16 \cos^2(\mu\pi/(n+1))} \right), \mu = 1, n/2, \quad (119)$$

where the plus/minus sign differentiates the occupied/virtual solutions. Similarly,

$$\begin{aligned} c_\mu^{iA} &= \sqrt{2/(2-\tau)} c_\mu^i, \\ c_\mu^{iB} &= \sqrt{2(1-\tau)/(2-\tau)} c_\mu^i, \end{aligned} \quad (120)$$

with  $c_\mu^i$  as in the homoatomic chain and  $\tau = \alpha/\epsilon_\mu$ .

It is not difficult to show that this is a gapped system. In the infinite  $n$  limit, using a  $1/n = \gamma$  expansion similar to that used before,  $\Delta(\gamma) = \alpha + 2\pi^2\gamma^2/\alpha + \mathcal{O}(\gamma^3)$ , and the gap approaches  $\alpha$  on growing chain size, the faster the larger the  $\alpha$  value. Figure 15 shows the evolution of  $\text{DI}(1, j)$  for the  $n = 10$  heteroatomic chain with three different  $\alpha$  values. Notice how the results collapse on the homoatomic ones if  $\alpha = 0$ , and how the metallic-like oscillations get damped for small

values of  $\alpha$  to completely disappear as this parameter increases. This is a very interesting insight. It is also pretty clear that heteroatomic DIs decay much faster than homoatomic ones. All DIs converge extremely fast to the  $n \rightarrow \infty$  limit. For instance, with  $\alpha = 2$ ,  $DI_{(1,2)}$  attains the limiting 0.368 value at  $n = 8$ , with just 4 AB units.

Figure 15 also shows the onset of the exponential decay of DIs for even pretty small  $n$  values. Our  $\delta^{1,j} = \delta(s)$  falls off exponentially with exponent  $\lambda$  approximately equal to 1.5, 1.8 for  $\alpha = 3, 4$  respectively. Our finite chain results support the proportionality between the gap and  $\lambda$  in the small gap limit. In this case,  $\Delta \approx \alpha \approx 2\lambda$ . The faster the decay rate, the larger the gap. This is a valuable insight in molecular calculations.

#### 4.5 PERIODIC ANALYTICAL MODELS

The calculation of DIs from TB models in one to three dimensions has been pioneered by R. Ponec, who first presented a simple calculation,[132] later extended and reformulated.[133] His second paper actually provides tight binding results under the Mulliken condensation approximation discussed previously. DIs from DFT calculations over QTAIM or ELI real space domains are available since the work of Kohout and co-workers.[18, 80] However, all these authors have been more interested in first or second-neighbour DI values than in the decay rate of the indices. We will focus here on this second aspect for homoatomic lattices, referring the reader to the above-mentioned papers for further details.

Imposing periodic boundary conditions (PBC) on a lattice with one primitive function  $\chi$  per site allows us to use Bloch's theorem[74] to immediately write the one-electron Bloch functions as

$$\psi_{\mathbf{k}} = (1/\sqrt{N}) \sum_{\mathbf{R}} \chi(\mathbf{r} - \mathbf{R}) e^{i\mathbf{k}\mathbf{R}}, \quad (121)$$

where  $\mathbf{R}$  runs over real space lattice vectors,  $N$  is the total number of sites, and  $\mathbf{k}$  runs over the first BZ. Under a nearest neighbours TB (or Hückel) hamiltonian, the above Bloch ansatz leads to the following one-electron eigenvalues:

$$\epsilon_{\mathbf{k}} = \alpha + \beta \sum_{\mathbf{R}_n} e^{i\mathbf{k}\mathbf{R}_n}, \quad (122)$$

where  $\mathbf{R}_n$  only covers nearest neighbours.

In a 1D lattice with lattice parameter  $a$ , where  $-\pi/a \leq k < \pi/a$ , we will have  $\epsilon_k = \alpha + 2\beta \cos(ka)$ , which may be compared with our previous finite 1D results. To obtain the DI between two lattice sites, let us centre our reference frame at one of them (the 0 site, with  $\mathbf{R} =$

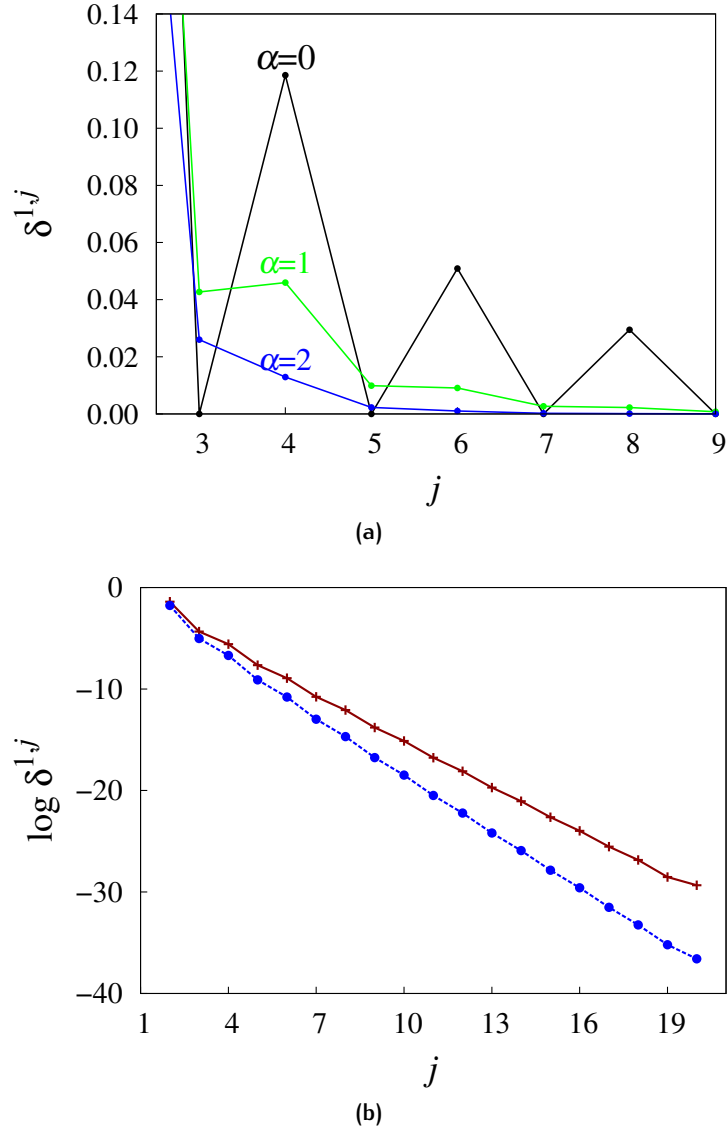


**Figure 8:** Top:  $\delta^{1,j}$  for the  $n = 10$  AB heteroatomic chain at  $\alpha = 0$  (black), 1 (green), and 2 (blue). Oscillations rapidly disappear as  $\alpha$  grows from 0. Bottom: Evolution of the logarithm of  $\delta^{1,j}$  for a  $n = 20$  chain with  $\alpha = 3$  (solid red with crosses) and 4 (dashed blue with dots).



0). The band (orbital coefficient) of this site is independent of  $k$ ,  $c_k^0 = 1/\sqrt{N}$ . That of site located  $r$  lattice parameters away,  $c_k^r = 1/\sqrt{N}e^{ikra}$ . Using then the Mulliken condensation scheme, and integrating over the BZ,

$$\delta^{0,r} = 4 \left\{ \frac{a}{2\pi} \int_{-\pi/(2a)}^{+\pi/(2a)} dk e^{ikra} \right\}^2 = 4 \sin^2(\pi r/2)/(r^2 \pi^2). \quad (123)$$

Of course, this result is equivalent to our previous infinite  $n$  limit, and shows that only if  $r$  is odd the DI does not vanish. PBC also leads to bond equalization. All nearest neighbour DIs are equal to  $4/\pi^2$ , independently of the lattice parameter  $a$ . This is of course a flaw of the TB hamiltonian. It is also relevant to comment on the on-site localization index (half the diagonal  $\delta^{0,0}$  value), which turns out to be equal to  $1/2$ , showing that half of the electron population is localized, half delocalized over the full lattice. Notice also that the sum rule  $1/2 \sum_B \delta^{A,B} = N_A = 1$  follows, since  $\sum_{i=0}^{\infty} 1/(2i+1)^2 = \pi^2/8$ .

Integration over the BZ in a 2D square lattice of lattice parameter  $a$  is again trivial, since the Fermi surface is a perfect square. Taking an arbitrary site of the lattice as origin  $O$ , we will label any other site with Cartesian coordinates  $(ra, sa)$  with the  $(r, s)$  integer pair,

$$\delta^{0,rs} = 4 \left\{ \frac{a^2}{(2\pi)^2} \int_{\text{FS}} dk_x dk_y e^{i(ra k_x + sa k_y)} \right\}^2, \quad (124)$$

which reduces to

$$\delta^{0,rs} = \begin{cases} 16/(\pi^4(-r^2 + s^2)^2) & r + s \text{ odd} \\ 0 & \text{otherwise.} \end{cases} \quad (125)$$

Our results show a more complex landscape than that provided by Taraskin and co-workers, who would describe an inverse third power decay. Here we show that the decay rate depends on the direction, following an inverse fourth power law envelope along the  $(1,0)$  direction. The localization index of each site is again equal to  $1/2$ .

The oscillatory pattern found in 1D is seen here to propagate in 2D. From a given site, the network of nodes with non-zero DIs resembles a check board. This behaviour is clearly related to the ability of this lattice to be decomposed into two  $45^\circ$  rotated interpenetrating alternate sublattices, like in alternate hydrocarbons. It seems that DIs between elements of the same sublattice vanish. Again, this may be understood in terms of charge fluctuation (covariance) if the allowed Pauling resonance structures are examined. Several interesting investigations regarding this should be undertaken. On the one hand, it would be interesting to check the behaviour of frustrated lattices. On the other, it would be of great interest to study also the chemical consequences (as noticed with mesomerism in 1D) of these patterns.

For the time being, it is relevant to shift to the crystalline coordinates of the sublattices. This can be done by using two new orthogonal coordinates  $p = r + s$ ,  $q = r - s$ . With this,

$$\delta^{0,pq} = 4/(\pi^2 p^2) \times 4/(\pi^2 q^2), \quad (126)$$

with  $p, q$  both odd, and  $\delta = 0$  otherwise. We thus see that the square lattice behaves as a Cartesian product of two 1D networks. With this expression, it is straightforward to show that the sum rule adding to the site population of 1 electron is also fulfilled.

Nodes along the (1,1) diagonal belong to the same sublattice ( $r + s$  is even, or  $q = 0$ ). The decay along  $p = \text{constant-odd}$  or  $q = \text{constant-odd}$  diagonals follows an inverse square power law, and if particular relations between  $p$  and  $q$  are satisfied along a nodes sequence, intermediate power laws also appear. We have found it difficult to obtain an analytical angularly averaged decay rate.

The non-trivial shape of the Fermi surface in the 3D case precludes an analytical integration over the BZ. Anyway, if we label nodes on the simple cubic lattice by the trio  $(r, s, t)$ , then

$$\delta^{0,rst} = 4 \left\{ \frac{a^3}{(2\pi)^3} \int_{\in \text{FS}} d\mathbf{k} e^{i(r,s,t)a\mathbf{k}} \right\}^2, \quad (127)$$

which may be reduced to simple numerical quadratures. The symmetry properties of the above expression allow us to assure that  $\delta^{0,rst}$  is only non-zero when  $r + s + t$  is odd, and we can again consider the lattice as composed of two interpenetrating sublattices such that  $\delta$  only communicates nodes belonging to different sublattices. We have no analytical decay rates, but clear numerical evidence points towards faster, likely inverse sixth power, decay speed. As an example,  $\delta^{0,100}$ , the nearest neighbours DI, is equal to 0.112 (to be compared to 0.405 and 0.164 in 1D and 2D, respectively).

Summarizing, extended TB models show algebraic decay of DIs in gapless homoatomic systems coupled to a very interesting interference cancellation that leads to wild oscillations that may be traced back to Friedel behaviour, from the physical point of view, or to resonance and mesomerism, from the chemical one.

## 4.6 SINGLE DETERMINANT (HF, KS) RESULTS

We will discuss here how the analytical models compare to actual one-determinant (or pseudo-determinant, in the case of DFT) calculations in hydrogen and lithium hydride toy systems. We have chosen interatomic separations for which these methods are known to provide reasonable answers, and a QTAIM space partitioning. We leave the true role of electron correlation aside, that we expect to consider

soon elsewhere. All calculations have been performed at fixed geometries. As we will see, the exact interference cancellation behind zero DIs disappears as we allow for the primitive functions to overlap. However, many of the insights developed from the Hückel or TB models remain valid.

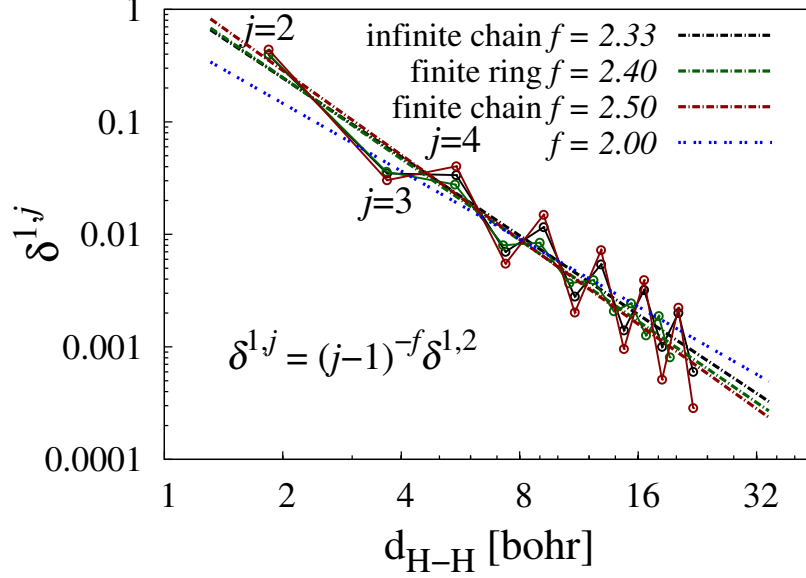


**Figure 9:** Logarithmic plot of  $\delta^{1,j}$  against the H-H distance in the H 1D infinite (black), cyclic finite with 42 atoms (green), and open-ended finite with 28 atoms (red) hydrogen chain. Linear fittings are superimposed to clearly observe the algebraic decay rate. The exponent of the power law decay,  $f$ , is to be compared with the Hückel or TB result,  $f = 2$ . This inverse square law is also represented in blue. The lattice parameter, or nearest neighbour H-H distance, is set to 1.84 bohr the theoretical limiting equilibrium parameter for a HF cyclic chain as  $n$  grows.

Figure 16 shows that actual calculations in 1D chains display deep oscillations, and that  $\delta^{1,2i+1}$  values are non-zero, but certainly much smaller than  $\delta^{1,2i}$  ones. Both odd and even envelopes evolve algebraically, with exponents larger than 2, but close to it. Several other points may be highlighted. For instance,  $f$  decreases approaching 2, as we move from open-ended finite to cyclic finite, and finally to PBC infinite chains. This is to be expected, since open finite chains differ considerably from the stringent approximations of the Hückel or TB models. We have also found that results in finite chains converge very quickly with size, as in the models, and that our computed values are quite close to those provided by the latter. For instance, DIs  $\delta^{1,2(4)}$  computed in the infinite chain are 0.44, 0.04, to be compared with the TB results, 0.39, 0.04, respectively.

Changing the lattice parameter does only introduce quantitative changes in the picture. For instance, at  $a = 2.5$  bohr, probably out of the confidence window where KS-DFT is reliable for this system (see

figure 17), the PBC chain  $f$  value equals 2.21, slightly closer to 2, the value that it should attain at dissociation values of  $a$ .

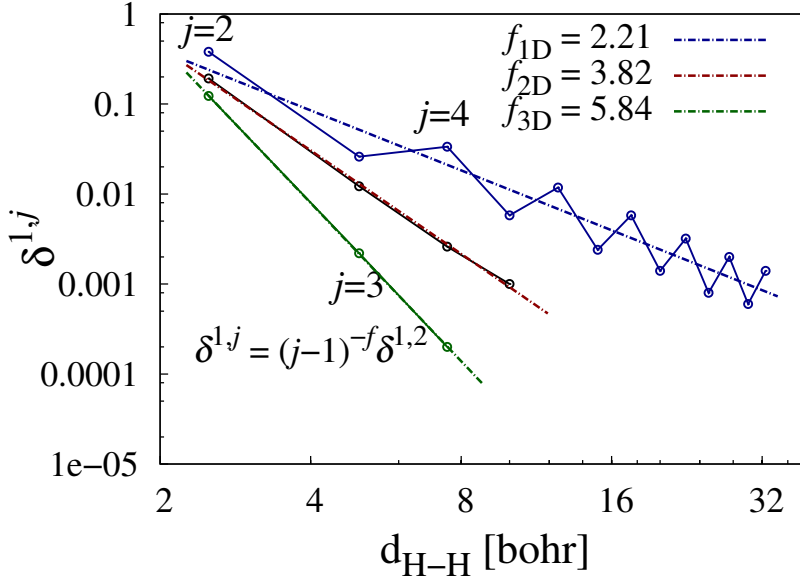


**Figure 10:** Logarithmic plot of  $\delta^{1,j}$  against the H-H distance in the H 1D (blue), 2D square (red), and 3D simple cubic (green) H infinite lattices for  $a = 2.5$  bohr along the 1, (1,0), and (1,0,0) directions, respectively.

Changing the dimensionality alters qualitatively the analytical results. We will show only PBC calculations in square and simple cubic 2D, and 3D H lattices, both computed at  $a = 2.5$  bohr. This is the lattice parameter used by Baranov and Kohout[18] (BK) in a seminal study of first neighbours DIs in solids. We use it here so that the reader may compare our values with those obtained by BK. Results at  $a = 1.84$  bohr do not differ qualitatively from those shown here. Figure 17 depicts that the decay is algebraic in the three cases, with  $f$  values roughly increasing in 2 units as we change dimension. What is noticeable is that oscillations disappear in 2D and 3D, while they widely persist in the TB models. We think that this is due to the increase in the number of neighbouring overlaps that contribute to the cancellation the destructive interference that lies behind the oscillations found in TB. In 1D, each site's primitive overlaps with 2 nearest neighbours, while in 2D and 3D this number increases to 4 and 6, respectively, or even more if we consider second neighbours. Be it as it may, our results clearly support an algebraic decay of DIs in gapless systems, with  $f$  values increasing steadily on going from 1D to 3D.

We now turn to insulating materials. This time we will present HF finite calculations in a (LiH)<sub>9</sub> 1D chain and a  $9 \times 9$  LiH square 2D foil, both with fixed Li-H distances equal to 3.0 bohr. In order to avoid as much as possible termination effects, we have built in each case models in which a Li or a H atom is placed at the centre of the chain (or foil). Figure 11 (top) shows the QTAIM DIs. As expected, their de-

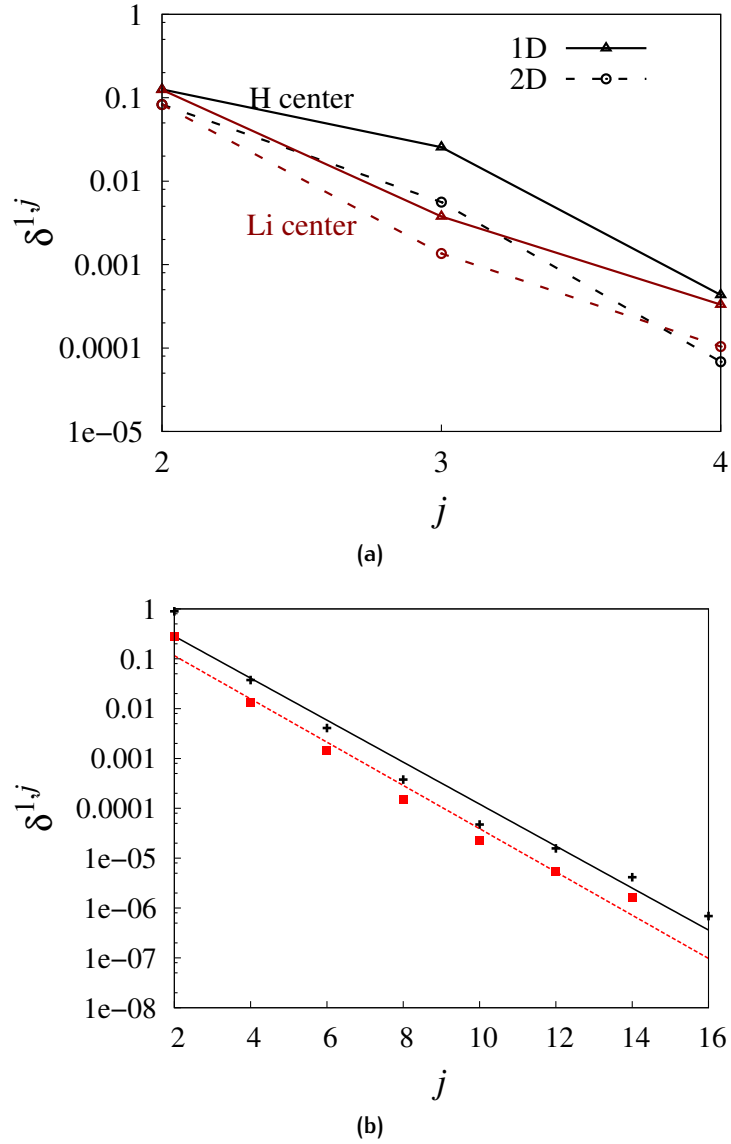


**Figure 11:** Top: Semilogarithmic plot of the QTAIM  $\delta^{1,j}$  against the node index in a LiH 1D chain (with 9 LiH units, solid line), and a LiH 2D square foil ( $9 \times 9$ , dotted line), both with  $a = 3.0$  bohr. The red (for Li) and black (for H) colours distinguish which atom is placed at the centre of the model and labeled as node 1. Only the  $(1,0)$  direction is shown in the 2D case. Bottom: Semilogarithmic plot of Löwdin  $\delta^{1,j}$  against the node index  $j$  in a LiH 1D chain of 17 LiH units, using also  $a = 3.0$  bohr. DI(Li,H) is shown with crosses, and DI(Li,Li) with squares. Minimum square lines are also shown just to aid the naked eye.

cay with distance is extremely fast. So fast, indeed, that we have not been able to obtain numerically reliable values beyond fourth neighbours. Notice that the existence of an AB lattice introduces three types of DIs: Li-Li, Li-H, and H-H. This is the origin of the kinks in the plot. For instance, the second neighbours ( $j = 3$ ) DI between Li atoms is almost one order of magnitude smaller than that between H atoms. With such a quick decay we have not enough data to support an exact exponential decay, but we can rule out a slow polynomial one. Notice also that the exponent seems to increase with dimensionality. This also explains why we have not added 3D data to the figure: numerical issues render even fourth neighbours unreliable for them. Decay rates do also depend on the direction, as expected, but numerical problems again preclude us from extracting precise conclusions. Numerical issues are much less important if instead of QTAIM basins we use equation 114 together with, for instance, Löwdin's orthogonalization. figure 11 (bottom) shows the exponential-like decay of these Löwdin DIs in a  $(\text{LiH})_{17}$  linear chain. DIs decrease 8 orders of magnitude on traversing the chain. Although the chemical interpretation of these Löwdin indices is prone to severe criticisms, they serve well our purpose of showing the evolution of decay rates.

Overall, analytical and real models support an exponential, non-algebraic decay of DIs in gapped systems.

Let us then wrap this Chapter up by gathering up the ideas we have been presenting. The search for real space descriptors that could discriminate metallic from insulating materials has been a recurrent quest in chemical bonding theory in the last decades. After the reformulation of Kohn's theory of the insulating state by Resta,<sup>[139]</sup> it is now known that electrical conductivity does not leave recognizable scars in the electron density itself. However, the modern theory of polarization, as the reformulation is known, points towards a possible link between electron delocalization measures and the insulating or conducting nature of a material. Previous knowledge in the physical literature had noticed that the decay rate of the 1-RDM changes from algebraic to exponential when going from metals to insulators in tight binding models. Here we have shown that since the delocalization index of real space theories of the chemical bond is dominated by the square of the 1-RDM, it must follow the same behaviour, so a link between bond orders (that is what the DI measures in isolated molecules) and conductivity appears.

To that end, we have solved several Hückel finite and TB extended models. As it turns out, even in fairly small molecular chains the shift from polynomial to exponential decay is evident when a gap is forced in the system, and the larger the gap, the faster the decay. Our results show that in metallic-like systems (because the gap does only close when we go from finite to infinite systems) the DI decays algebraically, wildly oscillating due to quantum mechanical interfer-

ence cancellations that annihilate the DI between nodes belonging to the same alternating sublattice. These oscillations have been shown to be intimately linked to Pauling resonant structures and chemical mesomerism, well known in alternant hydrocarbons. The dimensionality of the system simply changes the decay exponent, larger as we go from 1D to 3D.

Real computations within the HF or KS single (pseudo)determinant schemes together with a space partitioning according to the quantum theory of atoms in molecules, show that DIIs decay algebraically in metallic-like molecular systems, and very like exponentially, or at least extremely fast, in insulating-like ones. Oscillations persist after the inclusion of overlap in 1D chains, although the vanishing DIIs in the analytical models are now small, but non-zero. Overlap seems to block interference in larger dimensions, making oscillations to disappear (or at least dampen substantially).

Examining the decay of DIIs in real molecules and extended materials may provide very interesting clues to their conducting behaviour. Since DIIs may be computed between any pair of atoms, their decay may be followed along particular directions, making it possible to detect facile or non-facile conductivity channels. This may provide relevant information in material science and molecular electronics.

The impact of electron correlation on these results remains to be ascertained. We expect it to be small in simple systems at geometries close to equilibrium, but it should be important, yielding interesting insights into metal-insulator transitions, when the single (pseudo)determinant approximation ceases to be useful.

# 5

## DECAY OF DIS AND METALLICITY AT THE CORRELATED LEVEL

### 5.1 INTRODUCTION

Although the DIs have been computed in many systems, usually under the single determinant Hartree-Fock (HF) or Kohn-Sham (KS) approximations, the exact behavior of DIs is not known in general circumstances. This is particularly true as regards their response to changes in the A, B distance, since in most cases this implies an appropriate treatment of electron correlation. It has already been shown[57] that the profile of DIs along reaction coordinates reveals the nature of chemically relevant interactions, with sigmoidal profiles signaling the formation or breaking of chemical bonds and exponential shapes detecting non-bonding clashes. If read in terms of plain physical quantities, these findings tell us about the different patterns of electron delocalization taking place in both kinds of chemical processes.

As it was previously shown (see Section 4 and references[56, 56, 139, 158, 159]), in both finite molecules and extended systems DIs decay algebraically/exponentially for metallic-/insulating-like materials. This is true both in Hückel or TB models and in actual simple systems computed at the HF or KS levels. It was also found that DIs show an oscillatory behavior in metallic-like Hückel or TB models, vanishing whenever simple selection rules were satisfied. This behavior, related to quantum mechanical interference, persists in HF or KS calculations only in one-dimensional chains, disappearing in 2D and 3D systems. The oscillations observed in the DIs are interpreted in previous chapter in terms of the classical Pauling resonance theory or mesomerism, establishing a link between physical behaviour and chemical reactivity.

To close the loop, let us go one step further now and examine how the decay rate of DIs behaves under geometrical changes. In extended systems, this is coupled to the possible shift between a metallic and an insulating state, a metal-insulator transition (MIT). In molecules, to the shift from a sigmoidal to an exponential DI shape. Little is known about how DIs behave in these cases, since examining their long-range behavior in a geometrical rearrangement normally implies entering strong correlation regimes, which are difficult to deal with in large molecules.

To keep the discussion as simple as possible, the focus will be placed on the 1D cyclic hydrogen chain. This is no doubt one of



the simplest systems where a possible metal to insulator transition may occur, induced by the localization of electrons in their original potential wells as the H–H distance increases. This collective change is known as a Mott transition,[117] which is difficult to model with standard theoretical chemistry tools.

In a simple chemical language, increasing the H–H distance in the H-chain is equivalent to doing so in the  $H_2$  molecule. The simplest qualitatively correct solution in this case involves mixing two Slater determinants or, similarly, performing a complete active space CAS[2,2] calculation. Since the size of the CAS space explodes combinatorially if we consider a CAS[n,n] model when the number of atoms in the chain,  $n$ , increases, the problem soon becomes intractable with usual techniques. Notice that standard KS density functional theory (DFT) calculations are of no help here.

Many models have been proposed to cope with strongly correlated systems, being usually formulated in second-quantized language. For the problem treated here, the Hubbard hamiltonian[68] is the simplest one, since it allows for controlling the strength of electron correlation through a continuous parameter. When this parameter vanishes, the Hubbard model with nearest neighbour couplings falls onto the Hückel or TB one, so a relatively simple comparison with standard quantum chemical results is also at hand.

The Hubbard model has been extensively studied in one, two, three and infinite dimensions, at zero and finite temperatures, in all kind of lattices.[15] In 1968, Lieb and Wu[92] (LW) showed that the 1D Hubbard chain admits an analytical solution and that there is no Mott transition for this model, the ground state remaining a gapped anti-ferromagnetic singlet at any non-zero value of the correlating parameter. No analytical solutions have been found in 2D or 3D, but almost all approximate methods predict MITs.[15, 59]

Interestingly, a possible order parameter for the MIT is the so-called double occupancy,  $\mathcal{D}$ , that measures the probability of finding two electrons at a given node in the lattice (necessarily of opposite spin, for only one spinless state is available per site). At the MIT,  $\mathcal{D}$  drops to exactly zero, remaining so in the insulating phase. As it will be shown,  $\mathcal{D}$  is directly related to the real space (de)localization measures used in QCT, so another unexpected relation between seemingly unrelated concepts appears that deserves being considered.

This chapter will explore and compare the behavior of DIs in both the Hubbard model at different correlating parameters and in correlated descriptions of hydrogen chains. In the process, the origin of the sigmoidal shape of the DI in bond breaking processes will be proved to lie in the non-linear relation between the Hubbard correlating parameter and the interatomic distance. It will also be verified that the DI oscillations that characterize 1D metals in single determinant descriptions vanish as correlation increases and that their onset may be

understood as a transition from a tail-overlap-dominated regime to one in which quantum mechanical interference becomes prominent.

## 5.2 DELOCALIZATION MEASURES AND THE 1D HUBBARD CHAIN

The DI (equation 107) and the LI (equation 109) are defined as delocalization measures in real space, interpreted as descriptors that quantify the number of pairs of electrons shared (i.e. delocalized) between two real space domains of an N-electron system[10, 46].

As already noticed, the DI is a real space extension of the Wiberg-Mayer (WM) bond order[110, 162] (see equation 112). DIs and WM bond orders can be considered equivalent if we identify averaging over a real space domain with Mulliken condensation.[56, 106] DIs have been successfully used to quantify covalent bond orders for several decades, showing how a key chemical concept may be derived from orbital invariant quantities. The interacting quantum atoms (IQA) approach[51, 96] allows us to show that DIs are related to the covalent component of interatomic interaction energies.

Interestingly, as it is the case for the DIs (equation 115), the LIs also admit a statistical interpretation. It can be shown that

$$\lambda^A = n_A - \text{var}(n_A) = n_A - \langle (n_A - \langle n_A \rangle)^2 \rangle = n_A - (\langle n_A^2 \rangle - n_A^2). \quad (128)$$

Notice that only in the case that the electron population in a region does not fluctuate at all will  $\lambda^A$  be equal to  $n_A$ . The statistical connection introduces new insightful interpretations in chemical bonding theory. For instance, whenever the DI between two regions is non-zero, i.e. whenever they are *bonded*, the population of one responds to a fluctuation in the population of the other and vice versa. In other words, two regions are bonded together if there is a delocalization channel between them. In those circumstances, any perturbation in the electron population of one of them will be followed by a change in the population of the other. The interpretation of chemical bonding in terms of the fluctuation of electron populations or electron number distribution functions (EDFs) is being actively developed.[52, 54, 101]

Importantly, statistical variances and covariances may also be computed from EDFs, i.e. from the probabilities of finding a given number of electrons,  $p(n)$ , in each region. In this sense, it becomes clear now how the standard metal-insulator transition (MIT) order parameter, the probability of double occupancy of a site,  $\mathcal{D} = p(2)$ , is related to our real space descriptors. On the one hand,  $\mathcal{D}$  only vanishes for a Hubbard system when the variance at a site is zero. This is clear, but stems naturally from the average site population,

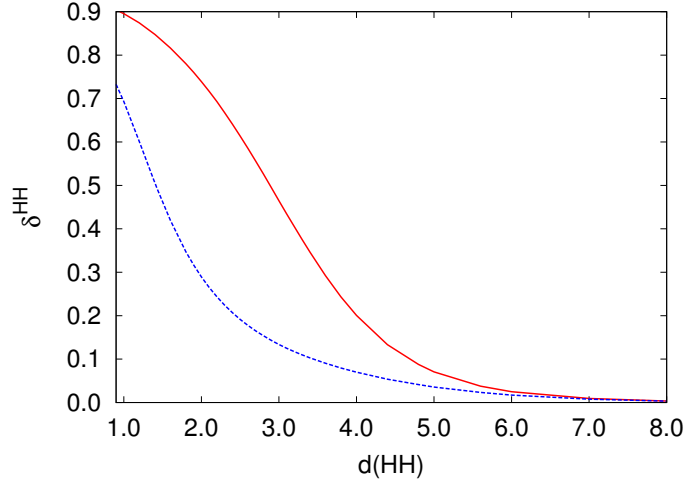


Figure 12:  $DI(H,H)$  for the  $X^1\Sigma_g^+$  (sigmoidal curve in red) and  $b^3\Sigma_u^+$  (blue) states of the  $H_2$  molecule computed at the CAS[2,2]//6-311++G(d,p) level.

$\langle n \rangle = 2p(2) + p(1) = 1$ , and the sum rule  $p(0) + p(1) + p(2) = 1$ . If  $p(2) = 0$ , then  $p(1) = 1$  and  $p(0) = 0$ . This means that, in terms of order parameters,  $\text{var} = 1 - \lambda$ , plays the same role as  $\mathcal{D}$ . Actually, the variance is more general and it only vanishes if the electrons are completely localized. It is also possible to resolve EDFs in spin components[101] and to define  $p(\uparrow\downarrow)$ , etc. It is also immediate to show that for the ground state H-chains with one average electron per site and using the symmetry  $p(2) = p(0)$ ,  $\text{var} = 1 - \lambda = 2p(2) = 2\mathcal{D}$ . With this, many of the results found in the physics literature about the Hubbard model can be directly read on the chemical scale.

Figure 12 shows the evolution of the DI with the internuclear distance in the singlet and triplet states of the  $H_2$  molecule, computed at the qualitatively correct CAS[2,2] level. This well-known behavior has been published many times[57] and is reproduced here for convenience.

Notice that in a diatomic,  $\text{var}(n_A) + \text{cov}(n_A, n_B) = 0$ , so  $\delta^{H,H} = -2\text{cov}(H, H) = 2\text{var}(H) = 4p(2) = 4\mathcal{D}$  is the direct analogue of the extended order parameter  $\mathcal{D}$ . As previously commented, the sigmoidal shape of the ground state DI is characteristic of (homolytic) bond breaking processes. The inflection point occurs at  $d(H, H) \approx 2.90$  a.u., where the DI is extremely close to half its maximum value. Similarly, the exponential behavior of the triplet is typical of non-bonded contacts. The origin of the ground state sigmoid is basically unknown. However, since the appearance of this shape is usually associated to cooperative effects, the relation between the DI and a phase transition order parameter points towards a possible clue that deserves further work.

### 5.2.1 The 1D Hubbard chain

One of the simplest models proposed to gain insight into the difficult strong correlation regime in the thermodynamic limit was proposed by Hubbard[68] and has been extensively studied so far. In its basic formulation it models a one-dimensional chain composed of identical single energy level sites (that can thus harbour two opposite spin electrons at most), subject to nearest neighbour interactions. In the half-filled band case, each site accommodates an electron on average, so it corresponds to an  $N$ -sites,  $N$ -electron problem. Usually, periodic boundary conditions are imposed and  $N$  is made to tend to infinity.

Two electrons are supposed to interact strongly only when located at the same site via a positive interaction energy  $U > 0$ , the so-called on-site Coulomb repulsion. They are also allowed to delocalize between neighbouring sites through a kinetic-like parameter  $t$ , known as the hopping energy, which is envisioned to be determined by the effective overlap of their site states. Although no exact link exists between the  $t, U$  Hubbard parameters and those of a conventional quantum chemical Hamiltonian, there have been many attempts that try to fit or approximate them. Particularly interesting in this sense is the work of Spalek and coworkers[86] who, through variationally determined renormalized single-particle wave functions, provide a chemically intuitive way to establish that connection.

With this, the Hubbard hamiltonian is now written in second quantized form as

$$H = -t \sum_{\langle i,j \rangle, \sigma} (c_{i\sigma}^+ c_{j\sigma} + c_{j\sigma}^+ c_{i\sigma}) + U \sum_i n_{i\uparrow} n_{i\downarrow}. \quad (129)$$

In the above expression, the  $c_{i\sigma}^+$  and  $c_{j\sigma}$  are fermionic operators that create or annihilate a  $\sigma$  spin electron at site  $i$ , respectively. They are subjected to standard anticommutator relations  $\{c_{i\sigma}, c_{j\sigma'}^+\} = \delta_{i,j} \delta_{\sigma,\sigma'}$ ,  $\{c_{i\sigma}, c_{j\sigma'}\} = \{c_{i\sigma}^+, c_{j\sigma'}^+\} = 0$ . The  $\langle i,j \rangle$  sum runs over first neighbours only, with each term describing the hopping of an electron from site  $j$  to site  $i$ . Notice that the anticommutation relation guarantees that the maximum occupation of a site is 2. Finally, the second term adds a Coulombic repulsion energy (a positive energy  $U$ ) to each site that is doubly occupied.  $t$  and  $U$  play opposing roles, so the model is conveniently described by the  $U/t$  dimensionless correlating parameter. Small  $U/t$  values favor hopping, thus delocalized solutions. As the correlating parameter increases, so does the penalty for electron hopping.

At a MIT, the system ceases to delocalize and each electron sits permanently at the same site. It is important to note on passing that the MIT parameter  $\mathcal{D} = p(2)$  equals  $\langle n_{i\uparrow} n_{i\downarrow} \rangle$ , so  $\mathcal{D} = de/dU$ ,  $e$  being

the energy per site. This means that if  $\mathcal{D} = 0$  in the Mott insulating state, the energy ceases to change with  $U$ .

From the quantum chemical point of view, it is interesting to examine the two sites Hubbard system, which is an analogue of the  $H_2$  molecule in a minimal basis. This textbook model is immediately solvable in the 6D space formed by the  $\binom{4}{2}$  states constructed by arranging two electrons in two nodes. Using  $r = U/(4t)$  as correlating parameter and defining  $\kappa = \sqrt{1+r^2} - 1$ , the two lowest states are a singlet, at energy  $E = -2t\kappa$ , and a triplet at energy  $E = 0$ . The probability of any electron configuration may be read directly from the square of the coefficients of the eigenvectors. The singlet is a mixture of Heitler-London-(HL) like covalent and ionic forms, while the triplet is fixed at its HL-like state. Notice that, since no explicit overlap appears, the triplet, for instance, is  $1/\sqrt{2}(\uparrow\downarrow + \downarrow\uparrow)$ . With this, it is clear that  $\mathcal{D} = p(2)$  vanishes for the triplet and that without overlap but with the antisymmetry restrictions, no interaction may occur, so  $E = 0$  constantly. Using the singlet eigenvector  $p(2) = 1/2 (\kappa/(1+\kappa^2))$ , which decays smoothly towards zero from its  $1/2$  starting value at  $r = 0$  as  $r$  increases. The statistics of the electron distribution for the singlet and triplet states follows the same trend as in a minimal basis full configuration interaction (FCI) under Mulliken condensation, and has the same  $r = 0, \infty$  limits. In this sense, the Hubbard model correctly captures the basic population correlations of the  $H_2$  molecule. Moreover, the  $U = 0$  limit of the Hubbard model may be mapped onto the Hückel (or TB) approximation if the Hückel  $\alpha$  and  $\beta$  parameters are set to 0 and  $-2t$ , respectively.

Surprisingly, Lieb and Wu (LW) showed in 1968[92] that the Hubbard infinite 1D chain has analytic solution and that the half-filled ground state is a gapped antiferromagnetic singlet at any  $U \neq 0$  value. The gap only vanishes at  $U = 0$ . There is no MIT transition, and the double occupancy  $\mathcal{D}$  ceases to behave as an order parameter, reaching zero only at its  $r \rightarrow \infty$  limit. No analytic solutions are known in 2D or 3D, but simulations[15, 59, 86] show that in these cases MITs develop at well defined  $r$  values.

It has also been shown[43] that, although not obvious from the Bethe Ansatz, all density-density correlations, i.e. the  $\langle n_i n_j \rangle$  expectation values for any two sites  $i, j$ , decay exponentially with intersite distance, as expected for an insulator. However, since at the  $U = 0$  limit the Hubbard solution falls into a metallic state with algebraic decay and oscillations in its DIs, it remains interesting to examine the behavior of this model and compare it with standard quantum chemical results.

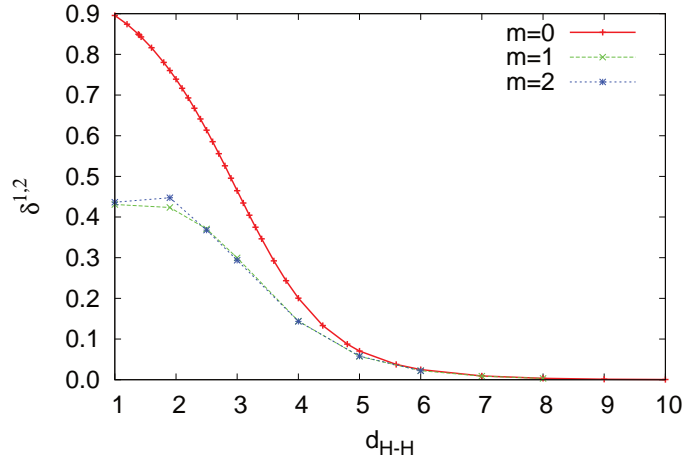
## 5.3 RESULTS

In this Section some results concerning the decay of DIs in Hubbard and real hydrogen chains are considered. To that end, Hubbard cyclic chains for lattices of increasing size with  $4m + 2$ ,  $m = 0, 1, 2, \dots$  sites have been exactly solved, examining their evolution with the correlating parameter  $r$ . 1D chains show very clear bond length alternation (precursors of Peierls distortions, as already shown[56]), so to simplify as much as possible, only aromatic-like cycles are considered. The Hubbard model effectively includes the Hückel or TB approximations when  $U = 0$ . Calculations have been performed using Lanczos diagonalization within the SPINPACK code.[144] As it will be shown, DIs (or density-density correlations) get quickly saturated towards the LW limit. The same H-cycles at different H-H distances  $a$  have been solved in regular polygon geometries with standard quantum chemical tools. Results at the HF, valence CAS, singles and doubles configuration interaction (CISD), and FCI levels using the GAMESS[142] code will be shown. Focusing on qualitative rather than on quantitative reasoning, simple 6-311+G, or even STO-3G basis sets in the FCI calculations, have been used. Delocalization measures have been obtained from QTAIM space partitionings, using the PROMOLDEN[2] code.

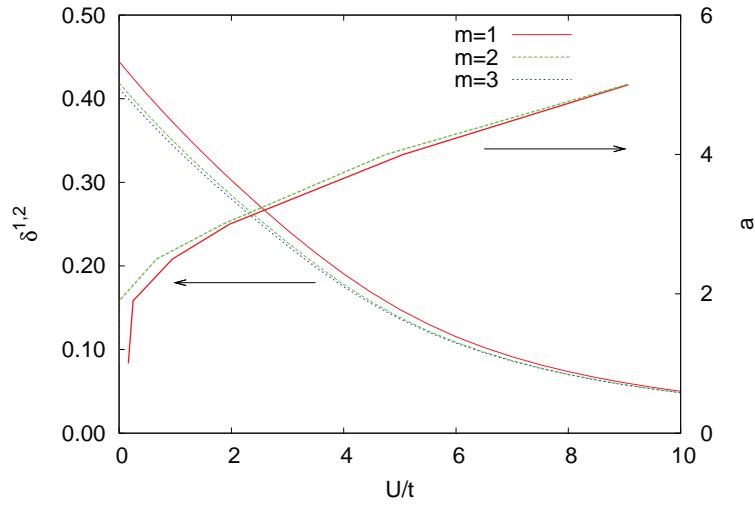
### 5.3.1 Saturation rate

The existence of the LW analytic solution allows to study the speed at which the quantum chemical or finite Hubbard chain results approach the infinite limit. There has been previous interest in the literature about the evolution of LIs or DIs in H-chains as regards their possible behavior as order parameters in MITs. For instance, Baranov and Kohout [17, 18] showed that symmetry broken (unrestricted KS, UKS) DFT LIs experience an abrupt transition from low to high LI as the lattice parameter of the infinite H-chain increases. Since many models, like the Gutzwiller Ansatz,[64] show a MIT in the 1D H chain, these results might simply signal that UKS displays a MIT transition, but do not help much in showing the proper behavior of the LI as  $r$  changes.

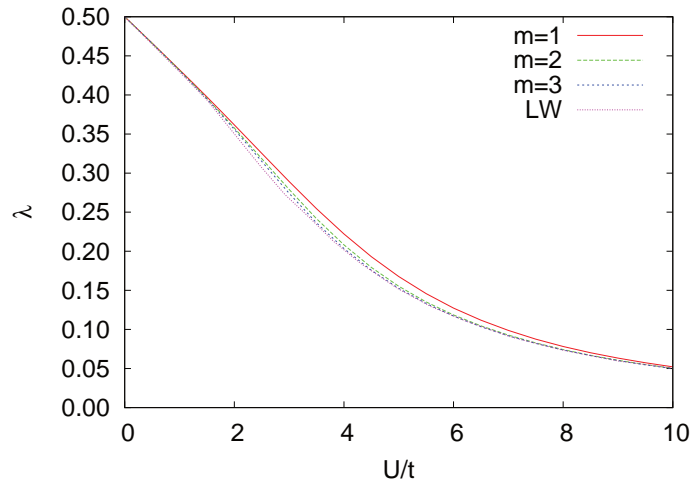
Figure 13 shows how size extensive valence CAS DIs, as well as finite Hubbard DIs and LI, behave with the lattice parameter  $a$  and  $4r = U/t$ , respectively, in cyclic chains with  $4m + 2$  nodes. Do not confuse the correlation strength  $r$  with the lattice parameter  $a$ . The saturation is very quick, at any  $a$  or  $r$  value, but only after comparing with the LW limit does it become clear that this rapid convergence is not an artifact of finite size models. Notice that it is possible to compare with analytic results at  $U/t = 0$ . In this case,  $\delta^{1,2} = 0.444, 0.419, 0.413, 0.409$  for  $m = 1, \dots, 4$ , respectively, and the  $n \rightarrow \infty$  value tends to  $4/\pi^2 \approx 0.405$ . All the CAS results show an in-



(a)



(b)



(c)

**Figure 13:** Saturation of LIs and nearest neighbour DIs with size for  $4m + 2$  cyclic chains. The upper diagram shows the evolution of DIs in valence CAS H-chains and the middle and bottom pictures those of DIs and LIs for Hubbard chains, respectively. The middle plot also shows a mapping of the  $\alpha, U/t$  relation, that should be read on the right scale, obtained from matching the CAS and Hubbard results. The bottom diagram contains the LW limiting LIs. All distances are in bohr.

flection point at about  $\alpha \approx 3.6$  bohr that is absent in the DI *versus*  $U/t$  Hubbard plots, much as shown in the  $H_2$  case. To understand the origin of the sigmoid from the CAS and Hubbard data a  $r(\alpha)$  map is generated. This has been done before with different models,[86] and as the middle plot in figure 13 reveals, the mapping is non-linear and quickly convergent. It appears that  $r$  grows slowly at small internuclear distances and faster as the distance increases.

The  $r(\alpha)$  non-linearity explains the sigmoidal shape of DIs as follows. A DI will show a zero second derivative with respect to  $\alpha$  due to the opposite signs of both terms in the following expression,

$$\frac{d^2\delta}{d\alpha^2} = \left(\frac{dr}{d\alpha}\right)^2 \frac{d^2\delta}{dr^2} + \frac{d\delta}{dr} \frac{d^2r}{d\alpha^2} \equiv ((r')^2\delta'' + \delta'r''), \quad (130)$$

so that the inflection point condition will be met when  $\delta''/\delta' = -r''/(r')^2$ . From the presented data, this occurs at about  $U/t \approx 4$  or  $r \approx 1$ , when the nearest neighbour DI is very close to half its maximum value (at  $r = 0$ ). This is an important insight, since it was previously shown[57, 102] that important chemical processes occur close to points where  $\delta \approx \delta^{\max}/2$ .

The saturation data show that the convergence of actual QTAIM LIs or DIs with  $n$  is similar to that shown by Hubbard models towards the LW solution. We are thus in a position to state that the evolution of either the LI or the nearest neighbour DI in the infinite H chain will be sigmoidal with  $\alpha$ , due to the non-linear  $r, \alpha$  map smoothly decaying with  $r$ , and that the discontinuity in the LI shown by UKS data[17] points to a fictitious MIT due to symmetry breaking.

### 5.3.2 Decay rate of DI(1,j)

The inter-site decay rate of DIs is a much less explored subject with possibly relevant repercussions on chemical thinking. Let us label the nodes of the cyclic chains from 1 to  $n$  and recall from a previous contribution that in the Hückel, TB, or Hubbard at  $U = 0$  models,  $\delta^{i,j}$  shows an oscillatory pattern, vanishing whenever  $i + j$  is even. This is a result of exact interference cancellation, that may be successfully interpreted in terms of Pauling resonance structures. In fact,[56] many important chemical effects, like mesomerism in conjugated systems, rely on this oscillatory propagation of electron delocalization. In the  $n \rightarrow \infty$  limit, the envelopes of all non-vanishing DIs decay with an inverse square law,  $\delta^{1,j} \rightarrow 4/(\pi^2(j-1)^2)$ . This signals the closure of the gap and the transition to a metallic extended system. It was also shown in that work that, although the long-range decay of the DIs for finite (gapped) chains might be exponential, their behavior for intermediate  $j$  values converges quite rapidly with  $n$  towards the inverse square law.



Exact vanishing of the odd  $j$  DIs is only observed if no direct through-space overlap between the nodes is allowed, as in the Hückel/TB cases. Real HF/KS calculations show that the oscillations persist in real systems when the geometries ( $\alpha$  values) lie in a range where we can trust in mean field calculations. However, exact cancellation conditions are now not met, and odd  $j$  DIs do not vanish, although their values are considerably smaller than their neighbouring even  $j$  partners. This is, in our opinion, sufficient to warrant mesomeric effects: non-monotonous decay of influence (delocalization) along the chain. Interestingly, exact cancellations do also occur in 2D and 3D Hückel/TB models, but seem to disappear in single-determinant computations.

The effect of electron correlation on this picture is not well known. On the one hand, on finite systems, correlation does not influence the presence of a gap, so the long-range decay of  $\delta$  should be exponential. On the other, the exact, true thermodynamic limit of the H chain is not available, but the LW solution also shows long-range exponential decay at any  $r$ . This does not preclude interesting chemistry at mid-range distances. By naïvely interpolating these ideas, a possible scenario appears in which, at large  $\alpha$  or  $r$  values DIs do not show any anomaly, decaying exponentially such that  $\delta^{1,i} > \delta^{1,j}$  if  $i < j$ . For small  $\alpha$  or  $r$  parameters, however, a transition towards an oscillatory pattern, converging on the  $j$ -parity rule, should be found.

Figure 14 shows the decay of  $\delta^{1,j}$  with the intersite H-H distance for a  $H_{14}$  cyclic chain with  $\alpha = 1.84$  bohr for several levels of theory. Each type of result has also been fitted to a polynomial decay law to show the shift in tendencies. As expected, once the zero  $j$  values have been removed from the Hückel results, we get the slowest decreasing model, with an exponent  $f \approx 1.43$ . This tends to exactly 2, the theoretical value in the  $n \rightarrow \infty$  limit. As it can be clearly seen, all the other theory levels predict oscillations compatible with mesomeric or medium-range delocalization effects, much as in a metallic-like system, but with all odd  $j$  DIs not vanishing now. Among the realistic models, the mean-field HF solution is the one with slowest decay, and the main effect of including electron correlation is a general decrease of all DIs. Interestingly, the situation is quite similar to that already examined in the  $H_2$  molecule, where the DI converges toward the exact value in a damped oscillatory pattern as the amount of correlation considered increases.

Inclusion of only static correlation at the CAS level has a large impact on DIs. As  $f$  tells us, the CAS data decay fastest of all. Addition of dynamical correlation at the CISD level dampens the CAS decrease and consideration of all possible excitations at the FCI level (even with a minimal basis) again reacts back slightly. In any case, at this internuclear distance where the HF approximation is still reason-

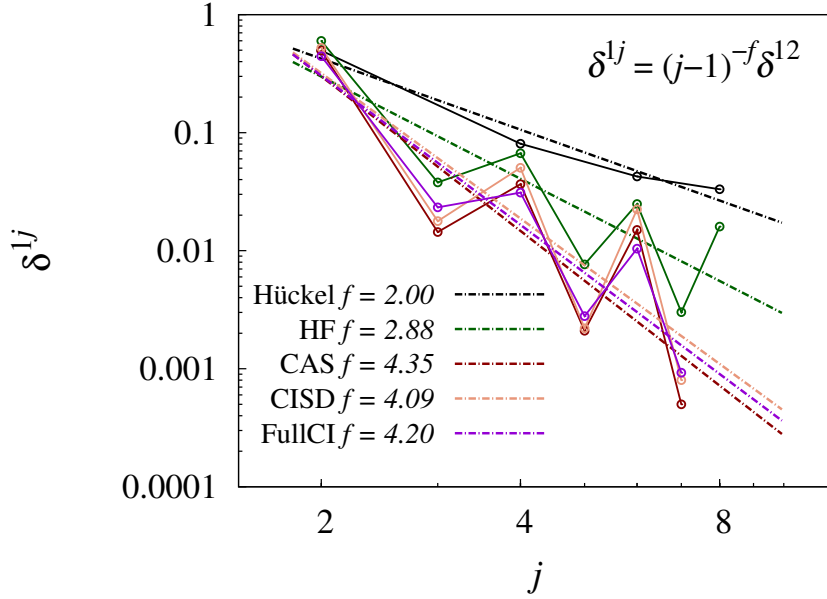
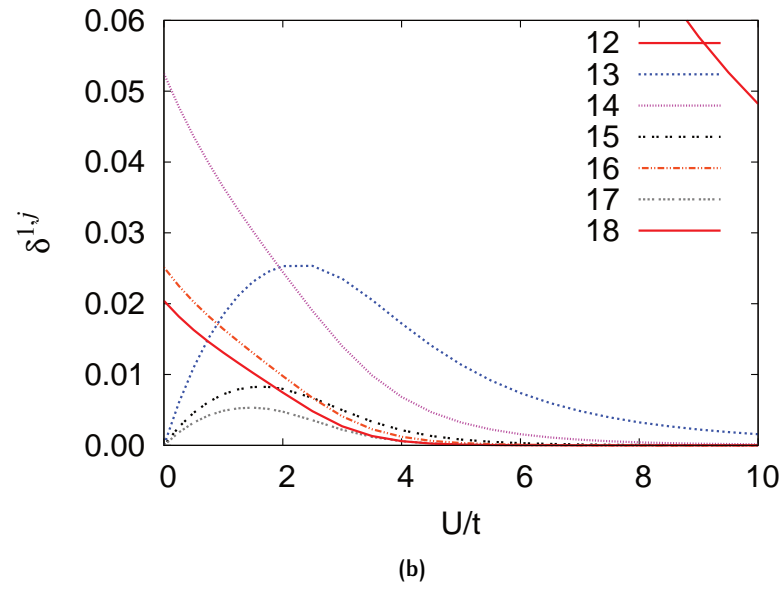
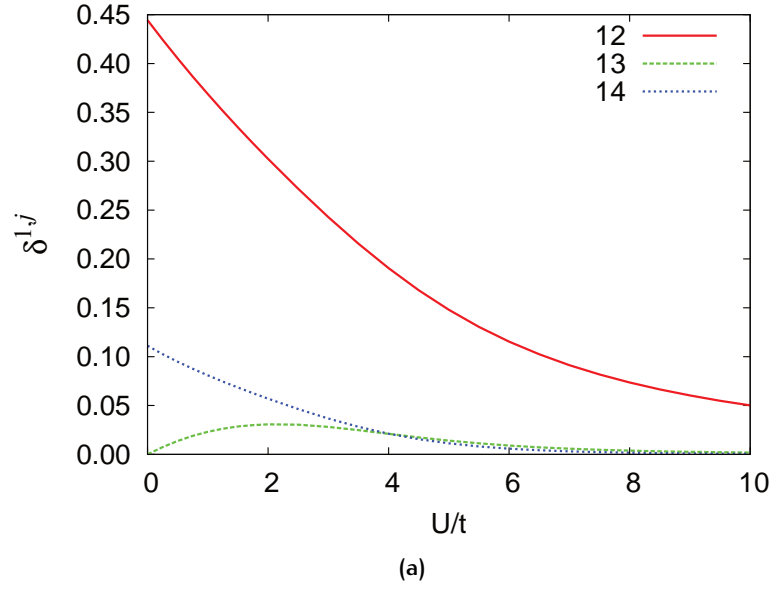


**Figure 14:** Evolution of  $\delta^{1,j}$  with  $j$ , equivalent to the intersite distance for the  $H_{14}$  cycle at different levels of theory, with  $a = 1.84$  bohr. Notice the double logarithmic scale. A linear fit of each set of data, with explicit description of the  $f$  exponent is also shown, so that  $\delta^{1,j} \approx (j-1)^{-f} \delta^{1,2}$ . Be aware that the fit is done with both high and low values. Odd  $j$   $\delta$ 's vanish at the Hückel level, so only even  $j$ 's are included in that case.

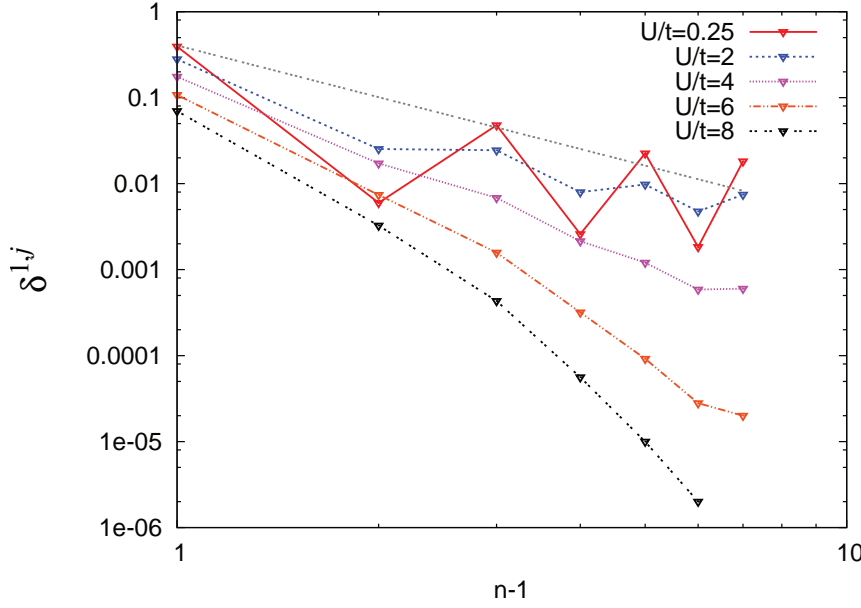
able, introduction of correlation seems to alter quantitative, but not qualitatively, the oscillatory decay.

Figure 15 shows two examples (with 6 and 14 sites) of the effect of the increase of  $r$  on the oscillatory pattern of DIs in the Hubbard chains used here. The behavior exemplified is general. At sufficiently large  $r$ , the canonical decay expected for an insulator is recovered and  $\delta^{1,j}$  decreases on increasing  $j$ . Decreasing  $r$  takes us to a point where a first crossing is met. This signals the onset of quantum mechanical interference in electron delocalization and once this barrier is crossed, the  $\delta^{1,j}$  order is no longer canonical. Successive crossings end up with the Hückel alternation, with vanishing odd  $j$  DIs. Interestingly enough, the first crossing between DIs on decreasing  $r$  occurs again, independently of  $m$ , very close to  $r = 1$  or to  $U/t = 4$ .

As expected, the Hubbard chains show a very interesting transition. Whatever the number of sites, the DIs go from an asymptotic regime with large  $r$ , decaying smoothly with intersite distance, to a regime at small  $r$ , where interference effects give way to a non-monotonous oscillatory decay. Since these oscillations are one of the fingerprints of mesomeric effects, we firmly think that electron correlation plays against it. This adds to other studies showing that the classical rules used in light element chemistry may not hold at all with heavy element analogues as electron correlation strengthens its role.



**Figure 15:** Decay of  $\delta^{1,j}$  for  $4m+2$  cyclic Hubbard lattices with  $m = 1, 3$  versus  $U/t$ .



**Figure 16:** Evolution of the decay rate of  $\delta^{1,j}$  for the 14 sites cyclic Hubbard chain with  $U/t$ . Notice the doubly logarithmic scale.

The transition from the oscillatory to the monotonous decay regime in the 14 sites chain is also shown in figure 16. Not surprisingly,  $r \approx 1$  (or  $U/t \approx 4$ ) is found to be the approximate boundary between the two situations. At  $U/t = 8$  delocalization is hampered so much that the asymptotic infinite  $n$  limit has been fully entered, which is found to be exponential.[43]

How this image readjusts in real H chains is the next focus. Figure 17 shows the quantum chemical results on the  $H_{10}$  chains, at several levels of theory and at varying  $\alpha$  values. Most of the relevant points regarding the behavior at small H-H distances have already been commented. The parity rule (odd-even  $j$  alternation) is obeyed at all theory levels, with damped CAS, CISD, and FCI alternation.

As  $\alpha$  increases, the mean-field, single-determinant HF model becomes unable to localize the electrons in their atomic domains (or sites), and the DI continues oscillating. At  $\alpha = 3.5$  bohr, close to  $r = 1$  according to the  $r, \alpha$  mapping, the parity alternation of DIs no longer holds for both the CAS and the FCI descriptions, but continues at the CISD level. At larger distances all signs of oscillatory behavior disappear for the CAS and FCI, and continue at the HF and CISD levels. A first obvious conclusion is immediate. In order to qualitatively follow the evolution of electron delocalization, size consistency is a must and the CISD method soon ceases to behave properly.

A second important point is that, once the consistency issue is assumed, quantum chemical and Hubbard data are surprisingly compatible, pointing towards the generality of our results. Although density-density correlations are known to decay exponentially in the

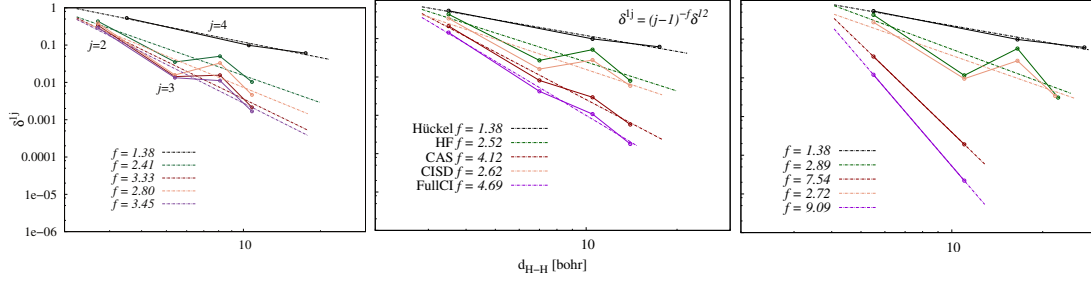


**Figure 17:** Decay of  $\delta^{1,j}$  for the  $H_{10}$  ring at three H-H distances: 2.7 (left), 3.5 (centre) and 5.5 (right) a.u., and various levels of theory. Notice that the fit includes all the data.

long range regime at any  $r \neq 0$  for the Hubbard infinite chain,[43] this by no means excludes interesting phenomena at short- or mid-range. We think to have convincingly shown that this is the case and that delocalization of electrons in real chains will suffer a transition from oscillatory to monotonous decay as correlation is increased.

To summarize, in this Chapter, the spatial decay rate of real space delocalization measures as electron correlation increases has been analyzed. After showing that DIs decay according to inverse power laws in metallic-like cases and exponentially in insulating-like moieties[56] for single-determinant and Hückel models, we go one step further, examining the validity of those insights when electron correlation is switched on.

The consideration of electron correlation as a variable opens the possibility of examining transitions between insulating and metallic phases upon simple geometrical rearrangements. These Mott insulating transitions (MIT) play an important role in contemporary condensed matter physics. Correlation also poses important problems for standard quantum chemical procedures, since MITs are collective phenomena (involving many particles) in the strong correlation limit (that needs from considering a combinatorial number of Slater determinants). It is therefore important to combine standard calculations with models of strong correlation to ascertain the reliability of the results. By using the standard Hubbard hamiltonian at half-filling, the amount of correlation can be controlled by a simple parameter  $r$ .

The systems analyzed here are restricted to simple finite and infinite H rings, examined under several standard quantum chemical theoretical levels and the Hubbard approximation. The latter admits an analytic solution in the infinite 1D chain, as found by Lieb and Wu[92] who showed that no MIT exists and that the system is an insulator for any  $r \neq 0$ .

A first insight is that the standard order parameter used to detect MITs, the double occupancy probability of a site, that vanishes at the MIT, is directly related to the localization index (LI). In fact, the latter is a generalization that might be used in general systems. LIs and

DIs show a quasi-universal sigmoidal behavior with intersite distance in bond breaking processes[57]. It is shown that the origin of this sigmoid lies in the non-linear relation between inter-site distance and the  $r$  correlating parameter, and that its inflection point is found at  $r \approx 1$ .

It has also become clear that DIs and LIs converge quickly with chain size. We can confidently state that the LI in the H chain will decay smoothly to zero as  $r$  or  $\alpha$  increases and that the jump shown in a previous work[17] is due to symmetry breaking.

Although DIs must decay exponentially at long range for the infinite Hubbard chain, light has been cast on the behavior of the metallic-like oscillations shown in mean-field models, that survive at short and midrange when  $r$  is small, to further disappear as  $r$  increases. At about  $r = 1$  they vanish and a clear exponential behavior sets in. Due to the link between DIs and core chemical concepts like bond order, bond conjugation, mesomerism, etc, these results imply a possible wide impact in chemistry. Conjugation and mesomerism, for instance, will not survive in strongly correlated analogues of alternant hydrocarbons.

Extension to further dimensions and/or systems should be done. As soon as the 1D chain is abandoned in favor of 2- or 3D analogues, true MIT will appear. After the analysis set forth, it comes out that the variance of the electron population at a given site (VAR, related to the LI) may be used as a general order parameter in real simulations. At a MIT, the VAR will show a jump, but will not vanish exactly, as it happens in the Hubbard model (where, for instance, VAR is null in the triplet state of  $H_2$ ). VAR will remain non-zero when computed quantum chemically, due to exponentially decreasing, but non-vanishing overlap of same spin electrons onto neighbouring atomic domains.

Finally, the results shown here have implications about the profile of DIs in chemical processes. Inflection points in those cases where sigmoidal shapes appear mark the switch from short to long range delocalization. At smaller  $\alpha, r$  values the regime is bonded, covalent-like, while at larger ones it turns to the non-bonded, exponential overlap region. Given the  $\alpha, r$  map, increased correlation will suppress covalency. This has been put forward repeatedly, but stems very neatly from our results.



## **Part IV**

# **The Electron Distribution Function (EDF) in the solid state**





## 6

ELECTRON DISTRIBUTION  
FUNCTIONS (EDF)[100]

As already mentioned above, the most common strategy to confront the study of the chemical bond is to partition the space into chemically meaningful regions. Among the many proposed schemes, the QTAIM [12] has been a rather successful one for it yields a partition in regions embodied with a very convenient physical meaning: once the space is divided into regions or basins, we can take any point of the 3D space  $\mathbf{r} \in \mathbb{R}^3$  and assign it to the atomic region  $\Omega_i$  that encloses it, or mathematically  $P : \mathbf{r} \rightarrow \Omega_i, \mathbf{r} \in \Omega_i$ . The partition  $P$  is exhaustive and can be envisaged as a coarse-grained mapping of the electron network since it consists of the replacement of every point inside a given basin by the basin itself. So gathering together all the information given in this paragraph, starting from a partition of the space in atomic regions that exhaustively fills the space, we make every electron correspond to its basin (or we coarse-grain, condense or basin average them) and we end up with a real space image of a resonance structure.

Let us make a set of snapshots of the positions of the electron of a system. Given a sufficiently large number of them, their statistics will be those of the quantum mechanical behavior. Let now a given number of electrons of the system  $c_A, \dots, c_M$  be condensed, i.e., always associated to them, over each of the  $m$  basins  $\Omega_A, \dots, \Omega_M$  in which we divide the system, and let us group them in the vector  $\mathbf{C} = (c_A, \dots, c_M)$ . Since not all the electrons are necessarily condensed, some of them can be left free, albeit still being assigned to a basin  $\mathbf{F} = (f_A, \dots, f_M)$  at each snapshot. If we do not distinguish between condensed and free electrons within each basin, we speak of a real space resonance structure,

$$\mathbf{S} = \mathbf{C} + \mathbf{F},$$

a partition of the electrons in regions, that describes the total number of electrons in each basin  $\mathbf{S} = (n_A, \dots, n_M)$ . In these expressions,  $c_j, f_j$  and  $n_j$  correspond to  $c^{\Omega_j}, f^{\Omega_j}$  and  $n^{\Omega_j}$ , respectively, and  $\sum_j c_j = i, \sum_j f_j = \mathcal{N}$  and  $\sum_j n_j = N$ . Note that we can condense any number of electrons  $0 \leq \mathcal{N} \leq N$ .

Both the partition and coarse-graining are now used to define from the  $N$ -electron density matrix (DM) or the probability density

$\rho_N(1, \dots, N) = \Psi^*(1, \dots, N)\Psi(1, \dots, N)$ , the coarse-grained density matrices (CGDMs), which have the form

$$\rho_i(\mathbf{r}_1, \dots, \mathbf{r}_i)[C] = I \int_{D_c} d\mathbf{r}_{i+1} \dots d\mathbf{r}_N \rho_N(1, \dots, N). \quad (131)$$

With  $D_c$  we mean a domain such that each of the condensed electrons is integrated over its associated basin: electrons  $(i+1)$  to  $(i+c_A)$  are integrated over basin  $\Omega_A$ , electrons  $(i+c_A+1)$  to  $(i+c_A+c_B)$  over basin  $\Omega_B$ , etc.  $I = N!/(i!c_A \dots c_M!)$  accounts for the indistinguishability of the electrons.

The sum over all possible condensations of the  $\mathcal{N} = N - i$  electrons over all the CGDMs yields the traditional total reduced DM

$$\rho_i(\mathbf{r}_1, \dots, \mathbf{r}_i) = \sum_{\{C\}} \rho_i(\mathbf{r}_1, \dots, \mathbf{r}_i)[C] \quad (132)$$

Let us now consider the special case where only one big basins exists,  $\Omega_i = \mathbb{R}^3$ . In that case  $F = 0$  since it is not possible to define free electrons as there is no neighbour basin they can move to, and only one resonant structure is possible, result of the condensation of all the electrons, so  $C \equiv S = (N)$ . The total reduced DM is  $\rho_0()[N] = 1$  since all the electrons have to exist within the basin and it carries no relevant information. However, in the case of a partition that results in  $m$  basins, the zeroth order CGDMs yields the probability of a total condensation of the electrons in a given configuration over the  $m$  regions the space was divided into, that is to say, the probability of a resonant structure, also called a coarse-grained probability distribution (CGPD) or electron distribution function (EDF). If we use  $p = \rho_0()$ , the probability of finding the  $N$  electrons distributed according to  $S \equiv C$  is given by

$$p(S) = \rho_0()[S \equiv C] = p(n_A, \dots, n_M) \quad (133)$$

Usually, one is only interested in a subset of the  $m$  atomic basins. Let us then call this subset  $k$  and define an additional basin formed by the union of the rest  $m - k$  basins. The total number of basins is then  $k + 1$ . The probability are obtained according to:

$$p(n_A, \dots, n_K, n_M) = \rho_0[n_A, \dots, n_K, (N - \mathcal{N})^{\bar{A}}] = I \int_D |\Psi|^2 d\tau, \quad (134)$$

where the electrons in the subset of interest are fully condensed  $N = n_A + n_B + \dots + n_M = \mathcal{N} + n_M$  and we have grouped together all the basins outside the subset of interest under the superbasis  $\bar{A} = \Omega_M$ . From equation 134 we obtain then the probabilities of finding  $n_A$  electrons within basin  $\Omega_A$ ,  $n_B$  electrons within  $\Omega_B$  and  $n_M$  electrons within basin  $\Omega_M$ .  $D$  specifies a domain where the  $n_A$  electrons are

integrated over basin  $\Omega_A$ , the  $n_B$  electrons over  $\Omega_B$  and the rest  $N - N$  electrons contained in the  $m - k$  over the superbasin  $\Omega_M$ .

The subindex  $i$  designates the nucleus of the atom embraced by the atomic basin  $\Omega_i$ , so that one possible resonant structure in Pauling's terms will be  $S = (n_A, \dots, n_M)$ , noting that any basin can be empty,  $n_i = 0$ . There are  $N_S = (N + m - 1)! / (N!(m - 1)!)$  of these structures, a combinatorial number that is 3 in  $H_2$ , 66 in  $H_2O$  or 286 in  $NH_3$ , but climbs to 76 223 753 060 in benzene. This number is in reality reduced to just a few chemically relevant structures. In the case of  $C_6H_6$  for instance, condensing all the 46 electrons in one H basin will have a negligible weight. The probabilities that result from the  $N_S$  resonant structures can be grouped in an EDF vector  $\mathbf{p}_N$ . The addition of all the probabilities follows of course

$$\sum_{\{S\}} p(S) = \sum_{\{S\}} p(n_1, \dots, n_m) = 1, \quad (135)$$

so  $p(S)$  can be considered as the weight of a certain resonant structure, that is obtained from the wave function of a system, or a model of it, regardless of the origin of it and with no previous assumptions or prescriptions.

## 6.1 THE 2-CENTER, 2-ELECTRON PARADIGM

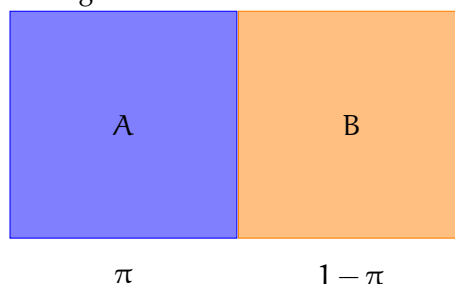
Let us consider a partition of the space into two distinct regions A and B as in figure 18. The probability of finding one electron in region A is  $p^1(1, 0) = \pi$ , and as the particle must exist somewhere, the probability of the same event in region B must be  $p^1(0, 1) = 1 - \pi$ . If we deal with independent particles, the probabilities resulting from adding one more independent particle to a system formed by one electron will be just products of the former probabilities  $p^2 = p^1 \otimes p^1 = (\pi, 1 - \pi) \otimes (\pi, 1 - \pi)$ . Following a Tartaglia-like order, the probability vector for a system of  $N$  electrons and two basins  $\mathbf{p}_N$  will be  $\mathbf{p}_N = (p(n_A = N, n_B = 0), p(n_A = N - 1, n_B = 1), \dots, p(n_A = 0, n_B = N))$ . In the case of 2 electrons in 2 regions

$$p^2((2, 0), (1, 1), (0, 2)) = (\pi^2, 2\pi(1 - \pi), (1 - \pi)^2), \quad (136)$$

and there are only three possible setups for both electrons between the two basins, distributions that are described by only one probability  $\pi$  in what we know as a binomial distribution (BD). It can be generalized as

$$p(n_A, n_B) = \frac{2}{n_A!n_B!} \pi^{n_A} (1 - \pi)^{n_B}. \quad (137)$$

**Figure 18:** The binomial distribution implies independent particles and only one probability suffices to describe all the possible ways of distributing two electrons in two basins.



Since for two electrons there are 3 probabilities, it is useful to visualize the probabilistic landscape in a triangular diagram, as shown in figure 19. Any point within figure 19 is fully determined once any two independent probabilities are fixed. Let us then carefully inspect this diagram and, passing through, take advantage of the fact that it also contains information on electron delocalization to introduce the connection between DIs and EDFs.

The three corners of the triangle correspond to the three possible ways of locating two electrons in two regions. The probabilities of each configuration are obtained from the axis clockwise from the corner it corresponds to. Besides the two bonding paradigms of non-interacting particles  $p(1,1) = 1$  and ionic bonding  $p(2,0) = p(0,2) = 1$  represented by the corners, there are two additional cases that are also chemically relevant: the covalent and charge-shift or VB ionic bonding situations. We will briefly go through all these four cases, which are summarized in figure 20.

Let us focus on the red curve of figure 19, which shows the independent particle situation where the electronic correlation is zero, and hence represents the BD described by Equation 136. As it was already mentioned, along the BD line the  $\mathbf{p}^2$  vector is fully determined by just one quantity  $\pi$ : the probability that one electron occupies one of the regions. Let us take the point of zero slope of the red curve (blue circle in figure 19) as an example of how to read the diagram. The probability of the (1,1) event is read in the right axis, which takes the maximum value at the (1,1) corner. We follow then the line parallel to the axis opposite to our corner rightwards (orange line in figure 19) and we will find a probability of 0.5. The event (2,0) has a value of 0.25 obtained by sliding upwards along a line parallel to the (1,1)–(0,2) axis that crossed the point we are analyzing (gray line). The same probability is obtained for the (0,2) event if we now go until the crossing between a line parallel to (2,0)–(1,1) that passes through the point of interest and the (2,0)–(0,2) axis (blue line). The dotted curves are there to help us find the different probabilities of any point within the triangle.

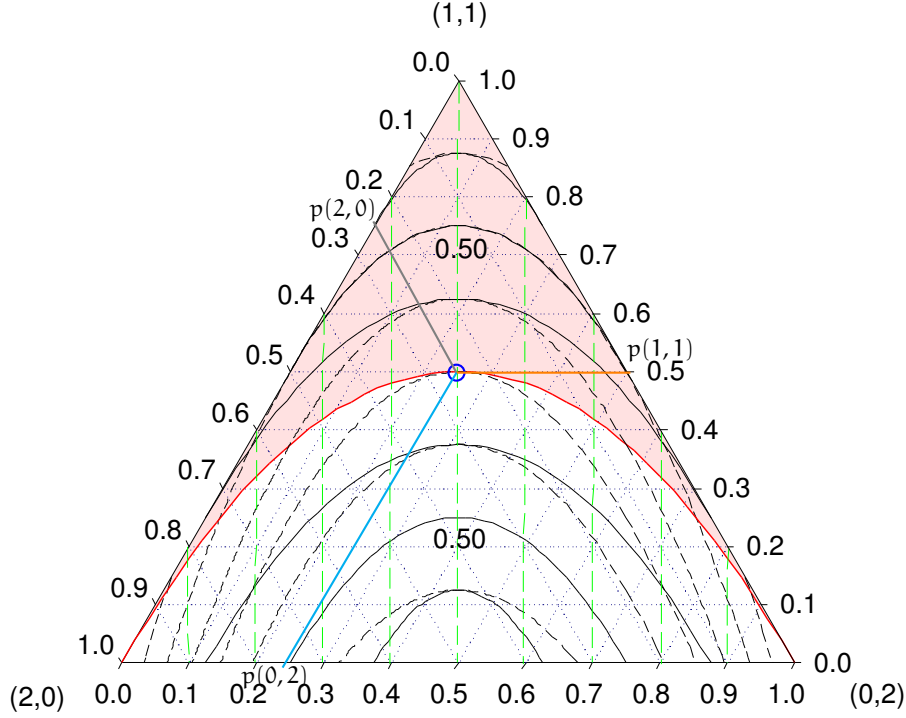


**Figure 19:** Ternary representation of the (2c,2e) EDF. Each corner represents the events  $p(1,1)$ ,  $p(2,0)$  and  $p(0,2)$  equal to unity, respectively, and in terms of which, the coordinates of any point in the diagram are given. As an example, the coordinates of the blue circle are obtained from the distances between the point and the side opposite to each corner, as the gray  $-p(2,0)-$ , orange  $-p(1,1)-$  and blue  $-p(0,2)-$  lines show (see text for details). Isolines of  $f$  start at the bottom ( $f = -1$ ) and increase in 0.25 units following the solid lines until the top corner ( $f = 1$ ) is reached. Dashed curves are  $\delta^{A,B}$  isolines that decrease 0.25 from  $\delta^{A,B} = 2$  at the bottom to  $\delta^{A,B} = 0$  at the top. Constant values of charge transfer (also constant  $\pi = (1 + q)/2$ ) are found along the vertical dashed lines, that increase 0.2  $e$  from  $q = -1 e$  to  $q = 1 e$  on going from left to right. Any point on the red curve would represent a  $f = 0$  binomial distribution  $p_2^b$ , which in turn separates the upper (shadowed) region of normal bonds (NBs) from the lower charge-shifted bonds or valence bond ionic (CSBs) region. The  $(1,1)$  corner and the middle point of the  $(2,0)$ - $(0,2)$  side are the  $p_2^n$  and  $p_2^{cs}$ , respectively.

This blue point has a probability vector of

$$\mathbf{p}_2^b(1/2) = (1/4, 1/2, 1/4), \quad (138)$$

which is the *real space* image of perfect covalency. The electrons move between both basins and can be found with the same probability either together in the same basin or in separate basins if we think of them as distinguishable particles.

As the real analogue to the 2-electrons-in-2-centers model, the EDFs for the  $\text{H}_2$  molecule have been evaluated. Following the prescription of the QTAIM to partition the space, the user ends up with a division of the space into basins that correspond to atoms (see section 3). A QTAIM partition of the  $\text{H}_2$  molecule yields then two atomic regions  $\text{H}_\text{A}-\text{H}_\text{B}$  that correspond to the two H atoms. If the EDF is now evaluated from a HF calculation, the most probable resonant structure exactly matches the perfect covalency scene of equation 138. For the sake of clarity, this situation is graphically represented in figure 20 (upper right diagram).

However, instead of an homopolar covalent bond as that of the  $\text{H}_2$  molecule, we could be facing a heteropolar union with an unequal sharing of the electrons, *i.e.*, one of the two atoms is more likely to retain the electron pair than the other. The limiting case of a complete electron transfer to one of the regions is depicted at both ends of the red line of BD: the lower corners of diagram 19. The bottom left corner represents a situation where the electrons are fully localized in region A  $\pi^\text{A} = 1$ , which is totally equivalent to the opposite case in which they are in region B  $\pi^\text{A} = 1$  and the probability vector

$$\mathbf{p}_2^b(1) = (1, 0, 0), \quad (139)$$

is that of an ionic bond. The lower left diagram of figure 20 graphically illustrates this case. We ask ourselves whether the EDF of a real ionic compound would be in agreement with the theoretical model, so we performed a HF calculation in the LiH molecule. Although we are now dealing with a 4-electron problem, it can be reduced and renormalized to a 2-electron case[99] and the probability vector of the real system will be

$$\mathbf{p}_2^{\text{LiH}} = (0.003, 0.096, 0.895),$$

that closely follows the theoretical vector 139.

The red line we have been discussing until now is that of a BD, *i.e.*, the line of zero electron correlation  $f = 0$ . A displacement upwards (downwards) from the BD curve gives rise to an increase (decrease) in the correlation in steps of 0.25 units and the binomial behaviour of the  $\mathbf{p}^2$  vector is of course destroyed. The  $f = 0$  line is the frontier between two chemically very relevant regions: an upper, negatively correlated  $-1 < f < 0$  and a lower, positively correlated  $0 < f < 1$

half. We already consider the importance of the frontier  $f = 0$  itself, let us now discuss the lower, positively correlated part.

In order to do so, let us go to a limiting situation, in which we move downwards from the blue point of a covalent bonding situation (see figure 19) following a straight line until we reach the (0,2) edge of the triangle. At that point,  $p(0,2) = p(2,0) = 1/2$ , which means  $p(1,1) = 0$ , the electrons always following each other, causing that way a charge shift to happen (see lower right diagram in figure 20). As already stated, this is a limit case of a positively correlated situation: the presence of an electron in basin A is favourable in order for a second electron to occupies the same region. The probability vector would now be

$$\mathbf{p}_2^{\text{cs}} = (1/2, 0, 1/2). \quad (140)$$

In such unusual scenery the Pauli principle, that states that two same-spin electrons cannot occupy the same region of the space, would be violated, event that yet feasible in theory, has yet never been described.

Any point lying below the  $f = 0$  line will correspond to a system of positively correlated electrons. In most cases, however, we will be dealing with systems whose description is found in the upper  $0 < f < 1$  part, that is, negatively correlated electron networks, where the presence of an original electron dampers the probability of second one to approach it, being zero at the coalescence.

At exactly the opposite side of the charge shift point, the limiting situation of non-interacting particles is found, just in the upper corner of the diagram labeled (1,1). We are now within the negatively correlated half of the triangle. As we see if we observe figure 19, going up from the charge shift case means a lowering in the probabilities of having both electrons on the same basin. If we are at the peak of the  $f = 0.5$  line for instance, the maximum the probability of both electrons occupying the same basin is  $\sim 0.13$ . The more correlation the larger the inclination of the electrons to be located on different atoms. Exactly at the corner, the correlation is at its maximum  $f = 1$  and as it is depicted in the upper left diagram of figure 20 the electrons do not interact with each other, therefore never sharing the same basin  $p(2,0) = p(0,2) = 0$  but being always separated  $p(1,1) = 1$ . The probability vector will now be

$$\mathbf{p}_2^{\text{n}} = (0, 1, 0). \quad (141)$$

Diagram 19 also contains information about the charge  $q$ . If we are in the (2,0)–(0,2) segment, the charge in region let us say A changes from  $q = -1$  on the left corner, where both electrons are in region A to  $q = +1$  in the (0,2) corner, situation in which region A has no electrons. Vertical dashed green lines are  $q$  isolines equispaced 0.2



electrons. Coming again to our demo point, we see that on average there is one electron per region, that is  $q = 0$ , as a consequence of the electrons being with the same probability in the same or in different regions  $p(2,0) + p(0,2) = p(1,1) = 0.5$ .

#### 6.1.1 Electron delocalization from the EDF

The DI is a measure of how often electrons travel out of the region they belong to, i.e., how likely it is to find the electron in a neighbouring region (see section 3.1 for a more in detail definition of the DIs). As we saw (see equation 107) the DI is defined from the exchange-correlation density  $\rho_{xc}$  but also admits a statistical interpretation. It can be defined as the covariance of the electron population between two regions A and B (see equation 115)

$$\delta^{A,B} = -2\text{cov}(n_A, n_B), \quad (142)$$

where  $n_A, n_B$  are the electron populations of regions A and B, respectively.

The EDF is a function out of which many relevant statistical measures can be constructed. From a given EDF, the covariance[23, 50, 98]

$$\begin{aligned} \text{cov}\{\mathbf{p}_B\} &= \langle (n_A - \langle n_A \rangle)(n_B - \langle n_B \rangle) \rangle \\ &= \int_{\Omega_A} d\mathbf{r}_1 \int_{\Omega_B} d\mathbf{r}_2 \rho_2^{xc}(\mathbf{r}_1, \mathbf{r}_2) \end{aligned} \quad (143)$$

allows us to connect with the DI:

$$\delta^{A,B} = -2\text{cov}\{\mathbf{p}_B\}. \quad (144)$$

In the special case of a perfect BD the covariance might be easily obtained from the probabilities given above as  $-2\pi(1 - \pi)$ .

The triangular diagram we are describing also contains information on the DI as a quantity related to the EDF. On it, the DI value changes from  $\delta = 2$ , which is a point exactly in the middle of the (2,0)–(0,2) segment to  $\delta = 0$  in the (1,1) corner, decreasing by intervals of 0,25 each indicated by a dashed curve from 0 at  $p(0,2) = 0.5$  to 2 at the (1,1) corner. If we consider again the blue point depicted in the figure, to the blue point corresponds a  $\delta^{A,B} = 1$ , indicating a situation in which the full electron pair is shared between the two regions. The use of the DIs as bond orders should be taken with care for strongly non-binomial EDFs. For instance, at the limit case of  $\mathbf{p}_2^s$ ,  $\delta^{A,B} = 2$ , which implies that two pairs of electrons are shared whereas we only have one.

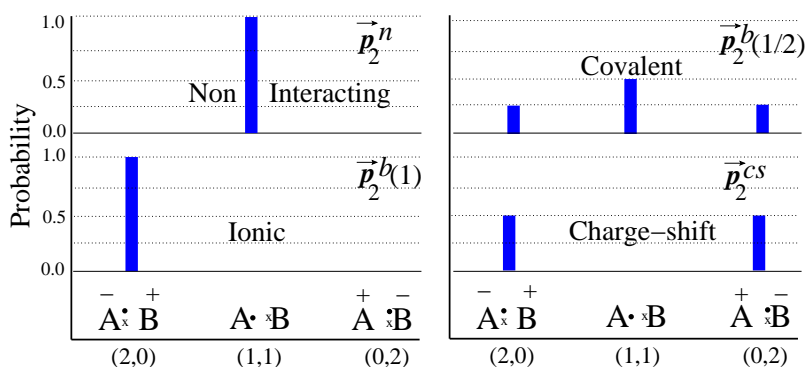


**Figure 20:** Electron number probability distribution functions in the real space description of the three model cases: non-interacting, covalent, ionic and charge-shift (or valence-bond ionic), for two-center (A,B), two-electron bonds (2c,2e). In the diagram the reader can find the probabilities of the different distributions together with the vector notation used. The abscissa contains the population of each basin A or B as well as the traditional Lewis-like diagrams.

## 6.2 ELECTRON DISTRIBUTION FUNCTIONS IN THE 1-DETERMINANTAL CASE

In the case described by equation 15, where the wave function  $\Psi$  is approximated as a single Slater determinant and the expression to find the EDFs, formulated in equation 131 adopts a specially simple form (see [30, 32, 141] for a more detailed description of how to obtain probabilities from monodeterminantal wave functions)

$$\begin{aligned}
 p(n_A, n_B, \dots, n_N) &= \frac{1}{\sqrt{N!}} \det[\Psi \Psi^t] \\
 &= \frac{1}{\sqrt{N!}} \sum_{k_1=1}^N \dots \sum_{k_N=1}^N \det \begin{bmatrix} \psi_1(k_1)\psi_1(k_1) & \dots & \psi_1(k_N)\psi_N(k_N) \\ \vdots & \ddots & \vdots \\ \psi_N(k_1)\psi_1(k_1) & \dots & \psi_N(k_N)\psi_N(k_N) \end{bmatrix},
 \end{aligned} \tag{145}$$

where only terms with all the  $k_j$  ( $j = 1, \dots, n$ ) different contribute to  $\det[\Psi \Psi^t]$ .

Each of the products of the determinant is an AOM of the form given in equation 100. If this expression is applied, equation 146 becomes

$$p(n_A, n_B, \dots, n_m) = \frac{1}{\sqrt{N!}} \sum_{\{k_j\} \in S_N} \det \begin{bmatrix} S_{11}^A(k_1) & \dots & S_{1N}^m(k_N) \\ \vdots & \ddots & \vdots \\ S_{N1}^A(k_1) & \dots & S_{NN}^m(k_N) \end{bmatrix}, \tag{146}$$

where  $S_N$  is the set of all  $N!$  permutations of  $\{1, 2, \dots, N\}$  and  $\{k_j\}$  is one of these permutations, satisfying that for  $k_j \in \{1, \dots, n_A\}$  integration is done over region A, for  $k_j \in \{n_A + 1, \dots, n_A + n_B\}$  over region B and  $k_j \in \{N - n_m + 1, \dots, N\}$  over region m.

The calculation of EDFs for one- and many-determinant wave functions has been implemented in the code EDF by Francisco and co-workers [53, 54].

# 7

## EDF IN THE SOLID STATE

As already mentioned (see Section 3.2), the calculation of the DI for extended systems is done from KS orbitals, according to a HF-like formula. The calculation of the EDF is analogous, for it derives as well from the exchange-correlation density and the only difference with respect to the 1-determinant expression introduced in the previous Section (see equation 146) is the form of the AOMs, which are now defined as in equation 108, for the one-particle spin-orbitals are now Bloch functions.

## 7.1 NATURAL ADAPTIVE ORBITALS

### 7.1.1 The domain average Fermi hole

The Fermi hole, which should be better called here the exchange-correlation hole, as it was defined in equation 55, describes the difference between the total density at the spin-spatial point  $\mathbf{x}_2$  and the conditional density of the situation in which one electron is at position  $\mathbf{x}_2$ , when another one is already at  $\mathbf{x}_1$ . In other words, it measures to what extent the probability of one electron to be at one point is depleted by the presence of other electron at another point of the space, i.e., the Fermi correlation.

However, the Fermi hole is a complex object as it depends on  $\mathbf{x}_1$  and  $\mathbf{x}_2$  and it is natural to think of the electrons, rather than being at a fixed point, occupying any position within a region  $\Omega$ . That way, we would obtain the Fermi hole averaged over a domain: the DAFH, introduced by Ponec [129, 130]

$$h_{\text{XC}}^{\Omega}(\mathbf{x}_1; \mathbf{x}_2) = \rho(\mathbf{x}_2) - \frac{\int_{\Omega} \rho_2(\mathbf{x}_1, \mathbf{x}_2) d\mathbf{x}_1}{\int_{\Omega} \rho_1(\mathbf{x}_1) d\mathbf{x}_1}, \quad (147)$$

where signs have been exchanged for convenience with respect to equation 55.

Taking into account that at  $\mathbf{x}_2$  the electron density is  $\rho(\mathbf{x}_2)$ , a charge-weighted Fermi hole is usually defined, named the charge-averaged Fermi hole, DAFH from here on, which can be formulated as

$$g^{\Omega}(\mathbf{x}_2) = \langle N_{\Omega} \rangle h_{\text{XC}}(\mathbf{x}_2). \quad (148)$$

The spinless DAFH can also be defined from the 2-RDM of equation 53 as

$$g^{\Omega}(\mathbf{r}) = \int d\sigma_1 \int d\sigma_2 \int_{\Omega} \rho_{\text{xc}}(\mathbf{x}_1, \mathbf{x}_2) d\mathbf{r}_1. \quad (149)$$

Let us consider only the spatial coordinates in what follows. Among the many interesting properties of the DAFH, we may point out that it integrates to the total number of electrons within a region

$$\int g^{\Omega}(\mathbf{r}) = N_{\Omega}. \quad (150)$$

For an exhaustive partition such as the QTAIM partition  $\cup_a \Omega_a = \mathbb{R}^3$  (see section 3 for a description of this partition strategy) it satisfies

$$\sum_a g^{\Omega_a}(\mathbf{r}) = \rho(\mathbf{r}), \quad (151)$$

which means  $g^{\Omega_a}$  yields a partition of the density at each point of the space into domain contributions.

On the other hand, as the DAFH derives from the same quantity as the delocalization measures LI and DI (see section 3.1), they are tightly related. In the special case where the Fermi hole lies completely within region  $\Omega$ , equation 150 becomes  $\int_{\Omega} g^{\Omega}(\mathbf{r}) = \lambda^{\Omega}$ , and the electrons are perfectly localized within the basin. As this is a limiting situation, usually the Fermi hole spreads out of the atomic basin<sup>1</sup> and  $\lambda^{\Omega} < \langle N_{\Omega} \rangle$ . The difference between both quantities is measured by the fluctuation, defined in equation 102, and gives us the fraction of electron pairs that are not contained in region  $\Omega$ , that is, delocalized across the system.

The charge delocalized to other regions different than  $\Omega$  is again captured by the DI, which in terms of the DAFHs can be calculated as

$$\delta^{\Omega, \Omega'} = \int_{\Omega} g^{\Omega}(\mathbf{r}) d\mathbf{r} + \int_{\Omega'} g^{\Omega'}(\mathbf{r}) d\mathbf{r}. \quad (152)$$

That way, the average population  $\langle N_{\Omega} \rangle$  is either localized within the region  $\Omega$ , which is measured by the  $\lambda^{\Omega}$  or it smears out and delocalizes to other neighbouring regions, which is felt by the  $\delta^{\Omega, \Omega'}$

$$\langle N_{\Omega} \rangle = \lambda^{\Omega} + \frac{1}{2} \sum_{\Omega' \neq \Omega} \delta^{\Omega, \Omega'}. \quad (153)$$

#### *The DAFH in the 1-Slater determinant case*

Let us now write  $g^{\Omega_a}(\mathbf{r})$  in the orbital basis. In the 1-determinant case, the exchange-correlation density takes the form of equation 60. The DAFH adopts in the monodeterminantal case the following shape

$$g^{\Omega}(\mathbf{r}) = \sum_{ij}^N \psi_i(\mathbf{r}) G_{ij}^{\Omega} \psi_j(\mathbf{r}), \quad (154)$$

where

$$G_{ij}^{\Omega} = \sum_{ij}^N \delta(\sigma_i, \sigma_j) S_{ij}^{\Omega}. \quad (155)$$

The  $S_{ij}^{\Omega}$  are the *atomic overlap matrix* (AOM) defined in equation 100, which contains information about the overlap between the molecular spin-orbitals  $\psi_i$  and  $\psi_j$  within region  $\Omega$ .

The matrix  $\mathbf{G}^{\Omega} = \mathbf{S}^{\Omega}$  represents the Fermi hole in the orbital basis. The set of eigenvalues and eigenvectors resulting from a diagonaliza-

<sup>1</sup> We assume here a QTAIM partitioning, but any other strategy to partition the space is up to the user's will.

tion  $\mathbf{G}^\Omega \mathbf{U} = \mathbf{U} \mathbf{n}$ , given the unitary transformation  $\mathbf{U}^\dagger \mathbf{U} = \mathbf{I}$ , contain information about how the electrons are distributed in an arbitrary region  $\Omega$ . The eigenvectors define a new basis of occupied orbitals, the DAFH orbitals  $\boldsymbol{\phi} = \chi \mathbf{U}$ , in terms of which the Fermi hole  $g^\Omega(\mathbf{r})$  can be rewritten as

$$g^\Omega(\mathbf{r}) = \sum_i^N n_i |\varphi_i(\mathbf{r})|^2. \quad (156)$$

The functions  $\varphi_i$  are effective monoelectronic states, called *domain natural orbitals* (DNOs), that were introduced by Ponec[129, 130]. The hole  $g^\Omega$  can be understood as a 1-order density confined to the domain  $\Omega$ , so that the  $\varphi_i$  functions can be seen as orbitals describing the distribution of the electron population within the region  $\Omega$ . The partition of the electron population of atomic basins into orbital contributions has been analyzed in molecules, see for instance [33, 134, 135], and in the solid state, see the work by Baranov[19]. The eigenvalues  $n_i$  are understood as occupation numbers for they resemble the occupation numbers of the natural orbitals[157] and also recover the average population of the region

$$\sum_i n_i = \langle N_\Omega \rangle. \quad (157)$$

### 7.1.2 Natural adaptive orbitals

We are going to recall here the cumulant densities (CD), previously introduced in section 1.5.2. Based on the idea that  $\nu$ -centre bonding is a measure of the  $\nu$ -centre statistical dependence that simultaneously occurs among the electron population of those regions. The  $\nu$ -centre bonding indices are obtained by domain-averaging the appropriate CDs. Making use of the CDs, it is therefore possible to define a set of functions that divide any bond index, no matter how many centers are involved, in monoelectronic contributions[55]. Let us call these monoelectronic functions, which are just a generalization of the DAFH (see section 147), natural adaptive orbitals (NAdOs)[113].

As they are obtained from the CDs, they inherit the extensivity (equation 63)—they integrate to the total number of electrons—and the recurrence properties (equation 62)—the CD of  $(\nu - 1)$ th-order can be obtained from the CD of higher order—. Under these conditions, in a partition of the space into  $m$  space-filling basins  $\Omega$ , the recurrence property of equation 62, if we domain-integrate  $\rho_C^{\nu+1}$   $\nu$

times we obtain a partition the electron density  $\rho(\mathbf{r}) = \rho_c^1(\mathbf{r})$  into  $\nu$ -centre contributions

$$\begin{aligned}\rho(\mathbf{r}) &= \sum_{AB\dots\nu} \rho_{AB\dots\nu}^1(\mathbf{r}) \\ &= \sum_{AB\dots\nu} \int_{\Omega_a} d\mathbf{r}_2 \int_{\Omega_b} d\mathbf{r}_3 \cdots \int_{\Omega_\nu} d\mathbf{r}_{\nu+1} \rho_c^{\nu+1}(\mathbf{r}, \mathbf{r}_2, \dots, \mathbf{r}_{\nu+1}).\end{aligned}\quad (158)$$

If for instance, among all these domain-partitioned densities, we write  $\rho_{AB\dots\nu}^1(\mathbf{r})$  in terms of the occupied MOs  $\psi_i$ ,

$$\rho_{AB\dots\nu}^1(\mathbf{r}) = \sum_{ij} \psi_i(\mathbf{r}) \mathbf{G}^{AB\dots\nu} \psi_j(\mathbf{r}), \quad (159)$$

where  $\mathbf{G}$  is a Hermitian matrix. Diagonalization of the above expression

$$\rho_{AB\dots\nu}^1(\mathbf{r}) = \sum_i n_i^{AB\dots\nu} |\varphi_i^{AB\dots\nu}|^2, \quad (160)$$

defines the  $\nu$ -centre NAdOs  $\varphi_i^{AB\dots\nu}(\mathbf{r})$  and their natural adaptive occupation numbers (NAdOcs)  $n_i^{AB\dots\nu}$ . The NAdOcs, generalizing equation 157, recover the  $\nu$ -centre DI

$$\sum_i n_i^{AB\dots\nu} = \langle N_{AB\dots\nu} \rangle. \quad (161)$$

If  $\nu = 1$ , the 2-CD  $\rho_c^2(\mathbf{r}_1, \mathbf{r}_2) = \rho_{xc}(\mathbf{r}_1, \mathbf{r}_2)$  and equation 158 becomes

$$\rho_c^1(\mathbf{x}) = \sum_A \int_{\Omega_a} d\mathbf{x}_2 \rho_c^2(\mathbf{x}_1, \mathbf{x}_2) = \sum_A \rho_A^1(\mathbf{r}). \quad (162)$$

In this particular case,  $\rho_A^1(\mathbf{r}) \equiv g^{\Omega_a}(\mathbf{r})$  is just the DAFH, which has been described more extensively in section 147. That way, the DNOs are recovered by expanding  $g^{\Omega_a}(\mathbf{r})$  in terms of the orbital basis as in equation 154 and after diagonalization (equation 156), the generalized densities are exactly Ponec's DAFH, and the  $\varphi_i^A(\mathbf{r})$ 's are the DNOs and the  $n_i^A$ 's their occupation numbers. If the one-electron function  $\varphi_i^A(\mathbf{r})$  spreads out of region  $\Omega_a$  into other regions  $\Omega_b \dots$ , the electrons in the former are sensed by the electrons in the other regions and a statistical dependence between both  $\Omega_a \Omega_b$  is established. In the opposite case, if a given  $\varphi_i^A(\mathbf{r})$  is fully contained in  $\Omega_a$ , exactly one electron will be localized in it. In other words,  $\rho_a^1(\mathbf{r})$  gives the average distribution of the  $\langle N_A \rangle$  electrons that should not be included in  $\rho$  when all the reference electrons in  $\Omega_a$  are considered. The DNOs defined that way constitute a description of the monoelectronic states that contribute to the population of the domain  $\Omega_a$ .



The same rule applied in equation 162 can be extended to  $\nu > 2$  and for the  $\nu = 3$  case,  $\rho_c^3(\mathbf{r})$  allows for a partition in 2 basins the 1-order cumulant  $\rho_c^1(\mathbf{r})$ :

$$\rho_c^1(\mathbf{r}) = \sum_{AB} \int_{\Omega_a} d\mathbf{r}_2 \int_{\Omega_b} d\mathbf{r}_3 \rho_c^3(\mathbf{r}_1, \mathbf{r}_2, \mathbf{r}_3) = \sum_{AB} \rho_{AB}^1(\mathbf{r}), \quad (163)$$

which is a partition in two centres of the electron density.

The same procedure can be followed in the case of the 2-RDM, which can be obtained by condensation of higher-order CDs. In terms of the 3-RDM, for instance

$$\rho_c^2(\mathbf{r}_1, \mathbf{r}_2) = \sum_A \int_{\Omega_a} d\mathbf{r}_3 \rho_c^3(\mathbf{r}_1, \mathbf{r}_2, \mathbf{r}_3) = \sum_A \rho_{c,A}^2(\mathbf{r}_1, \mathbf{r}_2). \quad (164)$$

A schematic representation of  $\rho_A^1$  in a system divided into two regions A and B is shown in figure 21 (left side). As it can be deduced from there, integration of  $\rho_A^1(\mathbf{r})$  over the whole space yields the average population of fragment A

$$\int_{\mathbb{R}^3} \rho_A^1(\mathbf{r}) d\mathbf{r} = \langle N_A \rangle. \quad (165)$$

If  $\rho_A^1$  is totally contained in region A, the population is equal to the localization within this atomic region  $\langle N_A \rangle = \lambda^A$ . But in general, as the electronic population can delocalize  $\rho_A^1$  spreads out of A and into region B, so the domain-integration recovers the localization index  $\lambda^A$ , defined in equation 109

$$\int_A \rho_A^1(\mathbf{r}) d\mathbf{r} = \lambda^A. \quad (166)$$

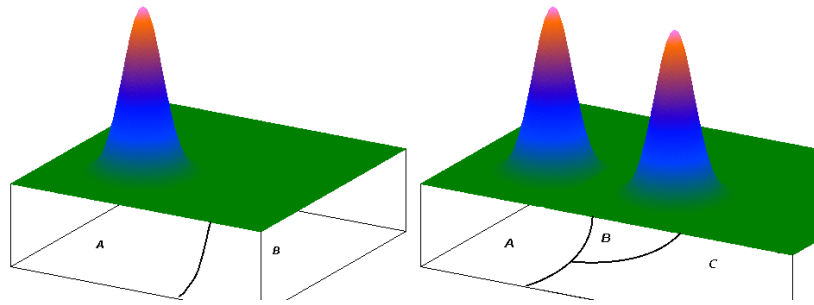


**Figure 21:** Schematic representation of the  $\rho_A^1$  and  $\rho_{AB}^1$  domain-partitioned electron densities, the space divided into 2 and 3 regions, respectively.

In the 2-centre case, equation 164 yields a description of how the A, B-delocalized electrons  $\langle N_{AB} \rangle$  are distributed in the space. The 2-centre electron density  $\rho_{AB}^1(\mathbf{r})$  is represented again schematically in

figure 21 (right side). If it spreads out of the  $\Omega_a \cup \Omega_b$  joint region there is, at least, three-centre statistical correlation and three-centre bonding, so that further condensation from  $\nu = 4$  or higher order-CDs is motivated. A integration of  $\rho_{AB}^1$  over the whole space yields  $\langle N_{AB} \rangle$ , which is half the delocalization index  $\delta^{A,B}$  (see equation 107 for definition)

$$\int_{\mathbb{R}^3} \rho_{AB}^1(\mathbf{r}) d\mathbf{r} = \langle N_{AB} \rangle = \frac{1}{2} \delta^{A,B}. \quad (167)$$

The  $\mathbf{G}^{AB\dots m}$  matrices are particularly simple in the case of single determinant wave functions, depending only on the so-called AOMs (see equation 100). If for  $\nu = 1$ ,  $\mathbf{G}^A = \mathbf{S}^A$  (see above), in the  $\nu = 2$  case,  $\mathbf{G}^{AB} = (\mathbf{S}^A \mathbf{S}^B + \mathbf{S}^B \mathbf{S}^A)/2$ . After diagonalization a new set of one-electron functions  $\varphi_i^{AB}$  or 2-NAdOs is obtained and associated, the occupation numbers denoted by  $n_i^{AB}$ . As it is usually the *modus operandi* in a DAFH analysis, plotting the 2-NAdOs (or simply  $\varphi$  in the following) would provide a MO-like representation, but now taking into account the bonding electrons rather than the electrons of the whole molecule, between 2 atomic regions, with the respective occupations.

The extensivity property of the cumulant densities (as formulated in equation 63) is noticeable here if the integrations in equations 162 and 164 are carried out over the remaining electron

$$\langle N_A \rangle = \int_A \rho_c^1(\mathbf{r}) d\mathbf{r} \quad (168)$$

$$\langle N_{AB} \rangle = \int_A d\mathbf{r}_1 \int_B \rho_c^2(\mathbf{r}_1, \mathbf{r}_2) d\mathbf{r}_2 = \frac{1}{2} \delta^{A,B}. \quad (169)$$

Note that likewise the integration of the 1-CD over region A yields the electron population within that basin  $\langle N_A \rangle$ , the same operation over the 2-CD recovers half the DI between regions A and  $B \neq A$ . The same procedure would allow to recover the  $\nu$ -center  $\delta$  from higher order  $\nu$ -CDs.

## 7.2 EDF RESULTS

As in the publication by Baranov and Kohout [18], for this is the first study where EDF are evaluated for solid systems, we have chosen model systems for each type of bonding situation: NaCl as ionic, diamond and graphite as covalent, Na in its *bcc* phase as metal. All those systems are described with a DFT wave function, obtained with the solid state FP-LAPW code Elk[1], using the local spin density approximation with the Perdew-Wang exchange-correlation functional[125]. All calculations were done using a fine logarithmic mesh, by setting the parameter `lradstp=1` in Elk. Additionally, a very small smearing width was used (usually `swidth`  $\approx 1e-08$ ) in order to avoid fractional occupations of the orbitals. The expansion cutoff for the wave function is 7.0 a.u. (parameter `rgkmax`). Default parameters were used except otherwise indicated. The posterior space partitioning into QTAIM basins, as well as the integration of the electron density to obtain the AOMs was carried out with the program DGrid[82] by M. Kohout, which also allowed, after an adaptation of the code done in collaboration with A. Baranov, the generation of the files for the representation of the NAdOs. The evaluation of molecular EDFs from both HF and correlated wave functions is implemented in the code EDF[54] by E. Francisco in our group. This is code used for calculating EDFs in the solid state, which required a generalization of the matrix diagonalization algorithm which must now handle complex matrices (AOMs), produced by DGrid. This also implies that the resulting orbitals are complex as well, so they are characterized by not only the amplitude, but by the phase too. Let us start then by discussing the ionic case.

### 7.2.1 The ionic case: crystalline NaCl

The NaCl molecule is a typical example of an ionic bond. The high electronegativity difference between both atoms makes the sharing of electrons to be asymmetric: the Cl atom keeps one electron that is stolen from the Na atom, the picture being  $\text{Na}^+\text{Cl}^-$ . The DIs and NAdOs were evaluated for the NaCl crystal from a calculation with  $4 \times 4 \times 4$  k-points, with a shift in the k-mesh of  $\mathbf{k}_{\text{shift}} = (0.25, 0.5, 0.75)$ , specified with the `vkloff` parameter. The localization within the QTAIM basins is found to be very high  $\lambda^{\text{Na}} = 9.9747$  and  $\lambda^{\text{Cl}} = 17.6911$  and is very similar to the QTAIM populations  $n_{\text{Na}} = 10.1418$  and  $n_{\text{Cl}} = 17.8582$ . The variance or the fluctuation in the electronic population, obtained as the difference between the QTAIM population and  $\lambda$  (see equation 102) can be considered to be low in both cases  $\sigma_{\text{Na}}^2 = \sigma_{\text{Cl}}^2 = 0.16710$ . High localization values that besides coincide to a large extent with the electronic population are in good agreement with the results obtained for the simplest prototype

of ionic bond LiH[10, 45], with fluctuations on the atomic populations having the values  $\sigma_{Li}^2 = \sigma_H^2 = 0.099$ [45]. The DI and LI values for the NaCl molecule are summarized in Table 2, to which we will be referring very often in the successive pages of our discussion.

As we have shown, the analysis of the EDF gives the probability of the different real space resonant structures (RSRS) in Pauling's terms of a system (see section 131 for a discussion on its usefulness and a more in detail definition of the EDF). According to the known nature of the chemical bond in the sodium chloride, it did not surprise us to obtain the configuration  $P^1(n_{Na} = 10) = P(n_{Cl} = 18) = 0.838$ , where the Na atom cedes an electron captured by the chlorine, as the most probable resonant structure of the NaCl molecule. This exactly corresponds to the expected  $Na^+Cl^-$  case. The probability of the sodium to loose an electron is identical to that of the chlorine to win an electron, originated from the fact that in the molecule there are only two atom basins, i.e., each electron has only one basin available to delocalize. Under this restriction, the electrons being shared by the sodium atom have hence no other possibility than going to the chlorine basin.

The scenario is quite different in the NaCl extended system. The delocalizing electrons are now allowed to go to any of the basins of the solid, either the Na or the Cl basins, with no restriction at all. The probabilities of the different resonant structures for the NaCl crystal are gathered up in Table 1. Let us start with the one centre probabilities, calculated letting  $n$  electrons be inside the Na or Cl basin, whereas the remaining  $N - n$  electrons are anywhere in the solid.

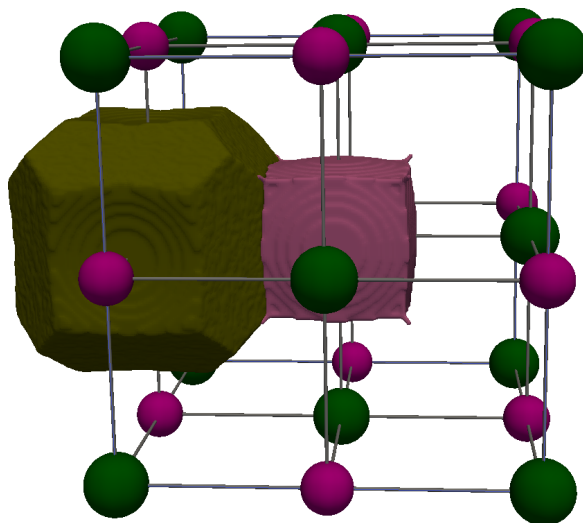


Figure 22: QTAIM basins of the NaCl, Na atoms are magenta and smaller than the Cl atoms, in green.

The most likely event that can happen to a Na atom is to loose one electron  $P^1(n_{Na} = 10) = 0.792$ , in agreement with our expectations.

The opposite one is the most probable event for the Cl atom: the gain of one electron  $P^1(n_{\text{Cl}} = 18) = 0.6197$ . The most probable situation therefore is the same as in the molecular case, with the important difference that however now both probabilities are not equal anymore  $P^1(\text{Na}^+) \neq P^1(\text{Cl}^-)$ . If we give the electrons freedom to delocalize over any of the atoms in an infinite network, the atom does not have to follow the restricted molecular situation, where only one basin was available for the electron to go. The electron that leaves its Na basin has now not one but infinite different chlorine basins where it can go to, although it mainly goes to the 6 closest ones.

The Na atom has a more rigid nature as a cation and is found as  $\text{Na}^+$  79% of the time, whereas the more flexible chlorine, as an anion, shares the electron it receives with other Cl atoms and has a lower probability 62.5% of being  $\text{Cl}^-$ . The difference between them resides in the amount of electronic charge that each atom exchanges with the second neighbourhood, which is formed by alike atoms. The Na shares electrons mainly with the Cl and not with the other Na atoms, but the Cl atom is a more bountiful species that shares its electron with other Cl atoms. The DI bolsters our interpretation: on the one hand the sodium has a much lower delocalization with the whole solid,  $\delta^{\text{Na,solid}} = 0.4549$ , than the chlorine,  $\delta^{\text{Cl,solid}} = 1.0378$  (see Table 2). On the other, taking a look at the delocalization between second neighbours, we see how the Cl atom behaves more covalently  $\delta^{\text{Cl,Cl}} = 0.0482$  in comparison with the tightfisted Na with  $\delta^{\text{Na,Na}} = 0.0002$ . This asymmetrical sharing tells us that the network formed by the Cl atoms behaves in a more covalent way although it is in an ionic context, for the  $\delta^{1,3}$  is similar to the equivalent value for the diamond system (see Table 2). On the contrary, the Na network is much more ionic, with a very small internal sharing as the second-neighbours DI suggests.

The covalent-like behaviour of the chlorine is nevertheless limited to the first Cl neighbourhood. To help the reader follow the numbers we present here, the QTAIM basins of the NaCl crystal are shown in figure 22. Proceeding in the same manner as Baranov and Kohout[18], we note that each chlorine atom has a sodium neighbourhood of 6 Na atoms and a chlorine neighbourhood of 12 Cl atoms. Thus the total delocalization between the chlorine and its first neighbourhood (including closest Na and Cl atoms) is  $6 \times \delta^{\text{Cl,Na}} + 12 \times \delta^{\text{Cl,Cl}} = 0.4416 + 0.5784 = 1.02$ , which means  $\delta^{\text{Cl,solid}} - 1.0200 = 0.019$  electron pairs shared with the atoms further away from the first vicinity. The same analysis in the case of the sodium yields  $6 \times \delta^{\text{Na,Cl}} + 12 \times \delta^{\text{Na,Na}} = 0.4416 + 0.0024 = 0.4440$ , and the sharing with atoms beyond the first vicinity is in this case  $\delta^{\text{Na,solid}} - 0.4440 = 0.011$  which is of the same order than that for chlorine. According to the expectations for an ionic compound, a very low delocalization with distant atoms is

**Table 1:** Probabilities of different RSRS for the NaCl crystal.  $p^1$  and  $p^2$  refer to one- and two-centre probabilities, respectively, indicating in brackets the species involved. The last column gathers a measure of the deviation from the independent particle situation, in which the product of the probability of the events should equal the probability of the joint event  $p_{NaCl}^2 = p_{Na}^1 p_{Cl}^1$ .

$n_{Na}$	$n_{Cl}$	$p^1(n_{Na})$	$p^1(n_{Cl})$	$n_{Na}$	$n_{Cl}$	$p^1(n_{Na}) \cdot p^1(n_{Cl})$	$p^2(n_{Na}, n_{Cl})$	$p^2 - p_{Na}^1 p_{Cl}^1$
10	18	0.7982	0.6197	10	18	0.4946	0.5086	0.0140
11	17	0.1537	0.2155	10	17	0.1720	0.1620	-0.0100
9	19	0.0335	0.1177	10	19	0.0939	0.0943	4.0e-04
12	16	0.0132	0.0326	11	18	0.0952	0.0851	-0.0101
13	20	0.0007	0.0110	11	17	0.0331	0.0428	0.0097
8	15	0.0006	0.0027	10	16	0.0260	0.0223	-0.0037

observed, only broken by the chlorine closest vicinity behaving in a more covalent-like manner.

This situation can be studied from the statistical point of view as well, since as we have seen the DI can also be seen as the covariance of the electron population[5, 13, 45, 107] (see chapter 3.1 for a deeper discussion). It can be said that the Cl atoms admit a higher mobility of the electrons, so that if we take a finite number of pictures of the electrons with their positions, the Na electrons will appear in the majority of them in their original Na basin but on the contrary, electrons in the Cl will be found with much higher frequency in other Cl atoms of its vicinity.

Let us now have a look at the 2-NAdOs for the NaCl crystal, for they may graphically illustrate the ideas we have just commented. As it was said in the introductory Section (see Section 7.1.2), the  $\nu$ -NAdOs are one-electron decompositions of any multicentre delocalization index: for  $\nu = 1$  the 1-NAdO  $\varphi^A$  (identical to the DNO or DAFH) is a partition of the A-domain population where the NAdO was evaluated. A  $\nu$ -centre NAdO is either partially or totally localized within the  $\nu$  centres. A total localization of the DAFH tells us this region does not take part in a bonding scenario (it is a core, lone pair, ...). Partial localization of the DAFH evidences a breakout of the population to the neighbouring basin and therefore the existence of at least 2-centre bonding. The DAFH were already analyzed by Baranov *et al.*[19] in the same typical ionic, covalent and metallic solid state systems. As it is usually found in ionic compounds, low delocalization values were expected in NaCl crystal. Accordingly, the cited work shows that 100% and 99% of the DAFH with the largest eigenvalue is contained within the Na and Cl basin, respectively, which tells us those are the core regions of the respective atoms. The second largest DAFH shows however larger delocalization, with values 99% and 95% again for the Na and Cl basins, respectively. Although small, this indicates that some 2-centre correlation is taking place, which would be better analyzed from the 2-NAdOs.

In an analogous manner as the DAFH, the 2-NAdO  $\varphi^{AB}$  is a decomposition of the delocalized electrons between regions A and B, i.e., of the  $\delta^{A,B}$ , which in the sodium chloride crystal is very low  $\delta^{Na,Cl} = 0.0736$  for it is an ionic compound. Equivalently as in the  $\nu = 1$  case, total localization of the orbitals within the Na–Cl region would mean a pure 2-centre bond, while delocalization to other regions is a sign that more basins are involved in the bonding scenario. The sum of the eigenvalues fully recovers the DI  $2 \sum_i n_i^{NaCl} = 0.0736$ , pointing out that no more than 2-centres are involved in the bonding. The two largest bonding and antibonding 2-NAdOs are depicted in figure 23. The bonding NAdOs are shown in the upper figures 23a and 23b, which together represent 98% of the DI. Looking at them it can be seen that the main contribution to the bonding is contained

**Table 2:** QTAIM populations  $n_A$  and localization indices  $\lambda^A$  for the analyzed compounds.  $\delta^{A,\text{solid}}$  refers to the delocalization between atom A and the rest of the system, and  $\delta^{1,2}$  and  $\delta^{1,3}$  is the DI between the first and second neighbours, respectively, specified by A-B. In diamond,  $C_{sb}$  stands for the superbasin formed by the four atomic basins forming a tetrahedron, as depicted in figure 25. The DI corresponds to bonded superbasins. In graphite,  $C-C_{||}$  stands for the DI between first-neighbour carbon atoms in the same layer and  $C-C_{\perp}$  between first-neighbours of different layers.

	A	$n_A$	$\lambda^A$	$\delta^{A,\text{solid}}$	A - B	$\delta^{1,2}$	$\delta^{1,3}$	$\delta^{1,4}$
NaCl molecule	Na	10.1418	9.9747		Na-Cl	0.3342		
	Cl	17.8582	17.6911					
NaCl solid	Na	10.1476	9.9201	0.4549	Na-Cl	0.0736		
	Cl	17.8524	17.3335	1.0378	Na-Na Cl-Cl		0.0002 0.0482	
Diamond	C	5.9940	3.8082	4.3716	C-C	0.9138	0.0388	
	$C_{sb}$	23.988	18.101	11.773	$C_{sb}-C_{sb}$	1.219		
Graphite	$C_{  }$	5.991	3.864	4.2795	$C-C_{  }$	1.2109		
	$C_{\perp}$	6.020	3.871		$C-C_{\perp}$	0.0196	0.0067	
Na <i>bcc</i>	Na	10.997	10.199	1.594	Na-Na(3.66Å)	0.0964	0.0030	0.0008
					Na-Na(4.22Å)	0.0588		



in the region formed by the joint of the Na and the Cl basin, the two basins represented in figure 22, and that the part of the DI that travels out of it goes almost exclusively to the closest 4 chlorine basins. In other words, if we focus on the Na–Cl pair of atoms (in orange in figure 23), the electron that the Cl atom gains comes mainly but not solely from the Na atom in front of it. On the contrary, it retains a part of this electron and the rest comes from other Cl around it, with whom it also shares. That way, once the electron leaves the Na atom, the electron travels from Cl to Cl according to the flexible nature of the anion. The Na on the contrary behaves in a more rigid way and does not share with other Na neighbours. The lower two figures 23c and 23d are the anti-bonding NAdOs with negative NAdOcs, so the sum of the percentages of the four orbitals is larger than 100%. In this case, the actual delocalization is larger than the DI shows, but some of it contributes negatively to the bonding. These negative contributions are of one order of magnitude smaller ( $-0.0081$  and  $-0.0034$ , against  $0.0591$  and  $0.0130$ ), but still non-negligible. A careful inspection of the NAdOcs provides hence a finer analysis of the actual bonding scenario.

It also informative to consider the RSRSs with smaller probability to occur. In figure 24 we represent the one-centre probabilities of the RSRS with the largest weights. The  $\Delta Q = 0$  bar corresponds to the most probable RSRS and positive (negative) values of  $Q$  mean the atom gained (lost) one electron with respect to it. In the case of NaCl, the blue and red bars stand for Na and Cl, which at  $Q = 0$  represent the most probable  $\text{Na}^+$  and  $\text{Cl}^-$ , respectively. Both atoms show a very asymmetrical distribution of their resonant structures, but differentiating in the tail width of the distribution. The chlorine, in its role of flexible atom shows a distribution with a notably wider tail than that of the sodium, reaching the threshold value of  $P \approx 1e^{-4}$  in the 7<sup>th</sup> most probable RSRS, whereas the sodium attains it in the 5<sup>th</sup>.

The consideration of resonant structures different from the most probable is one of the most interesting uses of the EDF, that makes it a powerful tool to analyze unexpected chemical behaviours, for it provides the information that allows us to take into consideration alternative chemical graphs that might surrogate the expected one in certain uncommon chemical scenario. Although it is clear to the expert eye what RSRSs will compete after the most probable corresponding to  $\text{Na}^+\text{Cl}^-$ , this might be not so predictable in more complex systems behaving atypically. It is in such cases where alternative explanations than those that are already part of the chemical intuition have to be given and where EDF has valuable information to offer. In the NaCl example that occupies us here, the ordering of the resonant structures is established by the EDF values as  $\text{Na}^+\text{Cl}^- > \text{NaCl} > \text{Na}^{2+}\text{Cl}^{2-} > \text{Na}^-\text{Cl}^+$ , with probabilities  $0.8388$ ,

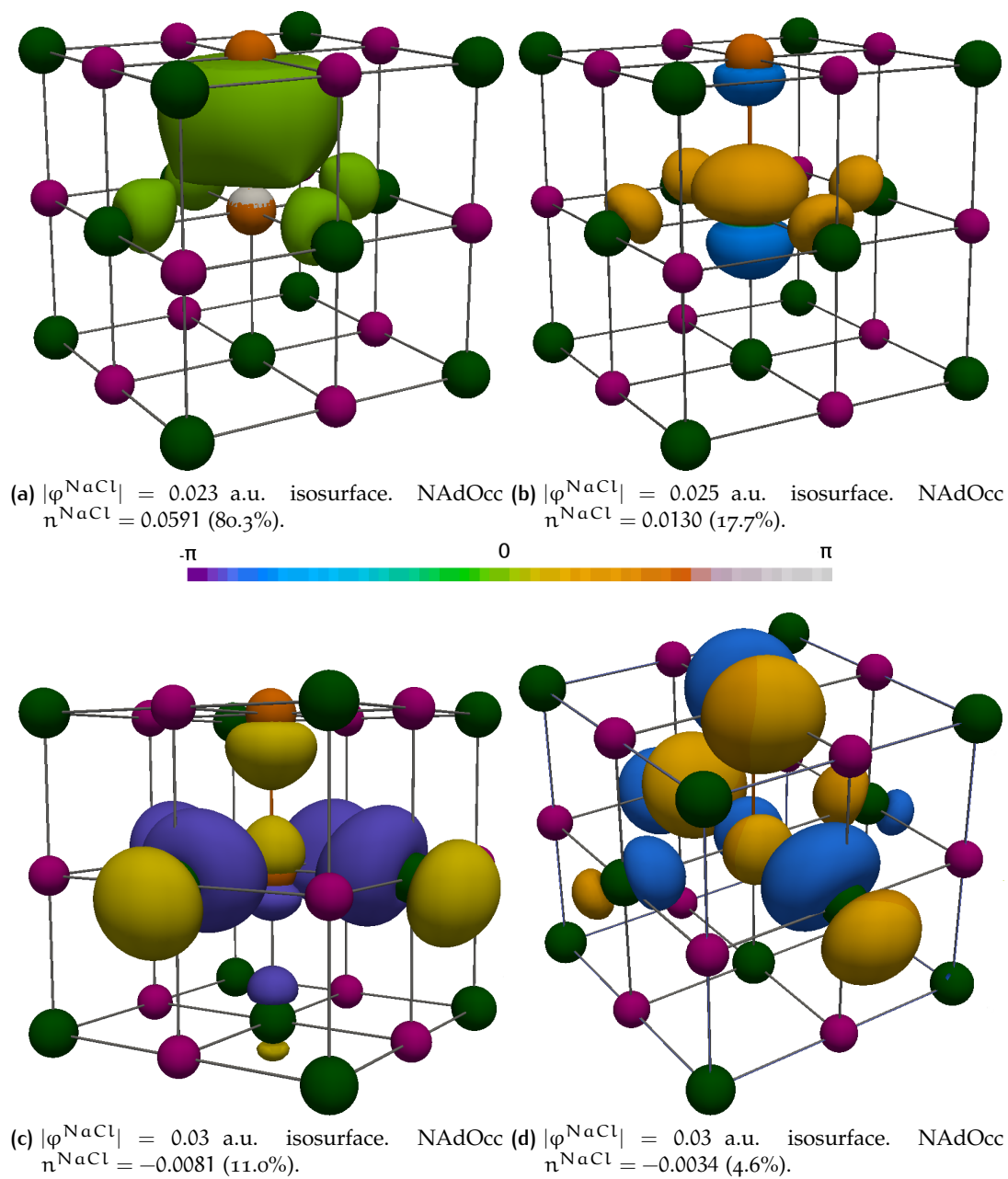


**Figure 23:** 2-centre (first-neighbouring Cl —green— and Na —magenta— atom basins, in orange in the figures) NAdOs  $\varphi^{\text{NaCl}}$  coloured with the phase according to the attached scale, with the largest (2 bonding and 2 anti-bonding) NAdOcs for the NaCl crystal.

0.1391, 0.0138 and 0.0080, respectively. This behaviour is in tune with the distributions found for the LiH molecule[99] and with data coming from ionization potentials. The high energetic cost of removing two electrons from an Na atom (47.286 eV) makes the  $\text{Na}^{2+}\text{Cl}^{2-}$  a very costly species. The  $\text{Na}^-\text{Cl}^+$  is in turn hindered by the expensive ionization of the chlorine (12.967 eV).

Let us now move on to the two-centre case and consider three units: the Na atom, the first Cl neighbour and the rest of the crystal. Joint probabilities are gathered in the right part of Table 1, where one can see that the most likely situation to be encountered is again the Cl taking one electron that the Na has lost  $P^2(n_{\text{Na}} = 10, n_{\text{Cl}} = 18) = 0.5086$ . It is interesting what comes up if we note that the product of the independent events of the Na atom having 10 electrons and the Cl atom 18  $P_{\text{Na}}^1 P_{\text{Cl}}^1 = 0.7982 \cdot 0.6197 = 0.4946$  is noticeably different than the joint event  $P_{\text{NaCl}}^2 = 0.5086$ , so one can conclude this is actually not the case of an independent particle situation, yet it is not very far from it neither: the difference  $P_{\text{NaCl}}^2 - P_{\text{Na}}^1 P_{\text{Cl}}^1 = 0.0140$  is in fact not very large. Table 1 shows the probabilities of the one-centre events (third and fourth columns), its product and the joint event probability (seventh and eighth columns), and the difference between both  $P_{\text{NaCl}}^2 - P_{\text{Na}}^1 P_{\text{Cl}}^1$  (last column).

RSRSs with lower probability than the usual  $\text{Na}^+\text{Cl}^-$  case may throw valuable information on the behaviour trends of the system. It is non negligible  $P(10, 17) = 0.1620$  the likelihood of the chlorine to loose one electron to the bulk of the solid, the system being  $\text{Na}^+\text{Cl}$ . One order of magnitude lower but with being still as frequent as 9.43%, 8.51%, 4.28% and 2.23% are the RSRS  $\text{Na}^+\text{Cl}^{2-}$ ,  $\text{NaCl}^-$ ,  $\text{NaCl}$  and  $\text{Na}^+\text{Cl}^{2+}$ , respectively (see Table 1). Again this results illustrate the reluctance of the sodium atom not to behave as a cation, which contrasts with the much flexible chlorine.

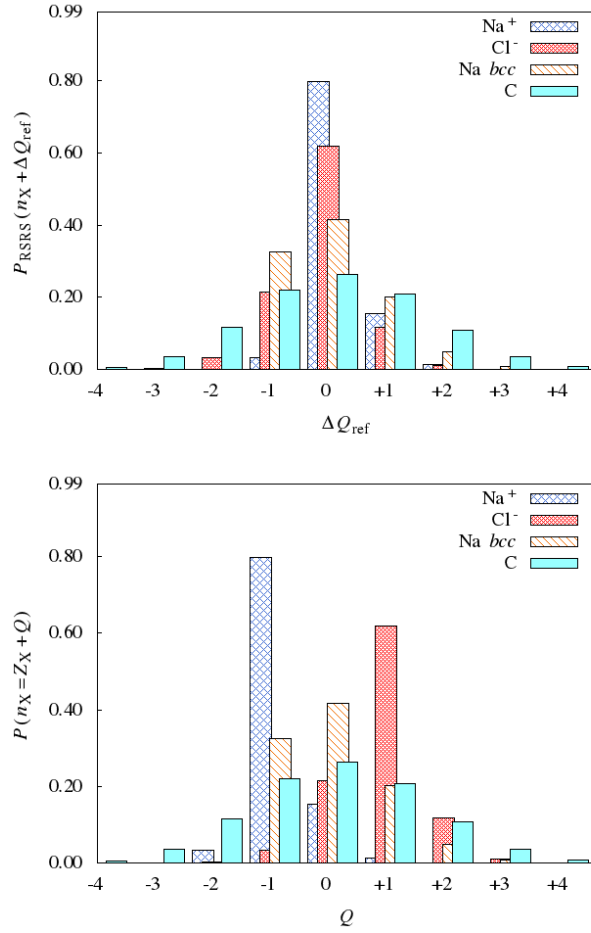


**Figure 24:** Bar chart representation of the largest one-centre probabilities for  $X = \text{NaCl}$ , diamond and  $\text{Na bcc}$ . Above:  $\Delta Q_{\text{ref}}$  refers to the deviations in the number of electrons  $n_X$  of the atoms in the most probable resonant structure  $P_{\text{RSRS}}$ , so that at  $\Delta Q_{\text{ref}} = 0$  all atoms have the electrons of the most probable RSRS. Below:  $Q$  refers here to a true charge and at  $Q = 0$  all atoms are neutral so the probability will be that of the atom having its atomic number  $Z_X$  electrons.

### 7.2.2 The covalent cases: diamond and graphite

Crystalline carbon provides us with two extensively studied systems with covalent bonding that suits our purpose of presenting the wealth of information that can be obtained from the analysis of the EDF, continuing our tour through the classic chemical bonding types. To a covalent bond, as a bonding scenario where electrons are being shared, we associate the image of tightly bound electrons occupying the physical space between the two bonded atoms.

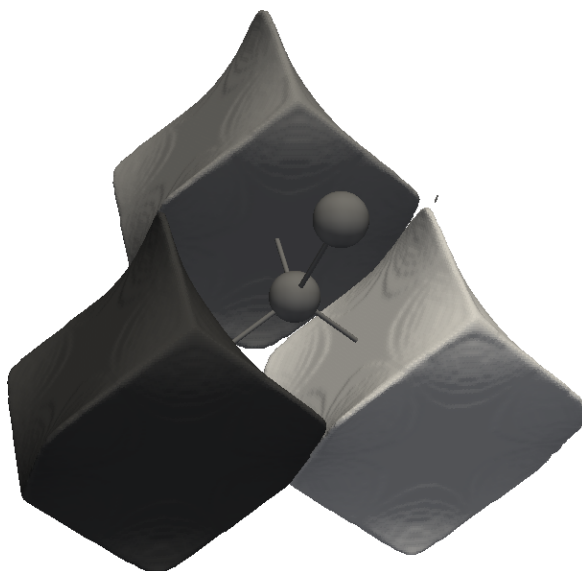


**Figure 25:** QTAIM basins of the diamond. The superbasin  $C_{sb}$  is formed by the joint of four basins: the three drawn and the one corresponding to the bare C atom in the middle. This C atom is bonded to another carbon atom, also bare in the figure, which equivalently forms the second superbasin with its three remaining direct neighbours. The bond between the two bare C atoms is therefore the bond between the superbasins too.

The wave function for diamond and graphite was obtained using a  $4 \times 4 \times 4$  and  $4 \times 4 \times 3$  k-mesh, respectively, in both instances shifted according to the vector  $\mathbf{k}_{\text{shift}} = (0.25, 0.5, 0.625)$ . The smearing width was increased in both cases up to  $1e-05$ .

Ionicity implies that in NaCl the electron is transferred from the cation  $\text{Na}^+$  to the anion  $\text{Cl}^-$  in an almost irreversible, electron transfer mechanism, which from a statistical point of view has consequently associated a very low variance of the electron population  $n_{\text{Na}} - \lambda^{\text{Na}} = 0.2275$ . The DI in NaCl is notably small when compared to the value for diamond  $\delta^{C,C'} = 0.9138$  and graphite  $\delta_{\parallel}^{C,C'} = 1.2109$ . The diamond shows as well a noticeably larger variance  $\sigma_{\text{diam}}^2(\text{C}) = n_{\text{C}} - \lambda^{\text{C}} = 2.1858$  as well as the graphite  $\sigma_{\text{graph}}^2(\text{C}) = 2.1270$ , according to the expectations for a covalent arrangement (see Table 2), where the electron moves back and forth from one carbon atom to the other in an electron sharing process. This difference in the variance

associated to the ionicity and covalency phenomena are graphically illustrated in figure 24, where the EDFs distribution of diamond is much wider than that of sodium chloride. The translation of DI into bond order is in a covalent context straightforward, and they are in harmony with the chemical wisdom in diamond and graphite, with bond orders of 1.0 and 1.5, respectively.

Although in both diamond and graphite the atoms are covalently connected, the bonding situation is different in both cases: single bond in diamond and delocalized  $\pi$ -system of intralayer atoms in graphite and weak interactions between layers. A  $\delta$ -analysis of both systems throws interesting insights. A diamond QTAIM basin (see the basins of diamond in figure 25) has a  $\delta^{1,2}$  very similar to the  $\delta^{1,2} = 0.988$  in the analogous C–C single bond in  $C_2H_6$ [45]. From the analysis of the DI between first- and second-neighbours, Baranov and Kohout[18] gave sharing values of 83% with the first neighbourhood, 11% with the second and 6% with the rest of the solid in diamond. In relative terms, 17% of the electronic population being shared goes to atoms beyond the second coordination sphere, which can be compared with the 5% and 2% of Na and Cl in NaCl, respectively[18]. Graphite has an almost identical relative distant sharing, with 15% of the shared electrons.

The carbon atoms in graphite arrange in a hexagonal pattern (see figure 26), as it does in the extensively studied case of benzene, the aromatic system *par excellence*: a cyclic compound that follows the rule  $N = 4n + 2, n \in \mathbb{N}$ , where  $N$  is the number of atoms, which is a configuration with a particularly high delocalization among the carbon atoms[44, 107, 108]. This confers a high DI values on the graphite for the shortest contact  $\delta^{1,2} = 1.2109$ , notably higher than in diamond  $\delta^{1,2} = 0.9138$  (see Table 2).

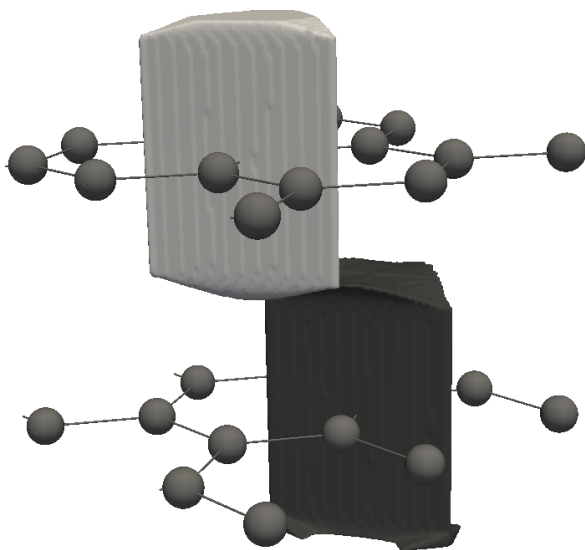


Figure 26: QTAIM basins of the graphite.

If we take a look at the largest probabilities for both diamond (Table 3) and graphite (Table 4), one observes no striking differences in the probabilities themselves nor in the electron distributions.

**Table 3:** Probabilities of different RSRs for the diamond.

$n_C$	$P^1(n_C)$	$n_C$	$n_{C'}$	$P^1(n_C) \cdot P^1(n_{C'})$	$P^2(n_C, n_{C'})$	$P^2 - P_C^1 P_{C'}^1$
6	0.2640	6	6	0.0697	0.0708	0.0011
5	0.2200	5	6	0.0581	0.0587	5.8e-04
7	0.2078	6	7	0.0549	0.0556	6.8e-04
4	0.1158	5	7	0.0457	0.0507	0.0050
8	0.1079	5	5	0.0484	0.0437	-0.0047
9	0.0363	7	7	0.0432	0.0392	-0.0040
3	0.0349	4	6	0.0306	0.0302	-4.0e-04

Let us now have a look at the one-centre probabilities. In Table 3 and 4 we see that the highest probability comes when a carbon atom has 6 electrons, which would be 26.4% and 26.7% of the times in diamond and graphite, respectively. In the same table, we see that the two-centre largest RSRS is again that of having 6 electrons, now in the region formed by the two first-neighbour atoms. If we now move to Table 6, the  $n = Z_A + Z_B$  column explains the chance of the same event, 6 electrons in the region formed by the first-neighbours, regardless in this case of the precise distribution of the electrons between the two atoms. In other words, it simply contains the sum of  $P^2(n_C, n_{C'})$  ( $P_{||}^2(n_C, n_{C'})$  in the case of graphite) satisfying that  $n_C + n_{C'} = 12$ . As we are now considering the union of two regions and each of them delocalizes to many other basins, the likelihood of such a circumstance  $P^2(12)$  has decreased and is now of 21.2% in diamond and 22.4% in graphite. It is not only smaller but actually also noticeably different in both systems: the electrons remain within the C–C superbasis with higher probability in graphite than in diamond.

The reader may find this result counterintuitive as we were expecting the graphite to be more delocalized than diamond. The reason behind it is that we are comparing two numbers that can not be directly compared: whereas the electron in the diamond system delocalizes in all directions, in graphite it does only in 2 dimensions, that is, within one of the layers[18]. Bearing that in mind, 77.6% of the electrons spread out in graphite in 2 dimensions, which is a higher delocalization degree than 78.8% in diamond in all 3 dimensions of the space. The DI indicates a much smaller interlayer delocalization in graphite  $\delta_{\perp}^{1,2} = 0.0196$ , in the same order of the  $\delta^{1,3} = 0.0388$  in diamond, also reflected in the probability of finding 6 electrons in first-neighbours located in different layers  $P_{\perp}^2(12) = 0.1905$ , 2 points smaller than the intralayer number. Travelling between different layers, even if the shortest way is taken, has a difficulty in the same order of magnitude for an electron in graphite than that of travelling between to the second neighbourhood in diamond.

**Table 4:** 1- ( $P^1$ ) and 2-centre probabilities between nearest neighbour C atoms in the same layer ( $P_{||}^2$ ) and between layers ( $P_{\perp}^2$ ) of graphite.

$n_C$	$P^1(n_C)$	$n_C$	$n_{C'}$	$P^1(n_C) \cdot P^1(n_{C'})$	$P_{  }^2(n_C, n_{C'})$	$P_{\perp}^2(n_C, n_{C'})$	$P_{  }^2 - P_{  }^1 P_{C'}$	$P_{\perp}^2 - P_{\perp}^1 P_{C'}$
6	0.2666	6	6	0.0711	0.0734	0.0708	0.0029	$3.0e^{-4}$
5	0.2187	5	6	0.0583	0.0592	0.0587	0.0019	$4.0e^{-4}$
7	0.2116	6	7	0.0564	0.0576	0.0565	$9.0e^{-4}$	$1.0e^{-4}$
4	0.1128	5	7	0.0463	0.0532	0.0469	0.0074	$6.0e^{-4}$
8	0.1094	5	5	0.0478	0.0414	0.0479	-0.0055	$1.0e^{-4}$
9	0.0358	7	7	0.0448	0.0392	0.0444	-0.0065	$-4.0e^{-4}$
3	0.0332	4	7	0.0239	0.0299	0.0244	0.0065	$5.0e^{-4}$
10	0.0070	5	8	0.0239	0.0302	0.0244	0.0063	$5.0e^{-4}$



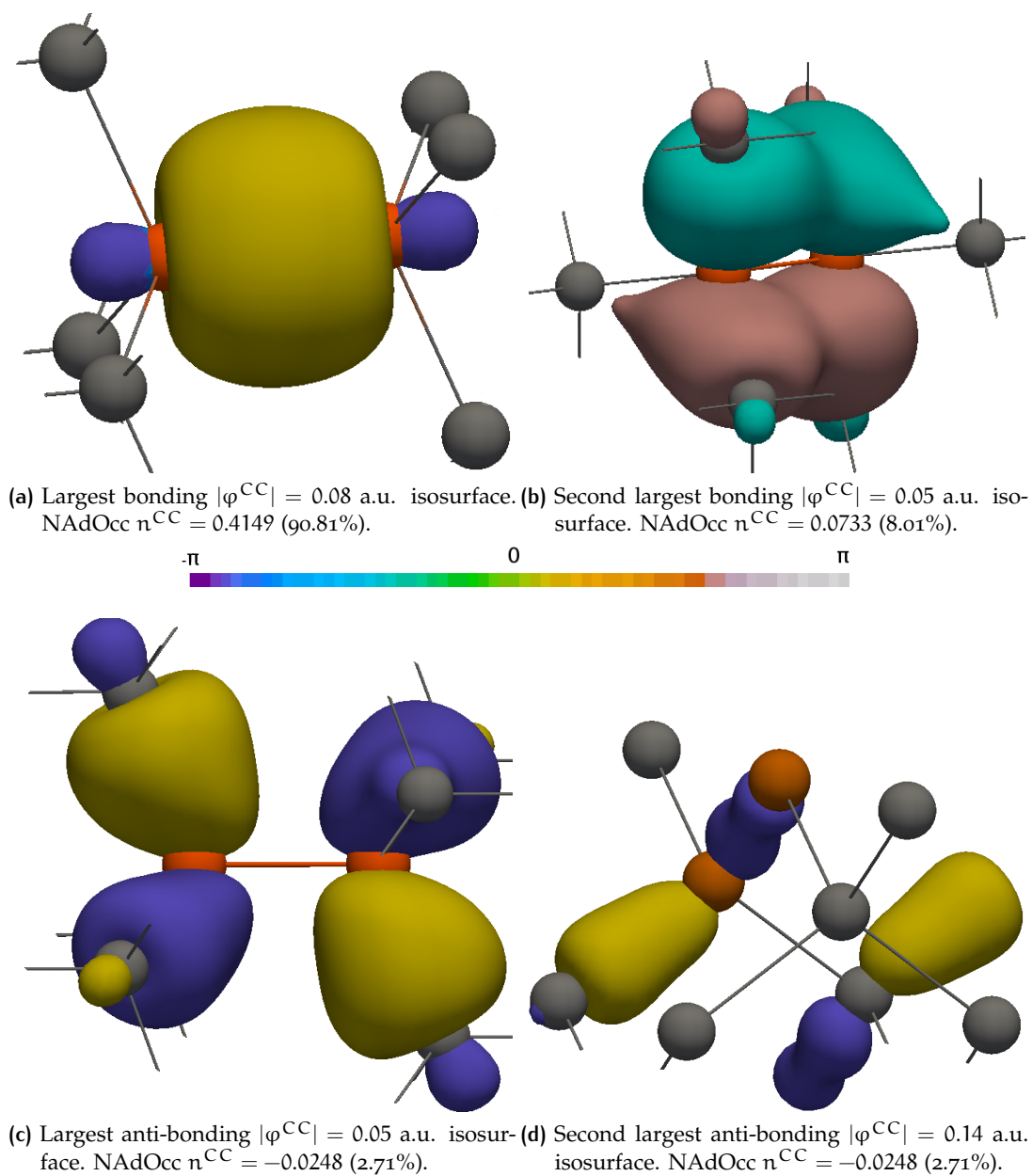


**Figure 27:** 2-centre (direct C neighbours, in orange in the figure) NAdOs  $\varphi^{CC}$  coloured with the phase according to the scale, with the largest (2 bonding and 2 anti-bonding) NAdOcs.

As it is discussed in the DAFH analysis of Baranov and co-workers, diamond has a core orbital almost completely contained within a C basin, but only 48% of the second largest eigenvalue is contained within the QTAIM basin, 43% is shared with the bonded neighbour and 6% delocalizes to basins located beyond the first coordination sphere of a C atom[19]. These the numbers for the bonding orbital of a system with much larger delocalization as it is a covalent electron network, and the DAFH analysis tells us there is a very important 2-centre correlation involving both basins of the bounded atoms. Actually, the population of a single C basin spreads also into other basins apart from the bounded neighbour, so higher order bonding is taking place in the diamond system.

A 2-NAdO  $\varphi^{CC}$  analysis is offered in figure 27. The largest eigenvalue of figure 27a corresponds to the main contribution to the C–C covalent bond in diamond. This orbital represents the highest contribution to the DI, i.e., to the bond order accounting to 90.81% of the total value. As it can be clearly seen in this picture, the NAdOs have symmetry: the irreducible representation of the  $\nu$ -centre group. A DAFH has the symmetry of the centre for which it was calculated, while it possesses the symmetry group of the bond in case of a 2-NAdO. As expected from the known bond order of 1 for diamond and from the DAFH drawings[19], the main largest bonding 2-NAdO is a  $\sigma$  contribution. The image thrown by the NAdOs is, as this also demonstrates, very much similar to the standard MO paradigm.

The second largest  $\varphi^{CC}$  contributes 8.01% and is of  $\pi$ -type. It is in this NAdO where we see that some of the DI is not contained within the C–C region, but invades other neighbouring areas, pointing towards a higher-order bonding paradigm. The anti-bonding contributions are, as in the NaCl crystal, much smaller than the bonding ones, though still noticeable. As the delocalization is larger in this case, the largest negative eigenvalues have a share in the total DI of 2.71%, smaller than in the NaCl instance.

**Table 5:** 1- and 2-centre probabilities between two bonded superbases (see figure 25), each of them formed by the four C atoms forming a tetrahedron in the diamond crystal structure, for different RSRs.

$n_C$	$P^1(n_C)$	$n_C$	$n_{C'}$	$P^1(n_C) \cdot P^1(n_{C'})$	$P^2(n_C, n_{C'})$	
24	0.1634	24	24	0.0267	0.0268	$\delta = 1.2193$ $\lambda = 18.1011$
23	0.1519	23	24	0.0248	0.0249	
25	0.1490	24	25	0.0243	0.0245	
22	0.1192	23	25	0.0226	0.0232	
26	0.1152	23	23	0.0231	0.0227	
21	0.0786	25	25	0.0222	0.0219	
27	0.0757	22	24	0.0195	0.0195	
20	0.0433	24	26	0.0188	0.0190	
28	0.0422	22	25	0.0178	0.0185	
29	0.0199	23	26	0.0175	0.0183	

**Table 6:** 1-centre ( $A - B$ ) probabilities of different RSRS of diamond, for nearest neighbours (n) and second-nearest neighbours (nn).  $P_{RSRS}(n = Z_A + Z_B)$  is the most probable event, and less probable resonant structures until  $P_{RSRS}(n \pm 2)$  are also shown.

	$A - B$	$P_{RSRS}(n = Z_A + Z_B)$	-1	+1	-2	+2
NaCl	n: Na-Cl	0.5594	0.1848	0.1894	0.0303	0.0290
	nn: Na-Na	0.6473	0.2464	0.0537	0.0448	0.0021
diamond	nn: Cl-Cl	0.4472	0.1464	0.2749	0.0253	0.0844
	n: C-C	0.2118	0.1821	0.1864	0.1188	0.1239
graphite	nn	0.1891	0.1669	0.1711	0.1190	0.1225
	n: (C-C) $_{  }$	0.2241	0.1918	0.1923	0.1206	0.1198
Na <i>bcc</i>	(C-C) $_{\perp}$	0.1905	0.1690	0.1722	0.1200	0.1233
	n: Na-Na	0.3149	0.2052	0.0639	0.2698	0.0973
	nn	0.3011	0.2179	0.2439	0.1038	0.0872

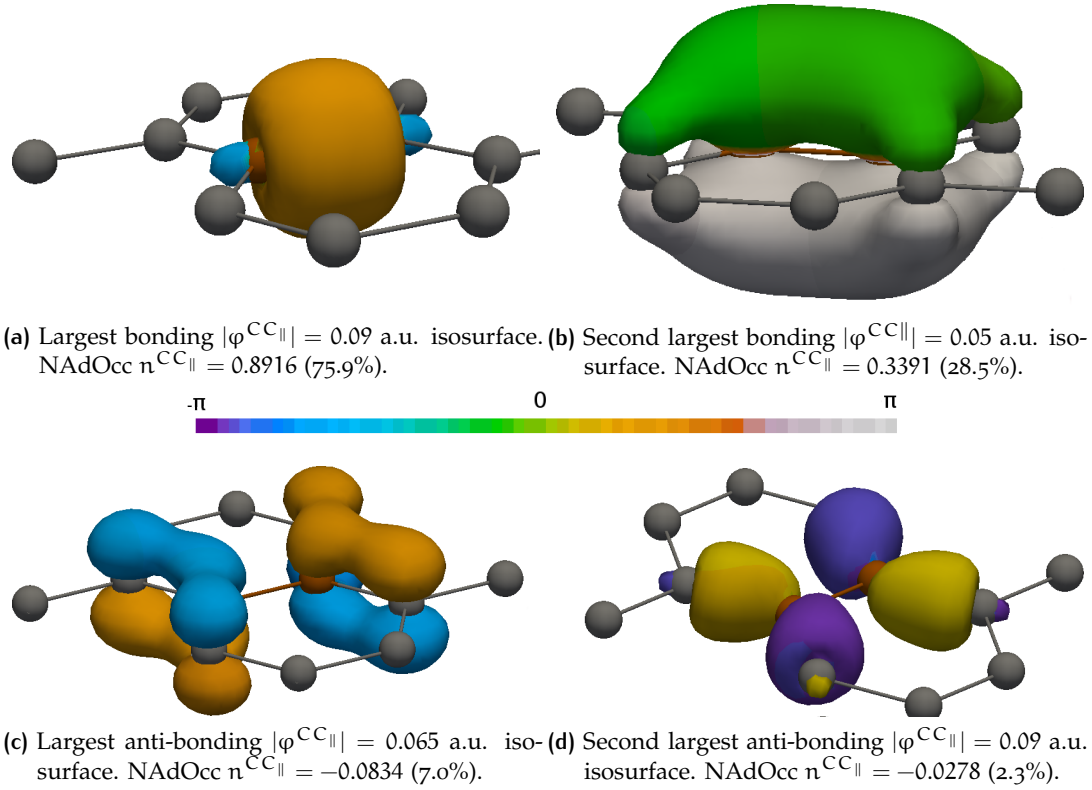


**Figure 28:** 2-centre (direct intra-layer neighbours, in orange in the figure) NAdOs  $\varphi^{CC||}$  within a layer of graphite, coloured with the phase according to the scale, with the largest (2 bonding and 2 anti-bonding) NAdOcs.

The first-neighbour NAdO analysis between carbon atoms is depicted in figure 27 and shows the major contribution to the bond of 90.81% to be  $\sigma$ -like (NAdO 27a). The second contribution is of  $\pi$  type and has a notably lower weight of 8.02%.

The intra-layer 2-NAdOs for graphite  $\varphi^{CC||}$  are shown in figure 28. Similarly as for diamond, the DAFH analysis shows, besides the usual core orbital, a  $\sigma$ -bonding orbital 51% of which is contained within the C basin, while 44% is contained in the basin of the bonded neighbour and just 5% is left for the remaining of the crystal[19]. This suggests a bonding scenario mainly ruled by 2 centres. The bonding 2-NAdO with the largest contribution has as in diamond the expected  $\sigma$  character as can be seen in figure 28a. The second largest  $\varphi^{CC||}$  is a  $\pi$ -like orbital (see figure 28b) and has therefore a rather different character, denoting a multi-centre delocalization. The DAFH analysis recovered a 46% localization within the C basin, and 12% of delocalization to the three closest C basin[19]. The 2-NAdO also points towards a multi-centre delocalization between carbon basins of the same layer. The largest anti-bonding orbitals are of both  $\pi$ - (figure 28c) and  $\sigma$ -character (figure 28d), which represent 7.0% and 2.3% of the  $\delta_{||}^{C,C}$ , respectively.

According to equation , the  $\delta_{||}^{C,C} = 1.2109$  can be divided into a  $\sigma$  contribution that participates with 0.8916 and a  $\pi$  one, which represents 0.3391, in very good coincidence with the classical bond orders of 1 and 1/3 for the  $\sigma$  and  $\pi$  components.

The intra-layer electron network is more delocalized in the case of graphite when compared with diamond, which is clear from the DI analysis (see table 2) and expected since the carbon atoms are arranged in an aromatic pattern within layers. This information is also obtained from the 2-NAdO analysis. The 2-NAdOs recover practically 100% of the DI in diamond, whereas in the case of graphite, 98.2% of the  $\delta_{||}^{C,C}$  is reproduced. Whereas the 2-centre analysis fully characterizes the diamond system, the 2-NAdOs tell us that we are considering a multi-centre bonding scenario within layers in the case of graphite.

It was said above that the delocalization in graphite is a within-layer delocalization, unlike in diamond, where the sharing of electrons is done in all the 3 directions. The inter-layer delocalization is consequently much smaller (see table 2). The 2-NAdOs between direct neighbour basins that belong to different layers (see figure 26 to get an image of how a C basin in graphite does look like) are depicted in figure 29. The 2-NAdO with the largest NAdOcc represents 137.6% of the DI, the  $\delta_{\perp}^{C,C}$  of figure 29a, which evidences that the inter-layer delocalization is mainly of  $\pi$ -type. As the NAdOcs can adopt negative values, the contribution of a single NAdO can be greater than the 100% and in this case, the anti-bonding orbitals heavily participate on the DI, being the largest (figure 29c) 46.4% of it, also of  $\pi$  type. The second contributions, both the bonding (figure 29b) and the antibonding (figure 29d) are much smaller and of similar importance, contribute 4.1% and a 3.1%, respectively and both are of  $\sigma$  symmetry. In all cases, the orbitals stretch out of the C–C region pointing towards a multi-centre delocalization.

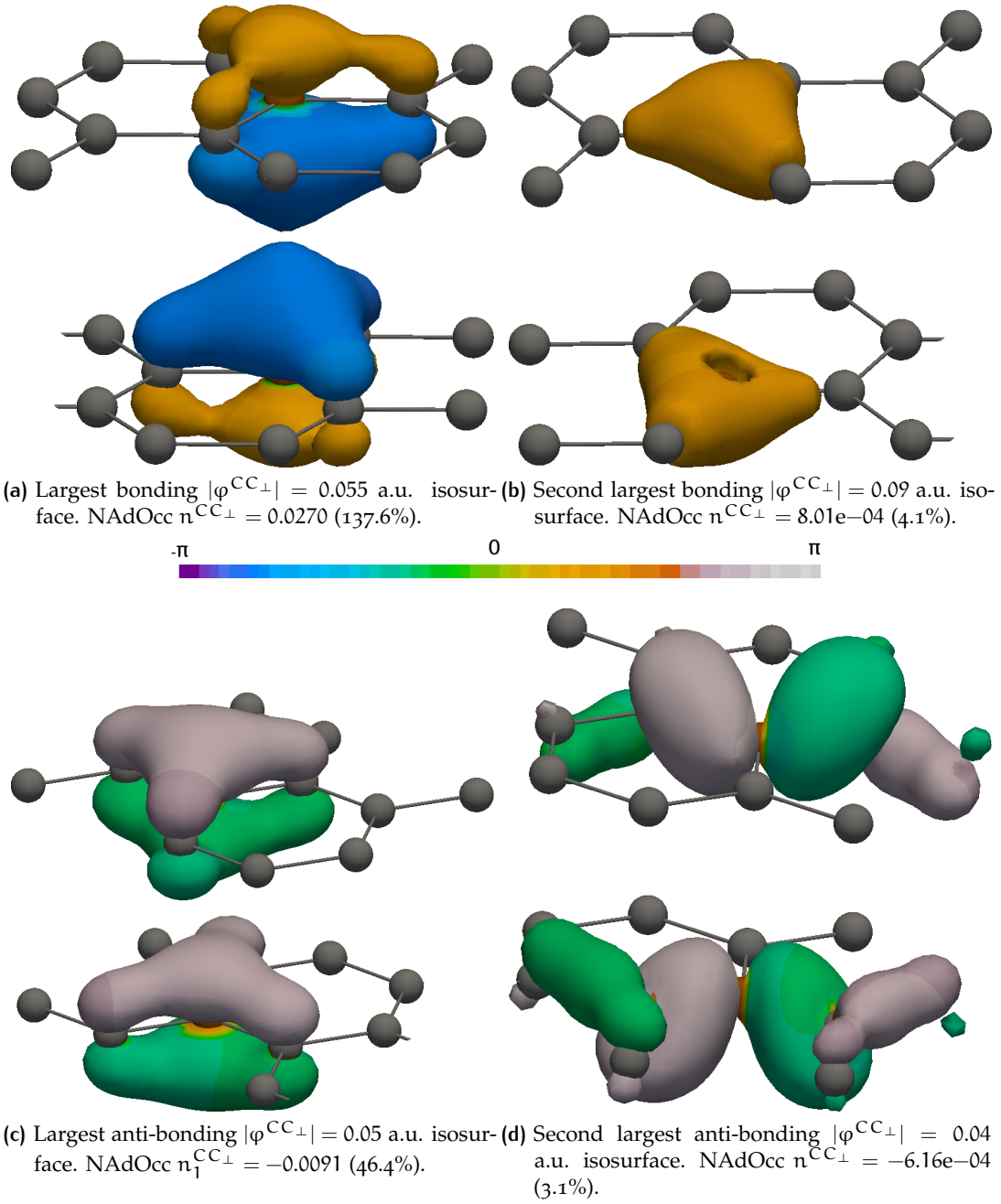


**Figure 29:** 2-centre (direct intra-layer neighbours, in orange in the figure) NAdOs  $\varphi^{CC\perp}$  between layers of graphite, coloured with the phase according to the scale, with the largest (2 bonding and 2 anti-bonding) NAdOcs.

7.2.3 A metal: Na *bcc*

The tight association between metallic bond and high long-range delocalization of the electron network has not only been put forward in many instances (see [19, 94, 149] and references therein), but has also been proven by us in reference [56] and in Section 5. Put it in Pauling's words, a metal can be seen as a system with its atoms bonded by a partially covalent tie[123]. This is confirmed by a DI value in crystalline sodium larger than in an ionic picture but smaller than that of a pure covalent bond  $\delta^{\text{Na,Cl}} < \delta^{\text{Na,Na}} < \delta^{\text{C,C}}$  (see table 2). The partial covalency of the metallic bond is also evidenced by the EDFs' distribution tail, wider than that of crystalline NaCl but narrower than the distribution in diamond, as shown in figure 24.

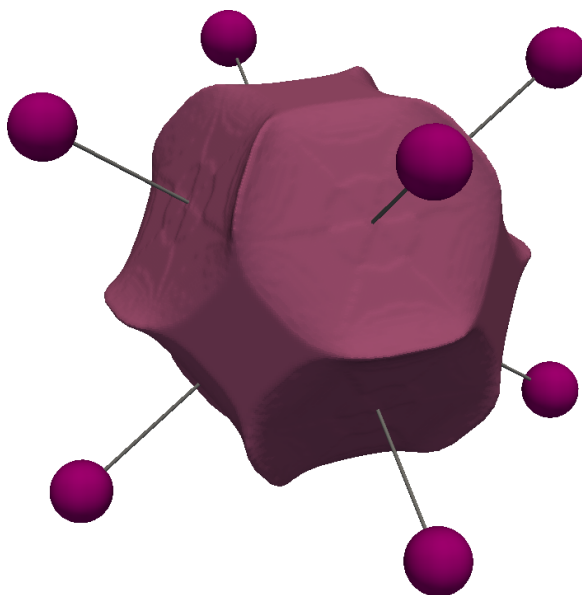


Figure 30: QTAIM basins of the Na *bcc*.

For alkaline metals such as Na *bcc* one awaits even higher delocalization values according to the band theory point of view, for *s*-electrons are thought to be nearly free in contrast to the in general localized *d*-electrons of transition metals. Accordingly, as the DIs are measures of the degree of delocalization, if they are truly sensitive high DI values are expected between distant basins. The inspection of the DIs in solid systems carried out by Baranov and Kohout[18] shows a distant sharing of 0.44 pairs for Na *bcc*, which is notably higher than the values obtained for NaCl crystal of 0.02 pairs but less than the distant sharing observed in diamond and graphite, with 0.74 and 0.64 pairs, respectively. It is even smaller than 0.66, the number of distant shared pairs in the metallic Cu *fcc* system. However, one must take into account that the Na atom has formally only one valence electron available for sharing. It is consequently informative to take a look at the fraction of distant pairs being shared, defined in

equation 105. This quantity indicates that the amount of distant sharing is, as expected, almost twice the value for graphite, diamond and crystalline copper[18].

Calculations were carried out in the case of Na *bcc* over a mesh of  $4 \times 4 \times 4$  k-points, with the same shift and smearing width as in crystalline NaCl. Each Na atom has 8 direct neighbours at a bond distance of  $3.66\text{\AA}$  those depicted in figure 30 which makes a total delocalization of  $8 \times \delta^{\text{Na},\text{Na}} = 8 \times 0.0964 = 0.7712$  (see table 2). Along this direction, the second neighbourhood is formed again by 8 atoms, which makes  $8 \times \delta^{1,3} = 8 \times 0.0030 = 0.0240$  and the third in turn also by  $8 \times \delta^{1,4} = 8 \times 0.0008 = 0.0032$  (table 2). The delocalization with the next nearest (*nnn*) and the next next nearest neighbours (*nnnn*) is far from non-negligible, always along the specified direction, specially noticing that we have considered neither the *nnn* nor the *nnnn* DI between sodium atoms along the direction of the  $4.22\text{\AA}$  bond.

The DAFH analysis tells us a similar interpretation[19]. The bonding DAFHs have  $\sigma$ - and  $\pi$ -character, of which 30% and 6% are contained within the basin. The part of the DAFH found in basins beyond the nearest neighbours at  $3.66\text{\AA}$  and the next nearest neighbours at  $4.22\text{\AA}$  is 14.4% for the s-DAFH and 34% for the p-like one, thus showing that the long-range delocalization is mainly of p-type[19].

The 2-NAdOs for the Na *bcc* crystal are shown in figure 31. The main contribution to the  $\delta^{\text{Na},\text{Na}}$  (figure 31a) is, according to the 1-NAdO analysis a  $\sigma$  orbital, which accounts for 108.2% of it. The  $\pi$ -bonding contribution (figure 31b) has a weaker implication in the DI, representing 5.0% of it. The anti-bonding  $\varphi^{\text{NaNa}s}$  with the largest and second largest NAdOcs (figures 31c and 31d, respectively), participate with 12.0% and 4.3% each. As suggested in reference [18], compounds with a low number of valence electrons often show multicentre bond in metals. Accordingly the 2-NAdO analysis offers a more adequate image of the bonding scenario, since the main contribution to the DI (figure 31a) is almost completely contained in the corresponding region (that formed by the union of two Na basins, depicted in figure 30), indicating that the s-interaction takes place mainly between 2-centres. The p-delocalization is however found to be the responsible for the long-range delocalization [19]. As it is observed, the remaining figures of 31 are p-orbitals and a smaller fraction of them is contained within the region they were calculated for, pointing out it is a bond in which more than 2 centres are involved.

Table 7 gathers up the largest EDFs for crystalline sodium. We can say that a metallic bond is a type of covalent bond in which the high electron sharing takes place with different spatial extension: it is long-range delocalization, instead of that happening in a pure covalent compound that on the contrary is observed at short distances. This fact motivated the analysis of Sections 4 and 5, that deal with the behaviour of the DI with distance. Unlike in diamond, where the



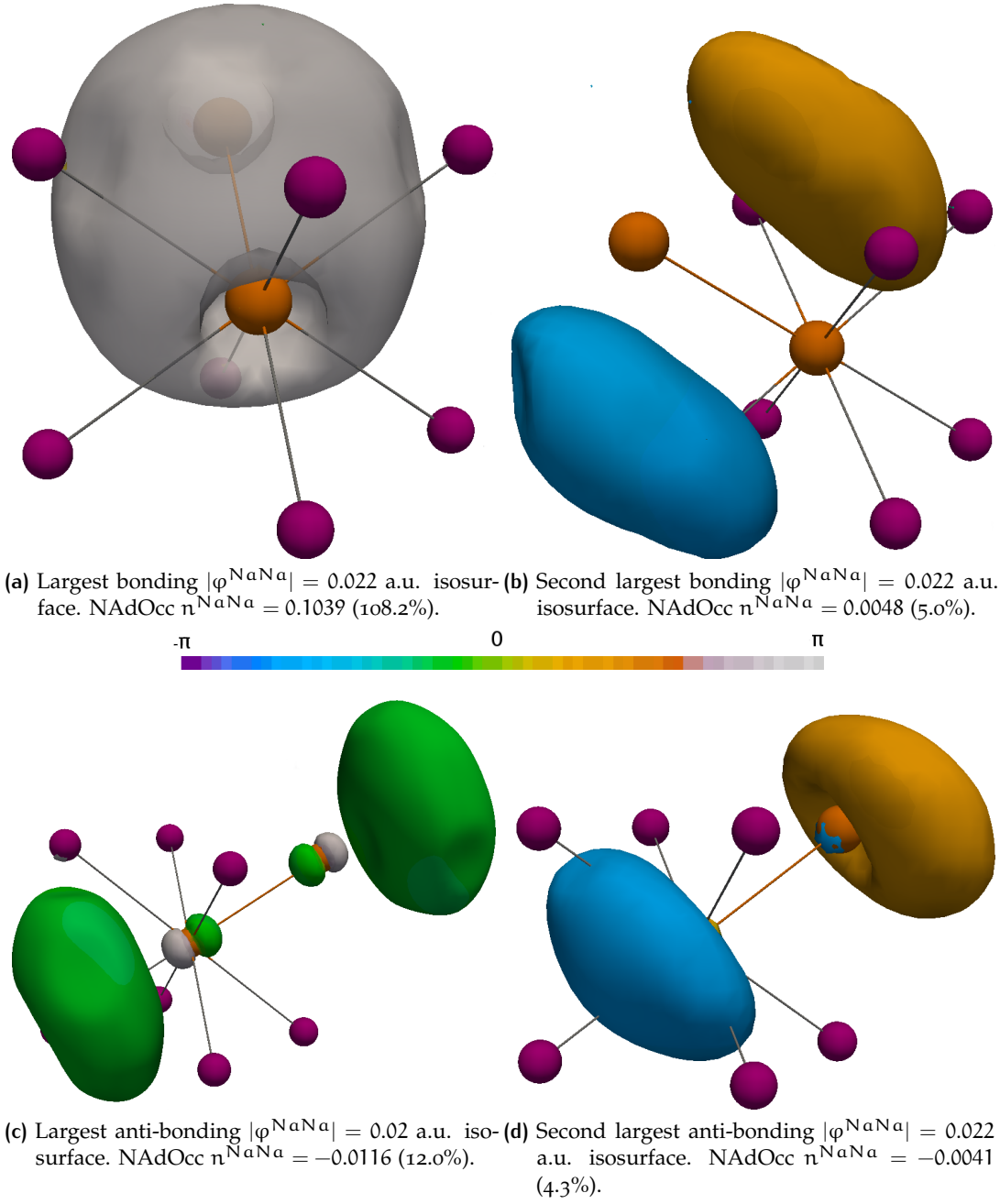


Figure 31: 2-centre (first-neighbouring Na atom basins, in orange in the figures) NAdOs  $\varphi^{\text{NaCl}}$  coloured with the phase according to the attached scale, with the largest (2 bonding and 2 anti-bonding) NAdOcs for the Na *bcc* crystal.

Table 7: Probabilities of different RSRs for the Na *bcc*.

$n_{Na}$	$P^1(n_{Na})$	$n_{Na}$	$n_{Na'}$	$P^1(n_{Na}) \cdot P^1(n_{Na'})$	$P^2(n_{Na}, n_{Na'})$	$P^2 - P^1_{Na} P^1_{Na'}$
11	0.4159	11	11	0.1730	0.1733	3.2e-04
10	0.3254	10	11	0.1353	0.1352	-1.0e-04
12	0.2019	10	10	0.1059	0.0971	-0.0088
13	0.0489	11	12	0.0840	0.0844	4.7e-04
14	0.0069	10	12	0.0657	0.0712	0.0055
15	0.0006	12	12	0.0408	0.0378	-0.0030
9	0.0003	11	13	0.0203	0.0205	2.0e-04
16	3.1e-04	10	13	0.0159	0.0186	0.0027

electrons that travel out of a C basin are most likely found in one of the nearest neighbouring basins, in a metal the electrons travel far away from the atoms they belong to. We could therefore talk of a short-range covalency, which would be that measured by the  $\delta^{1,2}$  between nearest neighbours and a long-range one, between atoms a given number of bond lengths away from each other, or simply characterized by the decay of the DI with distance (see 4 and 5).

The EDFs in the sodium metal show a narrower distribution than in diamond as it was said above (see figure 24 for a 2-centre EDF distribution scheme). As they are normalized and the sum of all of them gives the unity (see equation 135), this is translated in a fewer number of RSRs with a probability to happen above a certain threshold value than in diamond, but individually with a higher weight. It can be observed in table 7, that the first three RSRs occur with a probability of 41.6% if the Na atom keeps its 11 electrons, 32.5% when it becomes a cation and 20% as an anion. In the case of diamond, the largest 1-centre RSR had a weight of 0.2640 (see table 3). The 2-centre EDFs show something similar: both Na atoms are neutral with a probability of 17.3%, or one atom loses an electron with a likelihood of 13.5%, whereas in the case of diamond, the largest  $P^2$  does not reach the 10% (table 3). According to its very low covalent character, the NaCl crystal has only two EDFs with probabilities above the 10%, the largest reaching values of 50.9% (see table 1).

It is worth noting that, despite its reluctance to gain one electron, the  $\text{Na}^-$  event has a probability of 20.2%. If not staying neutral, the Na atom is inclined to lose one electron, but unlike in NaCl or other sodium ionic compounds, the electron that easily leaves its basin, travels a long way but must find a new basin at some point. Its very nature obliges the sodium to not only cede, but also accept electrons. For the same reasoning, the  $P^2$  probabilities tell us that the most likely events are those where either both atoms are neutral (17.3%) or just acts as a cation (13.5%). The circumstance of both atoms being cations is almost as likely to happen as one Na atom being an anion while the other stays neutral, with probabilities of 9.7% and 8.4%, respectively. One atom losing one electron is favourable, but losing two at the same time costs the same effort as one atom gaining one electron. The probability of both Na atoms being anions at the same time (3.8%) is notably smaller.

## Part V

# **The DI as a means to unveil the metal-to-insulator transition in MnO**



# 8

## MOTT INSULATORS

In 1937 de Boer and Verwey[38] presented conductivity data of various transition-metal oxides such as MnO, NiO or CoO among others which in spite of being insulators, were predicted by the band theory to be metals. These compounds are understood to be highly ionic, with oxygen moieties close to oxides,  $O^{2-}$ , and metallic cations with a nominal charge of +2 or +3 a.u. This would then partially fill the 3d bands of the system, and the solids arrangement showed be metallic according to the conventional theory. After that, it became clear that the band theory fails to describe systems where the electron interactions are crucial, in what are known as highly correlated systems, where the assumption that electrons do not interact with each other breaks down.

According to Peierls (1937) the electron-electron correlation is at the root of the origin of the insulating behaviour in systems with partially filled d-electron bands[71]. The explanation of Peierls and Mott (1937) consists in imagining a simple lattice of hydrogen atoms with a large lattice constant so that atoms can be considered as independent particles, one electron assigned to each site[26, 116]. The movement of an electron that leaves its original site and goes to a different location creates a charge flow which originates a conducting state. There are in this process two energies involved: the destabilization coming from pulling out one electron from its site (the ionization potential) and the stabilization achieved by occupying a free site away from the electron's original position (the electron affinity). In normal 3d oxides, this competence leads to highly mobile electrons and to metallic behaviour. However, in highly correlated systems the strong Coulomb repulsion among electrons prevents them from moving at all. At low temperatures, due to the electrostatic interaction the majority of the electrons are at their proper places in the ions and only a few overcome the energetic barrier and get to leave their place. Those must hence travel long in order to find an empty site and will spend time on already occupied ions, at a high energetic cost. The metallic behaviour is then strongly hindered by the nature of the electronic configuration of transition metals, as Mott reported based on Peierls' comments[115].

In the simple case of hydrogen atoms, the energetic penalty of locating two electrons at the same site from 1s orbitals is

$$\left\langle \phi_{1s}\phi_{1s} \left| \frac{e^2}{r_{12}} \right| \phi_{1s}\phi_{1s} \right\rangle. \quad (170)$$

The previous equation is the on-site Coulomb repulsion energy denoted by  $U$ . This Coulomb repulsion competes with the effect of the band width  $W$  in such a way that the actual insulating gap is given by  $U - W$ . To a large lattice parameter  $d$  corresponds a small band gap  $W$  and the potential energy dominates over the kinetic energy, which localizes the electrons and creates an insulating state. On the contrary, for small  $d$  the dominating magnitude is the band gap  $W$  and the system is metallic [26].

The prescription we just described is the basis of the Hubbard model and it is the first approximation to the treatment of a system considering an electron-electron correlation term of the form  $\frac{e^2}{r_{12}}$  that goes beyond the tight-binding approximation, which includes a term for the hopping of electrons between sites, but does not consider the electron-electron repulsion appropriately. The treatment of the Coulomb repulsion among electrons has made the Hubbard model a successful approach that has explained the insulating character of transition metal oxides and other materials with the same behaviour. It consists of a potential term  $U$  which takes into account the repulsion energy for two electrons on the same atomic site and a kinetic term that allows tunneling (hopping) of electrons between neighbouring sites. The latter is mathematically represented by a 'hopping integral' or 'transfer integral' that is directly related to the band width  $W$  [121].

As we have considered (see Section 5), some Transition Metal Oxides (TMOs) are typical examples of strongly correlated systems with partially filled d-bands that show insulating character in the ground state. After the development of the Hubbard model, the work of Mott pioneered the study of such systems and motivated the name of *Mott insulator*. In his explanation, Mott assumes each atomic site to be occupied by only one atomic orbital. In a situation with no electron-electron interactions a single band would be formed from the overlap of the atomic orbitals in a solid the same way as it was explained above. A fully occupied band would mean two electrons, one spin-up and one spin-down at each site. However the Coulomb repulsion would destabilize this situation and according to Mott, the band will split into two: the lower band filled with electrons occupying a free site and the upper one, formed by electrons located at a site already taken by another electron.

An alternative explanation by Slater [154] suggested the origin of the insulating state to be in the superlattice structure of the magnetic periodicity. The key point arises when we leave the Hartree and adopt the Hartree-Fock potential, that assigns different potentials for electrons of different spins. In a simple system of a one dimensional array of like atoms, in the antiferromagnetic case each atom would have one electron with  $\alpha$  and the next with  $\beta$  spin. This alternation causes the periodic potential to have a period of two atoms in the

Hartree-Fock potential, not a period of one, which means the bands will split into two with a gap in the middle. Now if we were dealing with half enough electrons to fill the whole band before splitting, this would mean not one half-filled energy band but a half-band completely filled, predicting the system to be an insulator. Nevertheless, several examples can be found of TMOs with no magnetic ordering, which points out that magnetism does not lie in the origin of the insulating character in Mott systems.

#### 8.0.4 DFT and Hubbard alliance: LSDA+U approach

Among the many attempts towards a satisfying description of Mott insulators using DFT, the LSDA+U has found particular success due to its low computational cost, which makes it an affordable method to treat the not only complex, but also large systems which are the targets of nowadays' interest. It consists of an LSDA functional plus a "Hubbard-like" term  $U$ , that is, an augmented LSDA functional that allows us to control how strong the on-site electronic repulsion is and gain this way a deeper insight of the nature of the Coulomb interactions. It also has an exchange interaction parameter  $J$ , which is the Hund's energy between electrons with like spin.

A major problem encountered when using LSDA+U comes from the fact that electronic interactions are already partially taken into account by the LSDA functional, therefore leading to double counting (DC) errors. All those errors are accounted for by an additional term that is subtracted from the total LSDA+U energy. The problem arises because, whereas the  $U$  and  $J$  quantities are calculated *ab initio*, only approximations to this "DC term" could be found till now, since there is no rigorous derivation of how to construct it.

#### 8.0.5 Mott transitions

Once we have introduced the Mott insulators and the standard method to correctly treat them (LSDA+U), we can go one step further and come closer to what it is our goal in this study. In short, a system undergoes a Mott transition when an alteration of its electric properties takes place, becoming conducting if it was an insulator or vice versa, as a consequence of a change in the strength of electron correlation. The reasons that might electronically alter a system might be of an assorted nature: modifications of the pressure, the composition, the strain... can lead to a change in the correlation strength with a concomitant switch in the ability of the system to conduct electric currents.

In the chemical literature, a metallic behaviour is naïvely associated to a large exchange of electrons among atomic sites, that is to say, to a high degree of delocalization of the electronic network across the



system. As we have shown, (see Sections 4 and 5) the DI conveys information about the insulating- or metallic-like properties of a system. We thus expect it to be an adequate tool to examine the insulator-to-metal transition and provide us with a better understanding of the process taking place in a Mott transition.

Once we have the theoretical basis that will provide us with the wave function of the system and the appropriate tool to capture the transition from metal to insulator, the last missing piece to carry out our study is the system that will be analyzed. Among all the TMOs that show insulating behaviour in their ground state, MnO is one of the simplest we can find, and as such, it is widely used as prototype, subject to many theoretical as well as experimental studies [6, 73, 85, 121]. MnO undergoes a first-order isostructural insulator-to-metal transition when subject to pressure [166]. The fact that this is not accompanied by a change in the crystal symmetry simplifies considerably the theoretical treatment previous to the analysis of the DIs itself, our final goal, making the MnO the most appealing system to this study.

## 9

A FAILURE STORY: DIS AND  
THE MOTT INSULATOR  
TRANSITION IN MNO

## 9.1 LSDA+U RESULTS IN MNO

We start with the real calculations by checking convergence of the Elk parameters against some ground features of the MnO such as the energy-volume (E-V) curve, using the LSDA+U approach.

Energy-volume curves are constructed by plotting the energy evaluated at different values of the lattice parameter. The minimum, corresponding to the equilibrium geometry, is found by a polynomial fitting of the E-V curve, done with the code `Gibbs2` [120]. The calculation with no magnetic ordering yields an equilibrium parameter of 7.6 bohr, 0.8 bohr different from the experimental value of 8.4 bohr [140], which is a too large deviation. Including antiferromagnetism in the calculation changes the bond parameter to 8.25 bohr, now only 0.15 bohr different from the experimental value. Nevertheless, we checked whether that deviation from experiment is due to a bad behaviour of the code, so we repeated the search for the equilibrium geometry using another code: VASP [83]. We see that the difference is also  $\approx 0.2$  bohr as with Elk, concluding the deviation does not lie in the code. Elk E-V curve with magnetic ordering using different values of  $U$  is represented in figure 32.

We will use from now on the equilibrium lattice parameter of  $a = 8.25$  bohr that we have found theoretically from the E-V curve. The effect of changing  $U$ , since it is a parameter that is just added to the energy, will consequently change the energy, so that the larger the value of  $U$ , the more positive the energy (see figure 32). The  $U$  values have been chosen taking as reference the value  $U = 6.9$  from [49], and adjusting it by increasing or decreasing this number.

The  $U$  parameter controls the separation between occupied and empty states, that is to say the band gap, as can be seen in figure 33 where the total Density Of States (DOS) is represented for different values of  $U$ . The LSDA+U is clearly able to recover the insulating character of the Transition-Metal Oxide (TMO), but we are interested here in the insulator-to-metal transition that takes place under pressure, so it must also correctly describe the metallic condition at the other side once the transition has occurred.

The Elk code does not include a keyword to explicitly control the pressure exerted on the system. Alternatively, the lattice parameter has to be manually tuned. MnO is known to change from insulator to

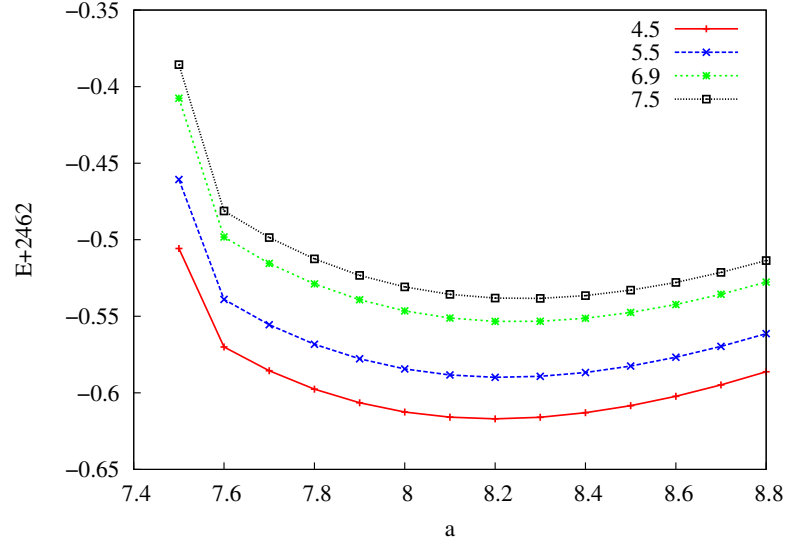


**Figure 32:** Energy-Volume curves for different values of the  $U$  parameter. The equilibrium lattice parameter is close to  $a = 8.25$  bohr, except for  $U = 7.5$ , where  $a = 8.33$  bohr. All values are in atomic units.

conductor under pressure, a transition that happens at around 90 GPa [121]. The performance of the LSDA+ $U$  goes however in the opposite direction: the band gap broadens as the pressure is increased (figure 34). At a value of around  $a \approx 8$  bohr an abrupt change of uncertain origin takes place. After that point, the band gap starts to get thinner until the interatomic distance is so small, that the muffin tins overlap. In the Elk[1] code (see Section 2 for a description on the electronic structure of solids), when the lattice parameter is sufficiently reduced, the muffin-tins overlap and instabilities appear. When this happens, the code automatically changes the radius of the spheres allowing for the calculation to proceed, but causing a leap in the gap, as can be seen at  $a \approx 7.6$  in figures 32 and 34.

To make sure we are obtaining reliable results from the LSDA+ $U$  calculations we also analyzed some thermodynamic properties of the MnO that will be compared with the experimental values. In Table 8 the values of three thermodynamic quantities (see table caption for details) are shown to confirm that no significant difference exists between them theoretical and experimental results.

In agreement with the results shown in reference [73], increasing the pressure beyond the point where according to the experiment the transition occurs does not cause a change in the conducting properties of the MnO. The LSDA+ $U$  method is not able to describe the insulator-to-metal transition, but points towards an insulator-to-insulator transition, whose origin we have not studied in detail.

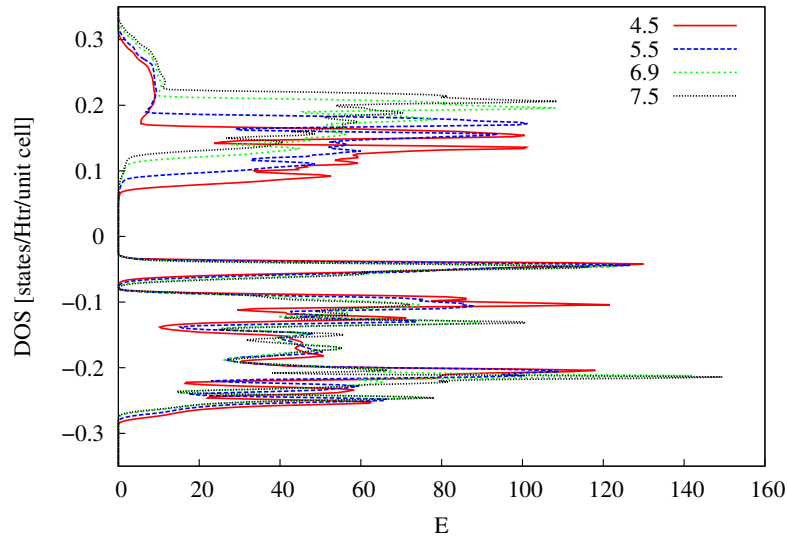


Figure 33: Total DOS at different values of  $U$  against energy. All values are in atomic units. Note the well-developed insulating gap.

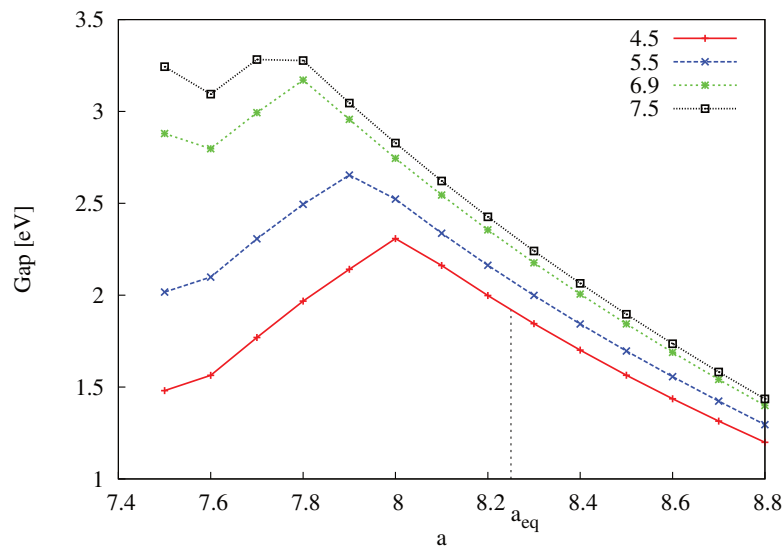


Figure 34: Band gap against pressure for different values of the  $U$  parameter. Except explicitly stated, all values are in atomic units.

**Table 8:** Comparison between experimental and theoretical values of the thermodynamic quantities: the heat capacity at constant pressure  $C_p = (dH/dT)[J K^{-1} mol^{-1}]$ , the adiabatic bulk modulus  $B_s = -V(dP/dV)[GPa]$  and the volumetric thermal expansion coefficient  $\alpha = 1/V(dV/dT)_p[10^{-5} K^{-1}]$ .

U		$C_p$	$B_s$	$\alpha$
	Exp	44.16	142-160	3.36( $\pm 0.37$ )
7.5	B-M(3)	41.528	158.809	3.739
	B-M(4)	41.544	158.644	3.831
6.9	B-M(3)	41.556	159.045	3.857
	P-T(3)	41.543	157.835	3.944
4.5	B-M(3)	41.436	161.617	3.741

Once we have discarded the LSDA+U method that fails to correctly map the transition, we search for an appealing alternative: reduced density matrix functional theory.

## 9.2 A ENCOURAGING ALTERNATIVE: THE REDUCED DENSITY MATRIX FUNCTIONAL THEORY

Reduced density matrix functional theory (RDMFT) is an alternative formulation of DFT originally developed by T.L. Gilbert in 1975 [60]. Gilbert introduced a generalization of the Hohenberg-Kohn theorem using instead of the density the first-order reduced density matrix  $\rho_1$  (1-RDM) defined in equation 49, also referred to as the 1-matrix.

In the single-determinant case, the diagonalization of the 1-matrix produces a set of natural orbitals  $\phi_{ik}$ , characterized by fractional occupation numbers  $n_{ik}$

$$\rho(\mathbf{r}, \mathbf{r}') = \sum_i n_{ik} \phi_{ik}(\mathbf{r}) \phi_{ik}^*(\mathbf{r}'). \quad (171)$$

In order to avoid confusion with the electron density  $\rho(\mathbf{r})$ , which is the diagonal part of the 1-RDM, let us rename it so that  $\rho(\mathbf{r}, \mathbf{r}') = \gamma(\mathbf{r}, \mathbf{r}')$ . To satisfy the N-representability condition of  $\gamma$ , the only requirement is that the occupation numbers must satisfy  $0 < n_{ik} < 1$  and sum to the total number of electrons,  $\sum_{ik} n_{ik} = N$ .

The generalization that Gilbert introduced guarantees in principle the existence of a functional of  $\gamma$  whose minimum yields the exact

ground state energy for systems characterized by an external potential  $V(\mathbf{r})$ :

$$E_v[\gamma] = \int d^3r \int d^3r' \delta(\mathbf{r} - \mathbf{r}') \left[ -\frac{\nabla^2}{2} \right] \gamma(\mathbf{r}, \mathbf{r}') \int d^3r V(\mathbf{r}) \rho(\mathbf{r}) + \frac{1}{2} \int d^3r \int d^3r' \frac{\rho(\mathbf{r}) \rho(\mathbf{r}')}{|\mathbf{r} - \mathbf{r}'|} + E_{xc}[\gamma]. \quad (172)$$

The first two terms account for the kinetic and the external potential energies, respectively. The third term describes the Coulomb repulsion between electrons whereas the last term is the exchange-correlation potential. The exact treatment of the kinetic energy in terms of the 1-RDM implies an advantage of RDMFT with respect to DFT. Although as in DFT the unknown part of the electron-electron interaction is gathered together into an exchange-correlation (xc) term  $E_{xc}$ , this does not include contributions to the kinetic energy, which is on the contrary treated exactly [161]. Approximate functionals for the xc energy in terms of the 1-matrix have been constructed, taking the original functional of Müller [118] as the starting point. One of them is the power functional [146], which describes the xc energy as

$$E_{xc}[\rho_1] = -\frac{1}{2} \int \int d^3r' d^3r \frac{|\rho_1^\alpha(\mathbf{r}, \mathbf{r}')|^2}{|\mathbf{r} - \mathbf{r}'|}. \quad (173)$$

The system-dependent parameter  $\alpha$  regulates the electron correlation included in the calculation. This functional interpolates between the  $\alpha = 1$  case which is the uncorrelated HF limit and the Müller prescription, which offers an alternative to the HF functional setting  $\alpha = 1/2$  but on the other hand overcorrelates the system [146]. The parameter  $\alpha$  has been found to have its peak performance at the value  $\alpha = 0.656$ , which is fixed for all our calculations [146].

Up to now RDMFT has been applied to both finite [88] and infinite systems [89, 146]. For extended systems, RDMFT faces the challenge of correctly describing the insulating nature of TMOs such as MnO or NiO in absence of magnetic treatment, where usual local/semi-local density approximations to the xc functional of DFT fail. The developers of Elk, the code we use in our solid state calculations, have implemented the RDMFT approach for many electron systems in their code [146] and have shown that, in principle, this method successfully describes the insulating state of MnO with no spin polarization [147], although antiferromagnetism had to be later considered [148].

Most approximations in RDMFT are explicit functionals of and minimized in terms of the natural orbitals  $\phi_j(\mathbf{r})$  (NOs) and their occupation numbers  $n_j$ . Unlike Kohn-Sham orbitals, which only accept being either fully occupied or empty, the NOs used by RDMFT have fractional occupations, which motivates their name despite the fact that  $\rho_1$  is not explicitly constructed. Contrary to what hap-

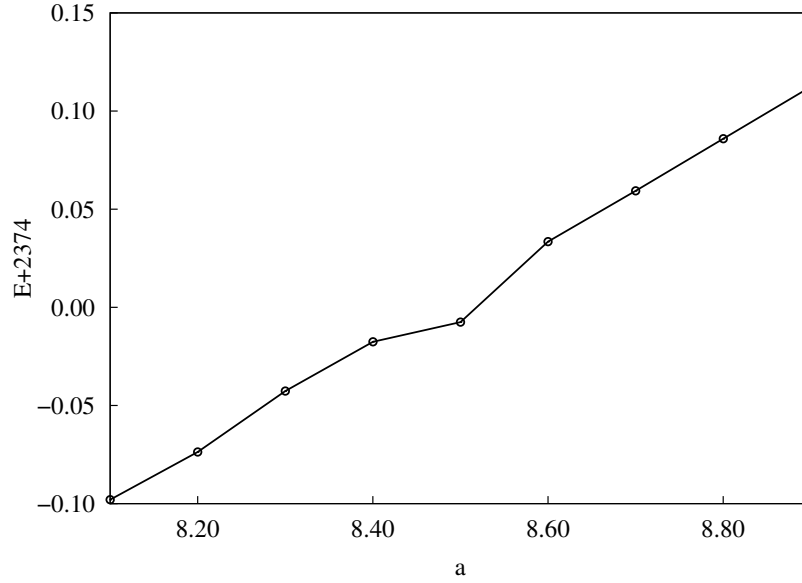


**Figure 35:** RDMFT ( $\alpha = 0.65$ ) energy-volume curve for MnO  $Fm\bar{3}m$  using a k-point shift  $vkloff=(0.25,0.5,0.625)$ . The experimental lattice parameter is  $a_{exp} = 8.40$ . Atomic units used throughout.

pens in classical DFT, the functional optimization with respect to the NOs does not reduce to an iterative eigenvalue problem, and specific techniques had to be introduced ([161] and references therein). On the other hand, it is favourable for us to deal with those “pseudo-NOs” since there is a way open for the evaluation of DIs from a RDMFT calculation. In their publication in 2002, Buijse and Baerends [28] provide us with a tool to approximately describe the exchange-correlation hole density and from it the 2-matrix, the required quantity for the evaluation of the DIs.

We hence performed test calculations adjusting the parameters of the code and tried to reproduce the equilibrium geometry. After a few trials we soon confirm that RDMFT does not reproduce the experimental equilibrium geometry of MnO (see figure 35). By establishing contact with the developers, they warned about the challenge that represents trying to reproduce equilibrium geometries with RDMFT. They suggested to instead try to reproduce the insulating nature of the MnO directly. As said before, the main bottleneck of RDMFT is its very demanding nature. A calculation of the MnO within a k-mesh of  $\mathbf{k} = (4, 4, 4)$  ( $4^3$ ) points, although it takes already a couple of weeks to complete, is too coarse and still non-converged, as it is revealed by the effect that shifting the k-point mesh has on the DOS (figure 36). The keyword `vkloff` is a vector, through which the displacement of the mesh with respect to the default settings is specified. By a shift in the k-point mesh, the actual number of k-points sampled in the calculation might be reduced according to the symmetry of the system treated, operation that by no means affects the final results. A calculation where using a specific `vkloff` causes a different DOS spec-

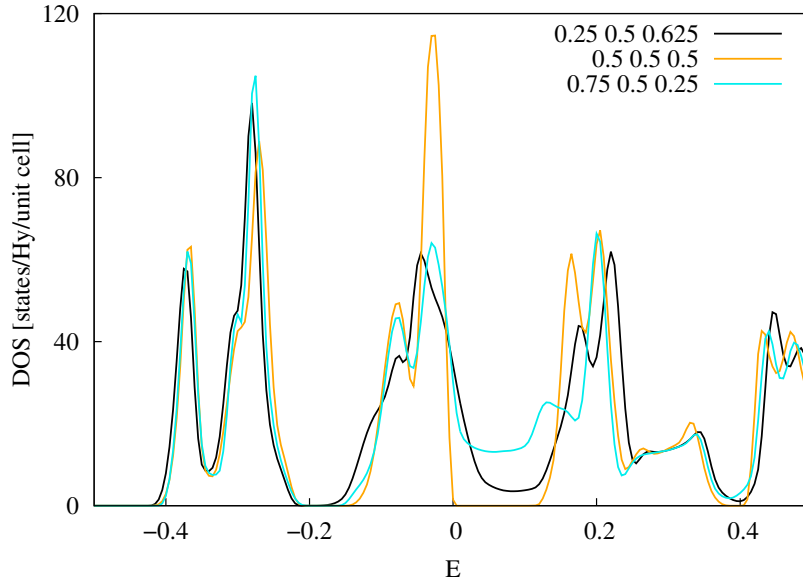


**Figure 36:** RDMFT ( $\alpha = 0.65$ ) DOS for MnO  $Fm\bar{3}m$  using a k-point mesh of  $4^3$  points shifted according to three different vkloff vectors. Atomic units used throughout.

trum, as it is our case, signals that convergence has not been attained yet (see figure 36). The k-point mesh used is still not fine enough, consequently yielding no reliable results. Improving the quality of the calculation by increasing the number of k-points is the immediate step, but means the computational time to complete the calculation will make it last more than one month in our cluster, which forces us to find another walk-around better than this.

One way to overcome that difficulty is to resort to more powerful computational resources: the Barcelona Supercomputing Center (BSC-CNS)<sup>1</sup>. This facility gives access to machines that are among the most powerful ones in Spain and is available for free for researchers working at a public institution. We submitted a project asking for stronger computational resources to test a solution to our problem and were assigned with calculation time in the Pablo Picasso node at the University of Málaga. Among all the machines available from the BSC-CNS, Pablo Picasso was the most convenient for us since it has the largest memory as well as the largest number of cores that can be used without the implementation of a protocol for node communication (MPI). The RDMFT algorithm, and we come here to another bottleneck of the theory nowadays, is still in an early phase of development, and the MPI protocol has not been implemented yet. This limitation in the parallelization adds to the large time demand, since the standard use of large number of cores in most supercomputers requires efficient communication between nodes. Although  $\approx 80$  processors were available by only using the OpenMP protocol, supported

<sup>1</sup> For more information about the BSC, check the web site: <http://www.bsc.es/>.



by RDMFT, this did not seem to speed up the calculation enough and did not allow us to have the calculations with large number of  $k$ -points done.

At the 2013 CECAM workshop about the Elk code celebrated in Lausanne a discussion related to this was held. It was discussed there that the calculations made in the original  $\text{MnO}$  RDMFT papers were done using  $\approx 300$  processors with only OpenMP implemented, something unreachable for us. Interestingly, the Elk authors suggested that the algorithm is still not mature enough in order to be used for scientific production. Accordingly we decided to follow the advise of the Elk programmers and leave the topic in standby for further study waiting for coming improvements.

# **Part VI**

## **Conclusions**



To wrap up, let us summarize some of the main conclusions that stem from our work:

Part III:

- The DI, as a real space index dominated by the square of the 1-RDM, is linked to conductivity.
- This link is perceptible in form of an exponential decay rate of the DI in insulators and algebraic in metals. The rate increases with the dimensionality of the system.
- This behaviour is present both in Hückel and TB models, as well as in real molecules, even if they are small and in solid state systems.
- The DI decays oscillating, which are linked to Pauling resonant structures and chemical mesomerism, well known in alternant hydrocarbons.
- Within the Hubbard model, correlation can be included through the parameter  $r$ . That way, transitions between insulating and metallic phases, where electron correlation plays a fundamental role can be studied, as well as the behaviour of the DIs and LIs under strongly correlated regimes.
- The costly correlated calculations restricted the systems analyzed to simple H finite and infinite rings, where both the DIs and LIs show a sigmoidal decay with the intersite distance.
- The origin of this sigmoidal decay lies in the non-linear relation between the intersite distance and the correlating parameter  $r$ .
- Both indices converge quickly with chain size. In the H chain, the LI decays smoothly to zero as either  $r$  or the chain size increases.
- In an infinite Hubbard chain, oscillations persist at small values of  $r$  to further disappear as  $r$  increases and a clear exponential decay sets in.
- If the dimension of the system is increased to 2D and 3D, a true MIT occurs and the variance of the electron population, related to the LI can be used as an order parameter to study the transition.

Part IV:

- The analysis of the electron distribution function (EDF) in the solid state provides us with a wide view of the possible real space resonant structures (RSRSs) —in Pauling’s terms— that a system can adopt and what is the probability of each of them to occur.
- For it derives from the same quantity as the DI, the EDF gives similar information but at a finer level, therefore complementing it.
- The high electron sharing of covalent compounds gives rise to a wide distribution of the RSRSs. The opposite situation of an ionic crystal has usually a single RSRS that represents its most common electron distribution. A metal, in agreement with Pauling words, is a partial covalent bond, which is confirmed by the EDFs which show an intermediate width.
- It is the long range delocalization that causes the EDF distribution to be narrower than that of a covalent compound, not its ionic character.
- RSRSs with probabilities below the most important one are revealing in atypical chemical behaviours.
- In graphite, the delocalization is mainly two-dimensional (intra-layer), whereas in diamond it spreads in the three directions.
- No higher orders than the 2-NAdOs are in most cases necessary to explain the bonding situation in a crystalline solid.
- Whereas in NaCl, Na *bcc* and diamond the bond is mainly a  $\sigma$ -type bond, in graphite the  $\pi$ -like contribution dominates.

#### Part V:

- The DIs are suitable tools to capture insulating and metallic behaviour, and it is therefore applicable to use them to map a Mott transition in a real compound, such as the MnO.
- Although it seemed that the band theory limitation to treat such oxides had been overcome, the published results were not reproducible in spite of the effort we put.
- We think the main reasons for that arise from the early stage of the development of the algorithms and the high computational resources associated with RDMFT.

## BIBLIOGRAPHY

- [1] (2013), «Elk 2.2.10», <http://elk.sourceforge.net>. {Cited on pages 45, 64, 112, and 144.}
- [2] A. MARTÍN PENDÁS, A. and FRANCISCO, E. (2016), «PRO-MOLDEN. A QTAIM/IQA code», (Unpublished). {Cited on pages 63 and 83.}
- [3] AMBROSCH-DRAXL, C. (2004), «Augmented planewave methods», *Physica Scripta*, vol. T109, p. 48. {Cited on page 45.}
- [4] ANDERSEN, O. (1975), «Linear methods in band theory», *Physical Review B*, vol. 12 (8), p. 3060. {Cited on page 47.}
- [5] ANGYAN, J., LOOS, M. and MAYER, I. (1994), «Covalent bond orders and atomic valence indices in the topological theory of atoms in molecules», *The Journal of Physical Chemistry*, vol. 98 (20), pp. 5244–5248. {Cited on pages 58 and 116.}
- [6] ANISIMOV, V., KOROTIN, M. and KURMAEV, E. (1990), «Band-structure description of Mott insulators (NiO, MnO, FeO, CoO)», *Journal of Physics: Condensed Matter*, vol. 2 (17), p. 3973. {Cited on page 142.}
- [7] ASHCROFT, N. and MERMIN, N. (1976), *Solid state physics*, New York, Saunder College Publishing. {Cited on page 37.}
- [8] BADER, R. (1991), «A quantum theory of molecular structure and its applications», *Chemical Reviews*, vol. 91 (5), pp. 893–928. {Cited on page 53.}
- [9] BADER, R. (1994), *Atoms in Molecules: A Quantum Theory*, International Series of Monographs on Chemistry, Clarendon Press. {Cited on pages 53, 54, and 55.}
- [10] BADER, R. and STEPHENS, M. (1974), «Fluctuation and correlation of electrons in molecular systems», *Chemical Physics Letters*, vol. 26 (3), pp. 445–449. {Cited on pages 6, 54, 59, 60, 79, and 113.}
- [11] BADER, R., STREITWIESER, A., NEUHAUS, A., LAIDIG, K. and SPEERS, P. (1996), «Electron delocalization and the Fermi hole», *Journal of the American Chemical Society*, vol. 118 (21), pp. 4959–4965. {Cited on page 54.}
- [12] BADER, R. F. (1990), *Atoms in molecules*, Wiley Online Library. {Cited on pages 6 and 95.}

- [13] BADER, R. F. and STEPHENS, M. E. (1975), «Spatial localization of the electronic pair and number distributions in molecules», *Journal of the American Chemical Society*, vol. 97 (26), pp. 7391–7399. {Cited on pages 54 and 116.}
- [14] BADER, R. F. W. (1990), *Atoms in Molecules*, Oxford University Press, Oxford. {Cited on page 59.}
- [15] BAERISWYL, D., CAMPBELL, D. K., CARMELO, J. M. P. and LOUIS, E., eds. (1995), *The Hubbard Model: Its Physics and Mathematical Physics*, Springer US. {Cited on pages 78 and 82.}
- [16] BAMBERG, J., CAIRNS, G. and KILMINSTER, D. (2003), «The crystallographic restriction, permutations, and Goldbach’s conjecture», *The American mathematical monthly*, vol. 110 (3), pp. 202–209. {Cited on page 38.}
- [17] BARANOV, A. I. and KOHOUT, M. (2011), *Acta Crystallogr. A*, vol. 67, p. C115. {Cited on pages 83, 85, and 91.}
- [18] BARANOV, A. I. and KOHOUT, M. (2011), «Electron localization and delocalization indices for solids», *Journal of computational chemistry*, vol. 32 (10), pp. 2064–2076. {Cited on pages 7, 57, 58, 68, 73, 83, 112, 114, 123, 124, 132, and 133.}
- [19] BARANOV, A. I., PONEC, R. and KOHOUT, M. (2012), «Domain-averaged Fermi-hole analysis for solids», *The Journal of chemical physics*, vol. 137 (21), p. 214 109. {Cited on pages 108, 116, 127, 129, 132, and 133.}
- [20] BAREISS, E. H. (1969), «Numerical solution of linear equations with Toeplitz and vector Toeplitz matrices», *Numerische Mathematik*, vol. 13 (5), pp. 404–424. {Cited on page 64.}
- [21] BECKE, A. and EDGECOMBE, K. (1990), «A simple measure of electron localization in atomic and molecular systems», *Journal of Chemical Physics*, vol. 92, p. 5397. {Cited on pages 6, 53, and 61.}
- [22] BESNAINOU, S., ROUX, M. and DAUDEL, R. (1955), «Retour sur leffet de la liaison chimique sur la densite electronique», *COMPTES RENDUS HEBDOMADAIRES DES SEANCES DE L’ACADEMIE DES SCIENCES*, vol. 241 (3), pp. 311–313. {Cited on page 59.}
- [23] BLANCO, M., MARTÍN PENDÁS, A. and FRANCISCO, E. (2005), «Interacting quantum atoms: a correlated energy decomposition scheme based on the quantum theory of atoms in molecules», *Journal of Chemical Theory and Computation*, vol. 1 (6), pp. 1096–1109. {Cited on page 102.}

- [24] BOHR, N. (1913), «I. On the constitution of atoms and molecules», *The London, Edinburgh, and Dublin Philosophical Magazine and Journal of Science*, vol. 26 (151), pp. 1–25. {Cited on page 3.}
- [25] BOYS, S. F. (1966), *Quantum Science of Atoms, Molecules, and Solids*, P. O. Lowdin, Ed. Academic Press, New York. {Cited on page 60.}
- [26] BRANDOW, B. (1976), «Theory of mott insulators», *International Journal of Quantum Chemistry*, vol. 10 (S10), pp. 417–434. {Cited on pages 8, 139, and 140.}
- [27] BREA, O., EL KHATIB, M., ANGELI, C., BENDAZZOLI, G. L., EVANGELISTI, S. and LEININGER, T. (2013), «Behavior of the position-spread tensor in diatomic systems», *Journal of chemical theory and computation*, vol. 9 (12), pp. 5286–5295. {Cited on page 60.}
- [28] BUIJSE, M. and BAERENDS, E. (2002), «An approximate exchange-correlation hole density as a functional of the natural orbitals», *Molecular Physics*, vol. 100 (4), pp. 401–421. {Cited on page 148.}
- [29] BURKE, K. (2007), *the ABC of DFT*, Rutgers University. {Cited on page 27.}
- [30] CANCÈS, E., KERIVEN, R., LODIER, F. and SAVIN, A. (2004), *Theor. Chem. Acc.*, vol. 111 (2-6), p. 373. {Cited on page 103.}
- [31] CAO, W. L., GATTI, C., MACDOUGALL, P. J. and BADER, R. F. W. (1987), «On the presence of non-nuclear attractors in the charge distributions of Li and Na clusters», *Chem. Phys. Lett.*, vol. 141 (5), p. 380. {Cited on page 59.}
- [32] CHAMORRO, E., FUENTEALBA, P. and SAVIN, A. (2003), «Probability Distribution in AIM and ELF basins», *J. Comp. Chem.*, vol. 24, p. 496. {Cited on pages 7 and 103.}
- [33] COOPER, D. L. and PONEC, R. (2013), «Bond formation in diatomic transition metal hydrides: Insights from the analysis of domain-averaged fermi holes», *International Journal of Quantum Chemistry*, vol. 113 (2), pp. 102–111. {Cited on page 108.}
- [34] COTTENIER, S. (2004), *Density Functional Theory and the family of (L) APW-methods: a step-by-step introduction*, to be found at [http://www.wien2k.at/reg\\_user/textbooks](http://www.wien2k.at/reg_user/textbooks), (Instituut Voor Kern-en Stralingsfysica, KU Leuven, Belgium). {Cited on pages 28 and 47.}
- [35] COTTON, F. A. (2008), *Chemical applications of group theory*, John Wiley & Sons. {Cited on page 39.}



- [36] COULSON, C. A., O'LEARY, B. and MALLION, R. B. (1978), *Hückel Theory for Organic Chemists*, Academic Press (London). {Cited on page 67.}
- [37] DAUDEL, R. (1968), *The fundamentals of theoretical chemistry: wave mechanics applied to the study of atoms and molecules*, Pergamon. {Cited on page 7.}
- [38] DE BOER, J. H. and VERWEY, E. J. (1937), «Semi-conductors with partially and with completely filled 3d-lattice bands», *Proceedings of the Physical Society*, vol. 49 (4S), p. 59. {Cited on page 139.}
- [39] EINSTEIN, A. (1905), «The photoelectric effect», *Ann. Phys.*, vol. 17 (132), p. 4. {Cited on page 3.}
- [40] EINSTEIN, A. (1906), «On the theory of light production and light absorption», *Annalen der Physik*, vol. 20, pp. 199–206. {Cited on page 3.}
- [41] EINSTEIN, A. and OTHERS (1905), «On the electrodynamics of moving bodies», *Annalen der Physik*, vol. 17 (10), pp. 891–921. {Cited on page 3.}
- [42] ESCHRIG, H. (2003), *The Fundamentals of Density Functional Theory (revised and extended version)*, vol. 9, Edition am Gutenbergplatz, Leipzig, Germany. {Cited on page 27.}
- [43] ESSLER, F. H. L. and FRAHM, H. (1999), *Phys. Rev. B*, vol. 60, p. 8540. {Cited on pages 82, 89, and 90.}
- [44] FEIXAS, F., MATITO, E., POATER, J. and SOLÀ, M. (2008), «On the performance of some aromaticity indices: A critical assessment using a test set», *Journal of computational chemistry*, vol. 29 (10), pp. 1543–1554. {Cited on page 123.}
- [45] FRADERA, X., AUSTEN, M. and BADER, R. (1999), «The Lewis model and beyond», *The Journal of Physical Chemistry A*, vol. 103 (2), pp. 304–314. {Cited on pages 56, 113, 116, and 123.}
- [46] FRADERA, X., AUSTEN, M. A. and BADER, R. F. W. (1999), «The Lewis Model and Beyond», *J. Phys. Chem. A*, vol. 103, pp. 304–314. {Cited on page 79.}
- [47] FRADERA, X., POATER, J., SIMON, S., DURAN, M. and SOLA, M. (2002), «Electron-pairing analysis from localization and delocalization indices in the framework of the atoms-in-molecules theory», *Theoretical Chemistry Accounts: Theory, Computation, and Modeling (Theoretica Chimica Acta)*, vol. 108 (4), pp. 214–224. {Cited on page 54.}

- [48] FRADERA, X., POATER, J., DURAN, M. and SOLÀ, M. (2003), «The delocalization index as an electronic aromaticity criterion: Application to a series of planar polycyclic aromatic hydrocarbons», *Chemistry-a European Journal*, vol. 9 (2), pp. 400–406. {Cited on page 54.}
- [49] FRANCHINI, C., BAYER, V., PODLOUCKY, R., PAIER, J. and KRESSE, G. (2005), «Density functional theory study of MnO by a hybrid functional approach», *Physical Review B*, vol. 72 (4), p. 045 132. {Cited on page 143.}
- [50] FRANCISCO, E., MARTÍN PENDÁS, A. and BLANCO, M. (2006), «A molecular energy decomposition scheme for atoms in molecules», *Journal of Chemical Theory and Computation*, vol. 2 (1), pp. 90–102. {Cited on pages 59 and 102.}
- [51] FRANCISCO, E., MARTÍN PENDÁS, A. and BLANCO, M. A. (2006), *J. Chem. Theory Comput.*, vol. 2, p. 90. {Cited on page 79.}
- [52] FRANCISCO, E., MARTÍN PENDÁS, A. and BLANCO, M. A. (2007), *J. Chem. Phys.*, vol. 126, p. 094 102. {Cited on page 79.}
- [53] FRANCISCO, E., MARTÍN PENDÁS, A. and BLANCO, M. A. (2008), *Comp. Phys. Commun.*, vol. 178, p. 621. {Cited on page 104.}
- [54] FRANCISCO, E. and PENDÁS, A. M. (2014), «Electron number distribution functions from molecular wavefunctions. Version 2», *Computer Physics Communications*, vol. 185 (10), pp. 2663–2682. {Cited on pages 7, 79, 104, and 112.}
- [55] FRANCISCO, E., MARTÍN PENDÁS, A., GARCÍA-REVILLA, M. and BOTO, R. Á. (2013), «A hierarchy of chemical bonding indices in real space from reduced density matrices and cumulants», *Computational and Theoretical Chemistry*, vol. 1003, pp. 71–78. {Cited on pages 33, 35, and 108.}
- [56] GALLO-BUENO, A., FRANCISCO, E. and PENDÁS, A. M. (2016), «Decay rate of real space delocalization measures: a comparison between analytical and test systems», *Physical Chemistry Chemical Physics*. {Cited on pages 7, 77, 79, 83, 85, 90, and 132.}
- [57] GARCÍA-REVILLA, M., POPELIER, P. L., FRANCISCO, E. and MARTÍN PENDÁS, A. (2011), «Nature of chemical interactions from the profiles of electron delocalization indices», *Journal of chemical theory and computation*, vol. 7 (6), pp. 1704–1711. {Cited on pages 7, 77, 80, 85, and 91.}
- [58] GATTI, C., FANTUCCI, P. and PACCHIONI, G. (1987), *Theor. Chim. Acta*, vol. 72, p. 433. {Cited on page 59.}

- [59] GEORGES, A., KOTLIAR, G., KRAUTH, W. and ROZENBERG, M. J. (1996), «Dynamical mean-field theory of strongly correlated fermion systems and the limit of infinite dimensions», *Rev. Mod. Phys.*, vol. 68, p. 13, URL <http://link.aps.org/doi/10.1103/RevModPhys.68.13>. {Cited on pages 78 and 82.}
- [60] GILBERT, T. (1975), «Hohenberg-Kohn theorem for nonlocal external potentials», *Physical Review B*, vol. 12 (6), p. 2111. {Cited on pages 9 and 146.}
- [61] GIMARC, B. M. (1979), *Molecular structure and bonding. The qualitative molecular orbital approach*, Academic Press, New York. {Cited on page 59.}
- [62] GOEDECKER, S. (1998), *Phys. Rev. B*, vol. 58, p. 3501. {Cited on page 61.}
- [63] GRIFFITHS, D. and HARRIS, E. (1995), *Introduction to quantum mechanics*, vol. 2, Prentice Hall. {Cited on page 3.}
- [64] GUZTWILLER, M. C. (1963), *Phys. Rev. Lett.*, vol. 10, p. 159. {Cited on page 83.}
- [65] HAMERMESH, M. (1962), *Group theory and its application to physical problems*, Courier Corporation. {Cited on page 39.}
- [66] HEITLER, W. and LONDON, F. (1927), «Interaction between neutral atoms and homopolar binding according to quantum mechanics», *Z. Physik*, vol. 44, p. 455. {Cited on page 4.}
- [67] HOHENBERG, P. and KOHN, W. (1964), «Inhomogeneous electron gas», *Physical Review*, vol. 136 (3B), p. B864. {Cited on pages 22 and 24.}
- [68] HUBBARD, J. (1963), «Electron Correlations in Narrow Energy Bands», *Proceedings of the Royal Society of London A: Mathematical, Physical and Engineering Sciences*, vol. 276 (1365), p. 238. {Cited on pages 78 and 81.}
- [69] HÜCKEL, E. (1930), «Zur Quantentheorie der Doppelbindung», *Zeitschrift für Physik*, vol. 60 (7-8), pp. 423-456. {Cited on page 4.}
- [70] HUND, F. (1932), «Zur frage der chemischen bindung», *Zeitschrift für Physik*, vol. 73 (1-2), pp. 1-30. {Cited on page 4.}
- [71] IMADA, M., FUJIMORI, A. and TOKURA, Y. (1998), «Metal-insulator transitions», *Reviews of Modern Physics*, vol. 70 (4), p. 1039. {Cited on page 139.}

- [72] IVERSEN, B. B., JENSEN, J. L. and DANIELSEN, J. (1997), «Errors in maximum-entropy charge-density distributions obtained from diffraction data», *Acta Crystallogr. A*, vol. 53 (3), p. 376. {Cited on page 60.}
- [73] KASINATHAN, D., KUNEŠ, J., KOEPERNIK, K., DIACONU, C. V., MARTIN, R. L., PRODAN, I. D., SCUSERIA, G. E., SPALDIN, N., PETIT, L., SCHULTHESS, T. C. and OTHERS (2006), «Mott transition of MnO under pressure: A comparison of correlated band theories», *Physical Review B*, vol. 74 (19), p. 195 110. {Cited on pages 142 and 144.}
- [74] KITTEL, C. (1995), *Introduction to Solid State Physics*, John Wiley & Sons, 7th ed., New York. {Cited on pages 7, 37, 60, 61, 65, and 68.}
- [75] KOCH, W. and HOLTHAUSEN, M. (2001), *A chemist's guide to density functional theory*, vol. 2, Wiley Online Library. {Cited on pages 15, 25, 27, and 29.}
- [76] KOELLING, D. and ARBMAN, G. (1975), «Use of energy derivative of the radial solution in an augmented plane wave method: application to copper», *Journal of Physics F: Metal Physics*, vol. 5, p. 2041. {Cited on page 47.}
- [77] KOHN, W. (1964), «Theory of the insulating state», *Phys. Rev.*, vol. 133 (1A), p. A171. {Cited on pages 7 and 60.}
- [78] KOHN, W. (1996), *Phys. Rev. Lett.*, vol. 76, p. 3168. {Cited on pages 60 and 61.}
- [79] KOHN, W. and SHAM, L. (1965), «Self-consistent equations including exchange and correlation effects», *Phys. Rev.*, vol. 140, pp. A1133–A1138. {Cited on page 24.}
- [80] KOHOUT, M. (2004), *Int. J. Quant. Chem.*, vol. 97, p. 651. {Cited on pages 61 and 68.}
- [81] KOHOUT, M. (2004), «A measure of electron localizability», *International journal of quantum chemistry*, vol. 97 (1), pp. 651–658. {Cited on pages 6 and 53.}
- [82] KOHOUT, M. (Radebeul, 2012), «DGrid 4.6», <http://www.cpfs.mpg.de/~kohout/dgrid.html>. {Cited on pages 64 and 112.}
- [83] KRESSE, G. and FURTHMÜLLER, J. (1996), «Efficiency of ab-initio total energy calculations for metals and semiconductors using a plane-wave basis set», *Computational Materials Science*, vol. 6 (1), pp. 15–50. {Cited on page 143.}
- [84] KUDIN, K., CAR, R. and RESTA, R. (2007), *J. Chem. Phys.*, vol. 126, p. 234 101. {Cited on pages 7 and 60.}

- [85] KUNEŠ, J., LUKOYANOV, A. V., ANISIMOV, V. I., SCALETTAR, R. T. and PICKETT, W. E. (2008), «Collapse of magnetic moment drives the Mott transition in MnO», *Nature materials*, vol. 7 (3), pp. 198–202. {Cited on page 142.}
- [86] KURZYK, J., WOJCIK, W. and SPALEK, J. (2008), *Eur. Phys. J. B*, vol. 66, p. 385. {Cited on pages 81, 82, and 85.}
- [87] KUTZELNIGG, W., MUKHERJEE, D. and OTHERS (1999), «Cumulant expansion of the reduced density matrices», *Journal of Chemical Physics*, vol. 110 (6), pp. 2800–2809. {Cited on page 34.}
- [88] LATHIOTAKIS, N., HELBIG, N. and GROSS, E. (2005), «Open shells in reduced-density-matrix-functional theory», *Physical Review A*, vol. 72 (3), p. 030 501. {Cited on page 147.}
- [89] LATHIOTAKIS, N., HELBIG, N. and GROSS, E. (2007), «Performance of one-body reduced density-matrix functionals for the homogeneous electron gas», *Physical Review B*, vol. 75 (19), p. 195 120. {Cited on page 147.}
- [90] LEVINE, I. N. (2013), *Quantum chemistry*, Pearson Higher Ed. {Cited on page 4.}
- [91] LEWIS, G. N. (1916), «The atom and the molecule», *J. Am. Chem. Soc.*, vol. 38, pp. 762–786. {Cited on page 4.}
- [92] LIEB, E. H. and WU, F. Y. (1968), «Absence of Mott Transition in an Exact Solution of the Short-Range, One-Band Model in One Dimension», *Phys. Rev. Lett.*, vol. 20, p. 1445, URL <http://link.aps.org/doi/10.1103/PhysRevLett.20.1445>. {Cited on pages 78, 82, and 90.}
- [93] LUAÑA, V., MORI-SÁNCHEZ, P., COSTALES, A., BLANCO, M. A. and MARTÍN PENDÁS, A. (2003), *J. Chem. Phys.*, vol. 119, p. 6341. {Cited on page 60.}
- [94] MACCHI, P. and SIRONI, A. (2003), «Chemical bonding in transition metal carbonyl clusters: complementary analysis of theoretical and experimental electron densities.», *Coordination chemistry reviews*, vol. 238, pp. 383–412. {Cited on page 132.}
- [95] MANDADO, M., GONZÁLEZ-MOA, M. J. and MOSQUERA, R. A. (2007), «QTAIM n-center delocalization indices as descriptors of aromaticity in mono and poly heterocycles», *Journal of computational chemistry*, vol. 28 (1), pp. 127–136. {Cited on page 6.}
- [96] MARTÍN PENDÁS, A., BLANCO, M. A. and FRANCISCO, E. (2007), *J. Comput. Chem.*, vol. 28, p. 161. {Cited on page 79.}

- [97] MARTÍN PENDÁS, A., COSTALES, A. and LUAÑA, V. (1997), «Ions in crystals: The topology of the electron density in ionic materials. I. Fundamentals», *Physical Review B*, vol. 55 (7), p. 4275. {Cited on page 53.}
- [98] MARTÍN PENDÁS, A., FRANCISCO, E. and BLANCO, M. (2005), «Two-electron integrations in the Quantum Theory of Atoms in Molecules with correlated wave functions», *Journal of computational chemistry*, vol. 26 (4), pp. 344–351. {Cited on page 102.}
- [99] MARTÍN PENDÁS, A., FRANCISCO, E. and BLANCO, M. (2007), «An electron number distribution view of chemical bonds in real space», *Physical Chemistry Chemical Physics*, vol. 9 (9), pp. 1087–1092. {Cited on pages 100 and 120.}
- [100] MARTÍN PENDÁS, A., FRANCISCO, E. and BLANCO, M. (2007), «Pauling resonant structures in real space through electron number probability distributions», *The Journal of Physical Chemistry A*, vol. 111 (6), pp. 1084–1090. {Cited on pages 7 and 95.}
- [101] MARTÍN PENDÁS, A., FRANCISCO, E. and BLANCO, M. (2007), «Spin resolved electron number distribution functions: How spins couple in real space», *The Journal of chemical physics*, vol. 127 (14), p. 144 103. {Cited on pages 7, 79, and 80.}
- [102] MARTÍN PENDÁS, A., FRANCISCO, E. and BLANCO, M. A. (2007), *Faraday Discuss.*, vol. 135, p. 423. {Cited on page 85.}
- [103] MARTÍN PENDÁS, A., BLANCO, M. A., COSTALES, A., MORISÁNCHEZ, P. and LUAÑA, V. (1999), *Phys. Rev. Lett.*, vol. 83, p. 1930. {Cited on page 60.}
- [104] MATITO, E., FEIXAS, F. and SOLA, M. (2007), «Electron delocalization and aromaticity measures within the Hückel molecular orbital method», *J. Molecular Structure: THEOCHEM*, vol. 811 (1), p. 3. {Cited on page 65.}
- [105] MATITO, E., POATER, J., SOLÀ, M., DURAN, M. and SALVADOR, P. (2005), *J. Phys. Chem. A*, vol. 109, p. 9904. {Cited on page 6.}
- [106] MATITO, E., POATER, J., SOLÀ, M., DURAN, M. and SALVADOR, P. (2005), «Comparison of the AIM delocalization index and the Mayer and fuzzy atom bond orders», *J. Phys. Chem. A*, vol. 109, pp. 9904–10. {Cited on pages 6 and 79.}
- [107] MATITO, E., POATER, J., SOLÀ, M., DURAN, M. and SALVADOR, P. (2005), «Comparison of the AIM delocalization index and the mayer and fuzzy atom bond orders», *The Journal of Physical Chemistry A*, vol. 109 (43), pp. 9904–9910. {Cited on pages 116 and 123.}

- [108] MATITO, E., SOLÀ, M., SALVADOR, P. and DURAN, M. (2007), «Electron sharing indexes at the correlated level. Application to aromaticity calculations», *Faraday discussions*, vol. 135, pp. 325–345. {Cited on page 123.}
- [109] MATTA, C. F. and BOYD, eds. (2007), *The Quantum Theory of Atoms in Molecules: From Solid State to DNA and Drug Design*, Wiley-VC. {Cited on page 59.}
- [110] MAYER, I. (1983), *Chem. Phys. Lett.*, vol. 270, p. 97. {Cited on pages 62 and 79.}
- [111] MCWEENY, R. (2002), *Symmetry: An introduction to group theory and its applications*, Courier Corporation. {Cited on page 39.}
- [112] MCWEENY, R. and SUTCLIFFE, B. (1969), *Methods of molecular quantum mechanics*, vol. 2, Academic Press London. {Cited on pages 29 and 30.}
- [113] MENÉNDEZ, M., ÁLVAREZ BOTO, R., FRANCISCO, E. and MARTÍN PENDÁS, Á. (2015), «One-electron images in real space: Natural adaptive orbitals», *Journal of computational chemistry*, vol. 36 (11), pp. 833–843. {Cited on pages 8 and 108.}
- [114] MORI-SÁNCHEZ, P., LUAÑA, V. and MARTÍN PENDÁS, A. (2002), *J. Am. Chem. Soc.*, vol. 124, p. 14 721. {Cited on page 60.}
- [115] MOTT, N. and PEIERLS, R. (1937), «Discussion of the paper by de Boer and Verwey», *Proceedings of the Physical Society*, vol. 49 (4S), p. 72. {Cited on page 139.}
- [116] MOTT, N. F. (1949), «The basis of the electron theory of metals, with special reference to the transition metals», *Proceedings of the Physical Society. Section A*, vol. 62 (7), p. 416. {Cited on page 139.}
- [117] MOTT, N. F. (1968), *Rev. Mod. Phys.*, vol. 40, p. 677. {Cited on page 78.}
- [118] MÜLLER, A. (1984), «Explicit approximate relation between reduced two-and one-particle density matrices», *Physics Letters A*, vol. 105 (9), pp. 446–452. {Cited on page 147.}
- [119] MULLIKEN, R. S. (1931), «Bonding Power of Electrons and Theory of Valence.», *Chemical Reviews*, vol. 9 (3), pp. 347–388. {Cited on page 4.}
- [120] OTERO-DE-LA ROZA, A., ABBASI-PÉREZ, D. and LUAÑA, V. (2011), «GIBBS2: A new version of the quasiharmonic model code. II. Models for solid-state thermodynamics, features and implementation», *Computer Physics Communications*, vol. 182 (10), pp. 2232–2248. {Cited on page 143.}

- [121] PATTERSON, J., ARACNE, C., JACKSON, D., MALBA, V., WEIR, S., BAKER, P. and VOHRA, Y. (2004), «Pressure-induced metallization of the Mott insulator MnO», *Physical Review B*, vol. 69 (22), p. 220 101. {Cited on pages 140, 142, and 144.}
- [122] PAULING, L. (1928), «The shared-electron chemical bond», *Proceedings of the national academy of sciences*, vol. 14 (4), pp. 359–362. {Cited on page 4.}
- [123] PAULING, L. (1960), *The Nature of the Chemical Bond*, Cornell Univ. Press., Ithaca, N. Y., third Ed. {Cited on pages 5 and 132.}
- [124] PAULING, L. and WILSON, E. B. (1935), *Introduction to quantum mechanics: with applications to chemistry*, Courier Corporation. {Cited on pages 3 and 4.}
- [125] PERDEW, J. P. and WANG, Y. (1992), «Accurate and simple analytic representation of the electron-gas correlation energy», *Physical Review B*, vol. 45 (23), p. 13 244. {Cited on page 112.}
- [126] PLANCK, M. (1901), «On the law of the energy distribution in the normal spectrum», *Ann. Phys*, vol. 4 (553), p. 90. {Cited on page 3.}
- [127] POATER, J., SOLÀ, M., DURAN, M. and FRADERA, X. (2002), «The calculation of electron localization and delocalization indices at the Hartree-Fock, density functional and post- Hartree-Fock levels of theory», *Theor. Chem. Acc.*, vol. 107, pp. 362–371. {Cited on page 6.}
- [128] POATER, J., FRADERA, X., DURAN, M. and SOLÀ, M. (2003), «The delocalization index as an electronic aromaticity criterion: application to a series of planar polycyclic aromatic hydrocarbons», *Chem. Eur. J.*, vol. 9 (2), p. 400. {Cited on page 65.}
- [129] PONEC, R. (1997), «Electron pairing and chemical bonds. Chemical structure, valences and structural similarities from the analysis of the Fermi holes», *Journal of Mathematical Chemistry*, vol. 21 (3), pp. 323–333. {Cited on pages 8, 106, and 108.}
- [130] PONEC, R. (1998), «Electron pairing and chemical bonds. Molecular structure from the analysis of pair densities and related quantities», *Journal of mathematical chemistry*, vol. 23 (1-2), pp. 85–103. {Cited on pages 8, 106, and 108.}
- [131] PONEC, R. (2005), «Chemical bonding in solids. On the generalization of the concept of bond order and valence for infinite periodical structures», *Theoretical Chemistry Accounts: Theory, Computation, and Modeling (Theoretica Chimica Acta)*, vol. 114 (1), pp. 208–212. {Cited on page 58.}



- [132] PONEC, R. (2005), «Chemical bonding in solids. On the generalization of the concept of bond order and valence for infinite periodical structures», *Theor. Chem. Acc.*, vol. 114 (1-3), p. 208. {Cited on page 68.}
- [133] PONEC, R. (2011), *J. Comput. Chem.*, vol. 32, p. 3114. {Cited on page 68.}
- [134] PONEC, R. and COOPER, D. L. (2007), «Anatomy of bond formation. Domain-averaged Fermi holes as a tool for the study of the nature of the chemical bonding in Li<sub>2</sub>, Li<sub>4</sub>, and F<sub>2</sub>», *The Journal of Physical Chemistry A*, vol. 111 (44), pp. 11 294–11 301. {Cited on page 108.}
- [135] PONEC, R., LENDVAY, G. and CHAVES, J. (2008), «Structure and bonding in binuclear metal carbonyls from the analysis of domain averaged Fermi holes. I. Fe<sub>2</sub> (CO)<sub>9</sub> and Co<sub>2</sub> (CO)<sub>8</sub>», *Journal of computational chemistry*, vol. 29 (9), pp. 1387–1398. {Cited on page 108.}
- [136] POPELIER, P. L. and AICKEN, F. M. (2003), «Atomic Properties of Amino Acids: Computed Atom Types as a Guide for Future Force-Field Design», *ChemPhysChem*, vol. 4 (8), pp. 824–829. {Cited on page 6.}
- [137] POPELIER, P. L. A. and BRÈMOND, E. A. (2009), *Int. J. Quant. Chem.*, vol. 109, p. 2542. {Cited on page 6.}
- [138] PRINCE, E., WILSON, A. J. C., HAHN, T. and SHMUELI, U. (1999), *International tables for crystallography*, International Union of Crystallography. {Cited on page 39.}
- [139] RESTA, R. (1998), «Quantum-mechanical position operator in extended systems», *Phys. Rev. Lett.*, vol. 80 (9), p. 1800. {Cited on pages 60, 75, and 77.}
- [140] RUHEMANN, F. (1935), «Temperaturabhängigkeit der Gitterkonstanten von Manganoxyd», *Physik. Ber.*, vol. 16, p. 2337. {Cited on page 143.}
- [141] SAVIN, A. (2002), «Probability distributions and valence shells in atoms», in SEN, K. D., ed., «Reviews of modern quantum chemistry: a celebration of the contributions of Robert G. Parr», vol. 1, p. 43, World Scientific, Singapore. {Cited on pages 7 and 103.}
- [142] SCHMIDT, M. W., BALDRIDGE, K. K., BOATZ, J. A., ELBERT, S. T., GORDON, M. S., JENSEN, J. H., KOSEKI, S., MATSUNAGA, N., NGUYEN, K. A., SU, S. J., WINDUS, T. L., DUPUIS, M. and MONTGOMERY, J. A. (1993), *J. Comput. Chem.*, vol. 14, p. 1347. {Cited on pages 63 and 83.}

- [143] SCHRÖDINGER, E. (1926), «Quantisierung als eigenwertproblem», *Annalen der physik*, vol. 385 (13), pp. 437–490. {Cited on page 4.}
- [144] SCHULENBURG, J. (2001), «Program Spinpack», URL <http://www-e.uni-magdeburg.de/jschulen/spin/>. {Cited on page 83.}
- [145] SHAIK, S. and FRENKING, G. (2014), *Front Matter*, pp. I–XXV, Wiley-VCH Verlag GmbH & Co. KGaA, URL <http://dx.doi.org/10.1002/9783527664696.fmatter>. {Cited on page 4.}
- [146] SHARMA, S., DEWHURST, J., LATHIOTAKIS, N. and GROSS, E. (2008), «Reduced density matrix functional for many-electron systems», *Physical Review B*, vol. 78 (20), p. 201 103. {Cited on page 147.}
- [147] SHARMA, S., SHALLCROSS, S., DEWHURST, J. and GROSS, E. (2012), «Spectrum of extended systems from Reduced Density Matrix Functional Theory», *arXiv preprint arXiv:0912.1118v2*. {Cited on pages 9 and 147.}
- [148] SHARMA, S., DEWHURST, J., SHALLCROSS, S. and GROSS, E. (2013), «Spectral density and metal-insulator phase transition in Mott insulators within reduced density matrix functional theory», *Physical review letters*, vol. 110 (11), p. 116 403. {Cited on pages 9 and 147.}
- [149] SILVI, B. and GATTI, C. (2000), «Direct space representation of the metallic bond», *The Journal of Physical Chemistry A*, vol. 104 (5), pp. 947–953. {Cited on page 132.}
- [150] SILVI, B. and SAVIN, A. (1994), *Nature*, vol. 371, p. 683. {Cited on page 61.}
- [151] SINGH, D. (1991), «Ground-state properties of lanthanum: Treatment of extended-core states», *Physical Review B*, vol. 43 (8), p. 6388. {Cited on pages 48 and 49.}
- [152] SINGH, D. (1994), «Plane waves, pseudopotentials and the LAPW method», Kluwer Academic, New York. {Cited on page 47.}
- [153] SJÖSTEDT, E., NORDSTRÖM, L. and SINGH, D. (2000), «An alternative way of linearizing the augmented plane-wave method», *Solid State Communications*, vol. 114 (1), pp. 15–20. {Cited on page 49.}
- [154] SLATER, J. (1951), «Magnetic effects and the Hartree-Fock equation», *Physical Review*, vol. 82 (4), p. 538. {Cited on page 140.}

- [155] SLATER, J. C. (1931), «Directed valence in polyatomic molecules», *Physical Review*, vol. 37 (5), p. 481. {Cited on page 4.}
- [156] SLATER, J. C. (1937), «Wave functions in a periodic potential», *Physical Review*, vol. 51 (10), p. 846. {Cited on page 45.}
- [157] SZABO, A. and OSTLUND, N. (1996), *Modern quantum chemistry: introduction to advanced electronic structure theory*, Dover Pubns. {Cited on pages 15, 20, and 108.}
- [158] TARASKIN, S. N., DRABOLD, D. A. and ELLIOT, S. R. (2002), *Phys. Rev. Lett.*, vol. 88, p. 196 405. {Cited on pages 61 and 77.}
- [159] TARASKIN, S. N., FRY, P. A., ZHANG, X., DRABOLD, D. A. and ELLIOT, S. R. (2002), *Phys. Rev. B*, vol. 66, p. 233 101. {Cited on pages 61, 66, and 77.}
- [160] TER HAAR, D. (1967), *The Old Quantum Theory*, Pergamon Press, 1st edition edition. {Cited on page 3.}
- [161] THEOPHILOU, I., LATHIOTAKIS, N. N., GIDOPOULOS, N. I., RUBIO, A. and HELBIG, N. (2015), «Orbitals from local RDMFT: Are they Kohn-Sham or Natural Orbitals?», *arXiv preprint arXiv:1505.00627*. {Cited on pages 147 and 148.}
- [162] WIBERG, K. B. (1968), *Tetrahedron*, vol. 24, p. 1083. {Cited on pages 62 and 79.}
- [163] WIKIPEDIA (2016), «Introduction to quantum mechanics — Wikipedia, The Free Encyclopedia», [https://en.wikipedia.org/wiki/Introduction\\_to\\_quantum\\_mechanics](https://en.wikipedia.org/wiki/Introduction_to_quantum_mechanics), [Online; accessed 11-February-2016]. {Cited on page 3.}
- [164] WIKIPEDIA (2016), «Quantum chemistry — Wikipedia, The Free Encyclopedia», [https://en.wikipedia.org/wiki/Quantum\\_chemistry](https://en.wikipedia.org/wiki/Quantum_chemistry), [Online; accessed 11-February-2016]. {Cited on page 4.}
- [165] WIKIPEDIA (2016), «Quantum mechanics — Wikipedia, The Free Encyclopedia», [https://en.wikipedia.org/wiki/Quantum\\_mechanics](https://en.wikipedia.org/wiki/Quantum_mechanics), [Online; accessed 11-February-2016]. {Cited on page 4.}
- [166] YOO, C.-S., MADDUX, B., KLEPEIS, J.-H., IOTA, V., EVANS, W., MCMAHAN, A., HU, M., CHOW, P., SOMAYAZULU, M., HÄUSERMANN, D. and OTHERS (2005), «First-order isostructural Mott transition in highly compressed MnO», *Physical review letters*, vol. 94 (11), p. 115 502. {Cited on page 142.}

## COLOPHON

This document was typeset in  $\text{\LaTeX}$  using the typographical look-and-feel `arsclassica`. Most of the graphics in this thesis are generated using Gnuplot, Paraview and pgf/tikz. The bibliography is typeset using natbib.